Identification of the causal PD risk gene(s) under GWAS peaks

Dissertation

zur Erlangung des Grades eines
Doktors der Naturwissenschaften

der Mathematisch-Naturwissenschaftlichen Fakultät
und
der Medizinischen Fakultät
der Eberhard-Karls-Universität Tübingen

vorgelegt
von

Weiping Wang
aus Shandong, China

2024

Tag der mündlichen Prüfung: 04.01.2024

Dekan der Math.-Nat. Fakultät: Prof. Dr. Thilo Stehle
Dekan der Medizinischen Fakultät: Prof. Dr. Bernd Pichler

1. Berichterstatter: Prof. Dr. Thomas Gasser

2. Berichterstatter: Prof. Dr. Peter Heutink

Prüfungskommission: Prof. Dr. Peter Heutink

Prof. Dr. Thomas Gasser

PD Dr. Christian Johannes Gloeckner

Prof. Dr. med. Olaf Riess

Erklärung / Declaration:

Ich erkläre, dass ich die zur Promotion eingereichte Arbeit mit dem Titel:

“Identification of the causal PD risk gene(s) under GWAS peaks”

selbständig verfasst, nur die angegebenen Quellen und Hilfsmittel benutzt und wörtlich oder inhaltlich übernommene Stellen als solche gekennzeichnet habe. Ich versichere an Eides statt, dass diese Angaben wahr sind und dass ich nichts verschwiegen habe. Mir ist bekannt, dass die falsche Abgabe einer Versicherung an Eides statt mit Freiheitsstrafe bis zu drei Jahren oder mit Geldstrafe bestraft wird.

I hereby declare that I have produced the work entitled “Identification of the causal PD risk gene(s) under GWAS peaks”, submitted for the award of a doctorate, on my own (without external help), have used only the sources and aids indicated and have marked passages included from other works, whether verbatim or in content, as such. I swear upon oath that these statements are true and that I have not concealed anything. I am aware that making a false declaration under oath is punishable by a term of imprisonment of up to three years or by a fine.

Tübingen, den 15.01.2024 .....

Unterschrift /Signature

Acknowledgment

First, I would like to thank my Ph.D. supervisor, Prof. Peter Heutink. I still remember how I felt when I first saw Prof. Heutink's profile on the DZNE website. What impressed me most was the friendliness of his photo compared to his outstanding scientific achievements. At that time, I wanted to join Peter's lab, but on the other hand, I felt that I was not strong enough. After thinking about it, I decided to give myself a chance to try, regardless of the result. After submitting my resume, I received a reply soon. After three rounds of interviews, I finally got into Peter's lab. Every time I see my progress, the person I want to thank most is my supervisor, Prof. Peter Heutink, for allowing me to be his student, to work with so many great colleagues, and to work on the projects I love. When I encountered problems, Peter always gave me a lot of valuable suggestions, and when I made presentations, Peter always gave me recognition, encouragement, and suitable suggestions. All of this has invariably influenced me to become better and more confident. I would like to pay my highest respect to Prof. Peter Heutink here.

I thank my current and former colleagues for their tolerance and help. Thanks to Joachim Taeger, who helped me adapt to the lab life during my PhD's initial phase, I learned many experimental techniques. We enjoyed sharing our ideas on my PhD project. Thanks to Noémia Alves Fernandes for giving me many suggestions and help with the RT-qPCR part of my experiments. Thanks to Melissa Castillo Lizardo for helping me with the mRNA sequencing part of the experiment. Thanks to Vikas Bansal, Natalia Savytska, Mohammed Dehestani, and Anastasia Illarionova for their guidance in analyzing my mRNA sequencing data. Also, thank Salvador Rodriguez-Nieto, Ashutosh Dhingra, and Elntem Sadikoglou for their advice on my experiments. I am lucky to have you as my colleague. You are serious and rigorous but always patient in experiments, and outside of experiments, we share different cultures and insights from different countries, which brings a lot of fun to my PhD life.

Thank my advisory board members, Prof. Thomas Gasser and Prof. Christian Johannes Gloeckner for their advice and support for my PhD project. Thanks to Prof. Thomas Gasser for the guarantees for my Ph.D. graduation. Thanks to Prof. Christian Johannes Gloeckner, for his valuable suggestions on this project.

Thank the Chinese government for training me and supporting my study abroad, and the China Scholarship Council (CSC) allowed me to expand my horizons and get to know the bigger world.

Thank my good friends Ping Liu, Shengjun Wen, and Martina Wagner. Thank Ping Liu and Shengjun Wen for always giving me valuable advice when I was lost and their encouragement and support when I was at a low point in my experiments. Thank Martina Wagner for bringing me a lot of enjoyable times in my life. Hanging out with her makes me feel relaxed, and we always sense each other and understand each other, and all these heal the tired mind.

Thank my family, they will always be my most substantial support. My mother, Ruifang Liu, has brought me many good qualities. She always taught me to be profound and practical, to persevere, and not give up lightly. These qualities have always influenced me until now. My mother is very selfless and giving, always giving me what I need. My brother, Guangan Wang, took on many responsibilities to care for and be with my mom while I was abroad. My husband, Jin Zhang, is doing his best to help me share the care and education of my son while completing his studies. Studying abroad has forced us to be more independent and more decisive, and this process has strengthened our relationship. My son Jingduo Zhang is now five and a half years old. However, he is just a child but very understanding. He plays by himself whenever I have to work overtime and never interrupts my work. I remember every moment we cooperated, taking him to work in the lab, taking him to training, bringing him to group meetings, etc. I am very grateful to him for his excellent behavior and the tolerance of my colleagues for my particular situation. Raising a child while studying for a Ph.D. is a tough and challenging task, but the joint effort of everyone makes the process less complicated and even more fun.

I keep my final thanks to myself for never giving up on trying and progressing. I have never given up lightly in my more than 20 years of study life. For every choice I made, I always chose to face challenges positively to pursue better educational resources, to experience a bigger world, to break the limitations of the status quo, and to make my mind more inclusive rather than resting on my laurels. Now, I am closer to my goal, and time will not disappoint those who strive hard. The next phase is about to begin, and I look forward to a better version of myself.

Table of Contents

Summary

Parkinson's disease (PD) is a neurodegenerative disease, the incidence of which increases with age. The prevalence of PD is rapidly increasing in the global aging population. With the increasing number of PD patients, the social and economic costs rise exponentially, emphasizing the immediate need to understand PD's pathogenesis and effective disease-modifying treatments (Tolosa et al. 2021; Trist, Hare, and Double 2019).

From the time PD was described by James Parkinson in 1817 to the present, several significant milestones have been reached. In 1912, Frederick Lewy discovered intracytoplasmic inclusion bodies ("Lewy bodies"), which were identified years later as the pathological hallmark of PD (Holdorff 2006, 2002). In 1957, Arvid Carlsson and Oleh Hornykiewicz pioneered the link between dopamine deficiency and PD (Fahn 2018; Hargittai 2023). In 1967, George Cotzias revolutionized high-dose levodopa therapy, leading to a breakthrough in the treatment of PD (Lees, Tolosa, and Olanow 2015; Patten 1983). In 1997, Polymeropoulos and colleagues identified the first mutation causing autosomal dominant PD in a large family that originated in Greece and immigrated to Italy. This gene mutation is a missense mutation (A53T) in the SNCA gene encoding α-synuclein (normal state of α-synuclein, same as below) protein located on chromosome 4q21-q23 (Polymeropoulos et al. 1997). Later, Spillantini and her colleagues discovered that α-synuclein is present in the Lewy bodies, a significant discovery that cemented the importance of α-synuclein and its central role in the pathogenesis of PD (Spillantini et al. 1997). A year after discovering the first mutation in the PD-associated gene SNCA, mutations in Parkin (PRKN) were found to cause autosomal recessive PD (Matsumine et al. 1997).

The discovery of PD triggered by a single gene mutation made PD as a complex disease that both rare and common genetic variants can influence. The heritability of PD is estimated to be about 35%, which includes risk factors such as GBA and MAPT etc. However, the variants identified by GWAS have modest effect sizes and collectively fail to account for current estimates of PD heritability. Larger sample sizes are required to identify other risk factors (Nalls et al. 2019). However, it also seems likely that additional rare alleles with larger effect sizes contribute to PD risk in the population (Blauwendraat, Nalls, and Singleton 2020).

Nalls et al. and Fu et al. have identified 90 significant risk variants across 78 genomic regions associated with PD in the European population and 2 from Asia population (Nalls et al. 2019; Foo et al. 2020). However, the underlying genes need to be known to develop disease-modifying therapeutic strategies. A complete list of candidate genes was generated in our lab after determining the associated genomic region flanking the associated single nucleotide polymorphisms (SNPs) based on linkage disequilibrium calculations, followed by determining the genes located in these regions. Our mission is to determine which of these genes under each locus are affected by the causal variants and how changes in the function or regulation of the causal genes lead to altered disease risk. Since most SNPs regulate the expression of one or more neighboring genes, their effect can be mimicked by gene knockdown using RNA interference (RNAi) technology or gene activation using clustered regularly interspaced short palindromic repeats (CRISPR) technology. In this study, gene knockdowns were performed by using RNAi technology, the effect of candidate genes on the change of mitochondrial dynamics on PD was investigated by performing mitochondrial morphology assay and Parkin translocation assay, the effect of candidate genes on α-synuclein proteins level was investigated by performing α-synuclein enzyme-linked immunosorbent assay (ELISA). In addition, mRNA sequencing was performed to determine the knockdown efficiency and the effect of gene knockdown on molecular pathways to learn more about potential novel PD-relevant pathways.

The robust strictly standardized median difference (SSMD) was calculated for hit selection of mitochondrial morphology assay and Parkin translocation assay. Effects were considered significant when most of the shRNAs targeting one gene the SSMD $\geqslant 3$ or $\leqslant -3$. The percentage of increased or decreased α-synuclein protein was calculated for hit selection of α-synuclein ELISA assay. Effects were considered significant when the percentage of increase of α-synuclein protein is $\geqslant 50\%$ of negative control, or the decrease of α-synuclein protein is $\leqslant 50\%$ of negative control for each treatment. Based on the result of functional assay and mRNA sequencing, a subset of priority genes per locus was selected from this study.

The data from this study helped us narrow down the list of risk genes for PD and suggested possible causative genes in each of the 78 known risk loci. Not only that, this study may also provide us with novel causative genes or novel roles of some genes in PD. Another critical point of this study is that our approach highlights a powerful experimental strategy that has broad applicability in

future studies of diseases with complex genetic etiologies. The selection of priority genes from a large number of candidates has advanced the study of the PD genome, but there is still some way to go before we can identify the actual causative genes. To achieve this goal, targeted experiments need to be designed to validate these prioritized genes. The future of PD-targeted therapy is bright as our understanding and research continue to advance.

List of Figures

List of Tables

List of Abbreviations

PD	Parkinson's disease
LBs	Lewy bodies
SNpc	Substantia nigra pars compacta
RNAi	RNA interference
CRISPR	clustered regularly interspaced short palindromic repeats
LCIG	Levodopa-carbidopa intestinal gel
MAOIs	Monoamine oxidase inhibitors
COMTIs	Catechol-O-methyl transferase inhibitors
DBS	Deep brain stimulation
STN	Subthalamic nucleus
hESCs	Human embryonic stem cells
iPSCs	Induced pluripotent stem cells
ATP	Adenosine triphosphate
GST	Glutathione S-transferase
S129	Serine 129
S87	Serine 87
TH	Tyrosine hydroxylase
UPS	Ubiquitin-proteasome system
ALP	Autophagy-lysosomal pathway
UCHL1	Ubiquitin carboxyl-terminal hydrolase L1
ER	Endoplasmic reticulum
ERAD	Endoplasmic reticulum-associated degradation
GSK-3β	Glycogen synthase kinase-3β
LRRK2	Leucine-rich repeat kinase 2
PFF	Preformed fibrils
MCI	Mitochondrial complex I

IMM	Inner mitochondria membrane
ROS	Reactive oxygen species
SNCA	α-synueclin gene
VPS35	Vacuolar protein sorting-associated protein 35
NESCs	Neuroepithelial stem cells
GCase	Glucocerebrosidase
PGC1α	Proliferation-activating receptor gamma coactivator 1-α
Drp1	Dynamin-related protein 1
OMM	Outer mitochondrial membrane
OPA1	Optic atrophy 1
UCP	Uncoupling protein
MPP+	1-methyl-4-phenylpyridine
PINK1	PTEN-induced putative kinase 1
PARKIN	Parkin RBR E3 ubiquitin-protein ligase
TOM	Translocase of outer membrane
MPTP	1-methyl-4-phenyl-1,2,3,6-tetrahydropyridine
mtDNA	Mitochondrial DNA
DAMPs	Damage-associated molecular patterns
PRRs	Pattern recognition receptors
Nr4a2/Nurr1	Nuclear receptor subfamily 4, group A, member 2
GIGYF2	Grb10-interacting GYF protein-2
GWAS	Genome-wide association studies
GBA	Glucosidase beta acid
UPR	Unfolded protein response
MAPT	Microtubule associated protein tau
SNP	Single nucleotide polymorphism
PRS	Polygenic risk score
KD	Knockdown

SD	Standard deviation
shRNA	Short hairpin ribonucleic acid
LB	Lysogeny broth
µg/mL	Microgram per milliliter
AMP	Ampicillin
FBS	Fetal bovine serum
µL	Microliter
CO2	Carbon dioxide
°C	Celsius degree
g	Gram
ng	Nanogramme
GFP	Green fluorescent protein
DMEM/F-12	Dulbecco's Modified Eagle/Nutrient Mixture F-12 Medium
DPBS	Dulbecco's Phosphate Buffered Saline
P/S	Penicillin/Streptomycin
PFA	Paraformaldehyde
nM	Nanomole
mM	Millimole
mm	Millimeter
min	Minute
CCCP	Carbonyl cyanide m-chlorophenyl hydrazine
ELISA	Enzyme-linked immunosorbent assay
rpm	Revolutions per minute
RIPA	Radioimmunoprecipitation assay
Tris-HCL	TRIS hydrochloride
NP-40	Nonidet P-40 Substitute
EDTA	Ethylenediaminetetraacetic acid
SDS	Sodium dodecyl sulfate

PMSF	Phenylmethanesulfonyl fluoride
FDR	False discovery rate
SSMD	Strictly standardized median difference
RIN	RNA integrity number
RT-qPCR	Realtime quantitative polymerase chain reaction
HK	Housekeeping
QC	Quality control
Rq	Relative quantification
SD	Standard deviation
GO	Gene Ontology
PCA	Principal component analysis
MAPK	Mitogen-activated protein kinase
IP3Rs	Inositol 1, 4, 5-triphsphate (IP3) receptors
AMPK	AMP-activated kinase
mTOR	Mammalian target of rapamycin
CDK	Cyclin-dependent kinases
ASK1	Apoptosis signal-regulating kinase 1
JNK	C-Jun-N-terminale Kinasen
CAMK	Ca2+/calmodulin-dependent protein kinase
AD	Alzheimer's disease
Aβ	β-amyloid protein (
BACE1	β-amyloid converting enzyme 1
HSP70s	Heat shock 70kD proteins
CTSD	Pre-cathepsin D
H3K4me3	Tri-methylated lysine-4 of histone H3

1. Introduction

Parkinson's disease (PD) is a neurodegenerative disorder with the prevalence increasing gradually with the increase in age. The global prevalence is expected to double from 6.2 million cases in 2015 to 12.9 million cases by 2040 (Blauwendraat, Nalls, and Singleton 2020). PD was first described as 'An Essay of the Shaking Palsy' by James Parkinson in 1871(Jagadeesan et al. 2017; Parkinson 1969). Patients with PD have a combination of progressive motor and non-motor symptoms affecting their quality of life, creating a substantial burden on healthcare systems. The motor symptoms mainly include slow movements, tremors, unstable posture, and rigidity. The non-motor symptoms include cognition impairment, emotion problems, sleep disturbances, and so on (Beitz 2014). The main pathological features of PD are progressive degeneration and loss of dopaminergic neurons in the substantia nigra, along with activation of glial cells and expression of inflammatory factors, as well as dysfunctional glucose metabolism, oxidative stress, apoptosis and aggregates of the α-synuclein (normal state of α-synuclein, same as below) protein into inclusions called Lewy bodies (LBs) (Lew 2007). According to the clinical diagnostic criteria, approximately 60-70% of nigrostriatal neurons are degenerated, and 80% of the striatal dopamine content is reduced before the diagnosis (Marino et al. 2012). Statistics show that approximately 1% of people over 60 years of age develop the disease (Tysnes and Storstein 2017). To date, the exact cause and pathogenesis of sporadic PD is largely unknown, but the onset of PD is undoubtedly not due to a single factor but rather to the involvement of multiple causative factors. The previously described risk factors of PD include increasing age, stress, male gender, environmental factors, genetic mutations, etc (Balestrino and Schapira 2020).

1.1 Genetic aspects of PD

The discovery of a familial form of PD caused by a single gene mutation has led to the current paradigm of PD as a complex disease that can be influenced by both rare and common genetic variants (Polymeropoulos et al. 1997; Blauwendraat, Nalls, and Singleton 2020). Genetic variants are estimated to contribute about 25% to the overall risk of developing PD (Day and Mullin 2021). The association of genetic variants and PD varies in frequency and risk (Figure 1).

On the one hand, the linkage analysis of affected PD families showed that monogenic or familial PD is characterized by rare high penetrance genetic variants. On the other hand, genome-wide

association studies (GWAS) have identified numbers of more common with low penetrance genetic variants that contribute to developing sporadic PD (Koros, Simitsi, and Stefanis 2017). In the middle of the two types of variants mentioned above, there are uncommon, but not rare variants that contribute moderately to the risk of developing PD, such as GBA and LRRK2 variants (von Linstow, Gan-Or, and Brundin 2020).

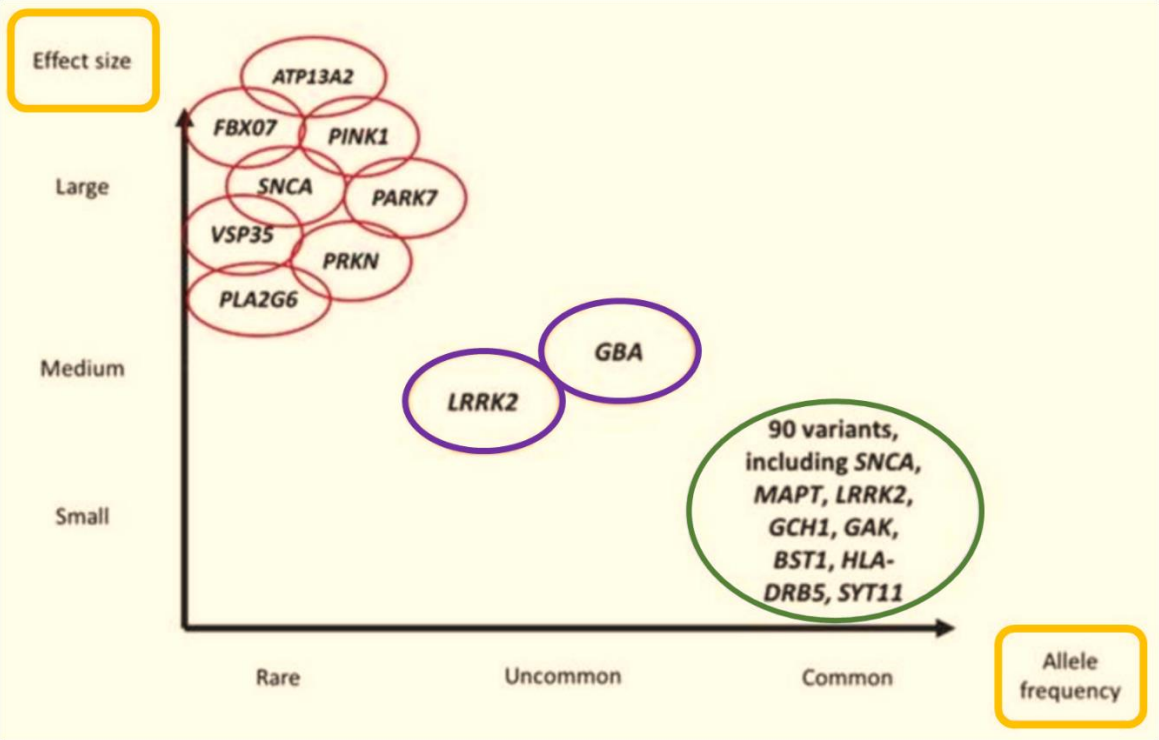

Figure 1. Summary of genetic variants in PD grouped according to allele frequency and associated risk of PD. (from (Day and Mullin 2021))

1.1.1 Familial PD

Familial PD (or monogenic PD) initially identified monogenic associations through studies of affected pedigrees. In 1997, Polymeropoulos and colleagues identified the first missense mutation in the SNCA gene encoding the α-synuclein protein located on chromosome 4q21-q23 (Polymeropoulos et al. 1997). Up to date, at least eight genes have been confirmed to be associated with familial PD including α-synuclein gene (SNCA), Parkin RBR E3 ubiquitin-protein ligase (PARKIN), PTEN-induced putative kinase 1 (PINK1), ATPase cation transporting 13A2 (ATP13A2), DJ-1 (PARK7), F-box protein 7 (FBXO7), phospholipase A2 group VI (PLA2G6)

and VPS35 retromer complex component (VPS35) genes (Hatano et al. 2009). Linkage analyses in autosomal dominant and autosomal recessive kindreds have identified genes resulting in Mendelian (single gene) forms of parkinsonism, which can explain 5-10% of PD cases (Klein and Westenberger 2012).

Monogenic PD usually has variants with large risk effects, resulting in changes in protein-coding or large differences in expression which makes it suitable for modeling using genetic methods in cellular and animal systems (Blauwendraat, Nalls, and Singleton 2020). Studies of the molecular mechanisms underlying monogenic PD have helped us to evaluate whether these mechanisms also apply to sporadic PD.

1.1.2 Sporadic PD

In contrast to familial PD, genetic studies of sporadic PD have been advanced primarily through the discovery of common genetic variants by using case-control cohorts GWAS, which made considerable progress in our understanding of sporadic PD (Jansen et al. 2017).

The first GWAS locus for PD was identified in 2009 (Figure 2). Until now, Nalls et al. and Foo et al. have identified 90 risk variants associated with PD in the European population and 2 from the Asian population (Nalls et al. 2019; Foo et al. 2020). These findings made a breakthrough in our understanding of the genetics of PD. They also provide us with a lot of important information and directions for doing more specific research. Since most of the studies used European cohorts, this limited the applicability of the results to the worldwide populations. In addition, the heritability of PD is estimated to be about 35%, which includes risk factors such as glucosidase beta acid (GBA) and microtubule-associated protein tau (MAPT), etc. However, the variants identified by GWAS have modest effect sizes and collectively fail to account for current estimates of PD heritability. Larger sample sizes are required to identify other risk factors. Considering the missing heritability of PD, additional rare alleles with larger effect sizes contribute to PD risk in the population (Jansen et al. 2017; Mullin and Schapira 2015). The development of high-throughput sequencing technologies has revolutionized human genetics, and hundreds of thousands of genomes have been sequenced worldwide, starting a new era of genetics.

GWAS has generated new loci relevant to the risk of developing PD. However, the underlying genes or gene markers need to be known to develop disease-modifying therapeutic strategies. The

associated single nucleotide polymorphisms (SNPs) from GWAS studies identify the genomic location (locus) for a genetic risk variant but do not identify the variant or the gene itself. Under each of the association peak, several genes can be located and considered candidate gene(s). Thus, the identification of the causal genes is challenging. If a SNP is located in a protein-coding region, this gene is likely causal. However, the vast majority of the SNPs identified in recent studies lie not in protein-coding regions of the chromosome. Several even in "gene deserts" which are regions of the genome that are devoid of protein-coding genes. Therefore, post-GWAS analyses are critical in assigning biological functions to GWAS variants (Gallagher and Chen-Plotkin 2018). These analyses include functional analysis, which is aimed at inferring the possible underlying disease biological mechanisms associated with the variants and calculating the polygenic risk score (PRS) to quantify a person's genetic risk of developing a trait.

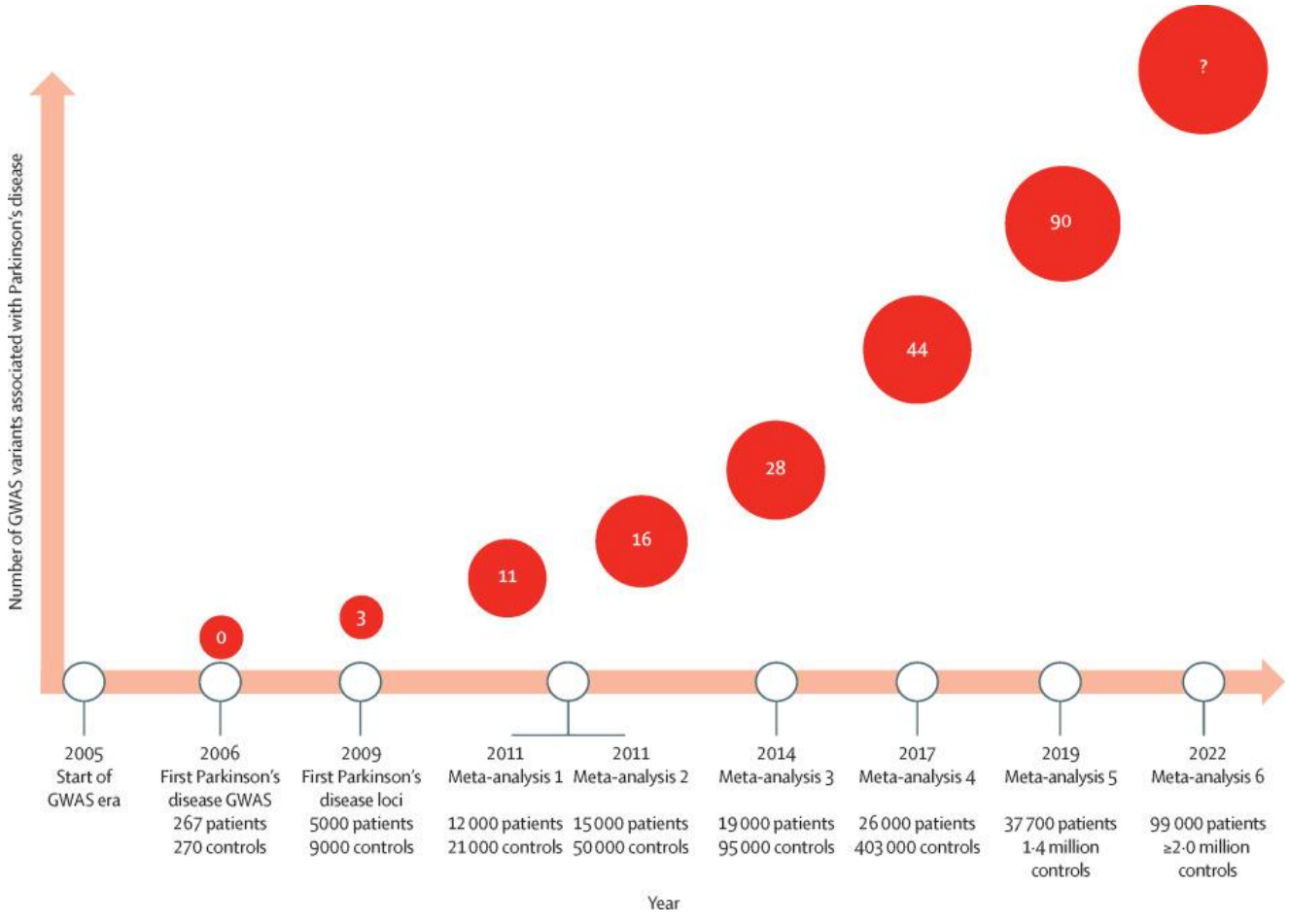

Figure 2. Timeline of genetic discoveries from GWASs for PD. (from (Blauwendraat, Nalls, and Singleton 2020), with permission from Elsevier)

1.2 Pathophysiology of PD

PD is characterized by several neuropathological hallmarks, including the degeneration of dopaminergic neurons in the substantia nigra and the aggregation of abnormal α-synuclein (Antony et al. 2013).

The main pathological change in PD is the degeneration of dopaminergic neurons in the substantia nigra (Y.-F. Zhu et al. 2020). Nigrostriatal dopaminergic neurons are involved in motor regulation in the basal ganglia by transporting dopamine to the striatum via the substantial nigra-striatal pathway. The regulation of motor function by the basal ganglia is achieved primarily through connections with the cortico-basal ganglia-thalamus-cortical circuit (Rodriguez-Sabate et al. 2019). In this circuit, the striatum receives projected fibers from the brain's sensorimotor cortex, and its emitted fibers reach the medial pallidum/ substantia nigra pars compacta (SNpc) reticular formation, the emitting unit of the basal ganglia emitted fibers via direct and indirect pathways. Dopaminergic fibers emanating from the SNpc project to the striatum for further coordinated control of the basal ganglia motor circuitry (Quartarone et al. 2020). In the direct pathway, dopamine binds to D1 receptors on the striatum, activating the direct pathway (Alexander, DeLong, and Strick 1986). In the indirect pathway, dopamine binds to D2 receptors on the striatum and inhibits the indirect pathway. In PD patients, there is a decrease in substantial nigra-striatum dopaminergic signaling, causing inhibition of the direct pathway, excitation of the indirect pathway, and ultimately causing symptoms of reduced movement such as hypokinesia and tonicity (Figure 3).

Another neuropathology hallmark of PD is the presence of intracellular inclusions termed LBs, which are composed of aggregates of abnormal α-synuclein (Dickson 2018). Normally, α-synuclein is a natively unfolded protein highly enriched in presynaptic and perinuclear cellular compartments in the central nervous system, which may modify synaptic vesicle release (Burré et al. 2010). In PD, the abnormal α-synuclein is a misfolded “amyloid-like” protein prone to aggregation, and has pathologic post-translational modifications (Choong and Mochizuki 2022).

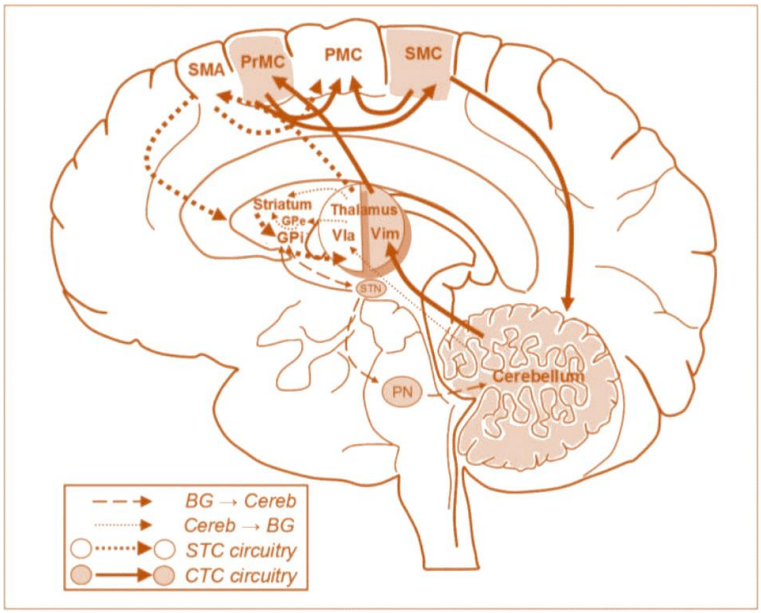

Figure 3. A conceptual framework for considering striatal-thalamo-cortical and cerebello-thalamo-cortical circuits. (from (Lewis et al. 2013))

1.3 α-synuclein and PD

α-synuclein is a small soluble protein encoded by the SNCA gene, with a molecular weight of 19 kDa, consisting of 140 highly homologous amino acids (Maroteaux, Campanelli, and Scheller 1988).

It has been previously suggested that a-synuclein is connected to PD pathogenesis via toxic gain-of-function and cytotoxicity rather than loss of function. Abeliovich *et al.* conducted with α-synuclein knockout mice, and the results showed that no such differences were observed between the structures of neurons and synaptic terminals in the α-synuclein-deficient mice and those in the normal mice. Although they showed some defects in the nigrostriatal dopamine pathway, they did not show any abnormalities or PD features (Abeliovich et al. 2000). A study from Stefanis further demonstrated that both the oligomeric and fibrillar species of α-synuclein are currently considered to be cytotoxic (Stefanis 2012). It was found that there is a dynamic balance between normal and misfolded α-synuclein and its oligomerization. When this balance is disturbed, the protofibrils rapidly aggregate into large, insoluble, fine fibers. Any factor that upsets this balance is disruptive and plays a key role in the development of PD (Mehra, Sahay, and Maji 2019; Gadhe et al. 2022).

The aggregation of α-synuclein can cause endoplasmic reticulum (ER) stress, ultimately leading to cell death. The ubiquitin-proteasome system (UPS) is an intracellular protein quality control system that selectively transports misfolded or denatured proteins to the proteasome in the cytoplasm for degradation (Omura et al. 2006). In this ER system, which is termed ER-associated degradation (ERAD), unfolded proteins are initially retrotranslocated from the endoplasmic reticulum to the cell membrane via transposition, polyubiquitinated by ubiquitin-binding enzymes (E2), ubiquitin ligases (E3), and other components. The ubiquitinated proteins are usually degraded by the 26S proteasome complex, which relies on ATP hydrolysis to function (Hershko and Ciechanover 1998). Cooper et al. found that the accumulation of α-synuclein impairs the degradation of ERAD substrates, leading to the accumulation of misfolded proteins in the ER and the associated ER stress. Apart from this, Cooper et al. also found that the yeast expressing the α-synuclein gene showed early impairment of ER to Golgi vesicle transport and that overexpression of Rab1 resisted the dopaminergic neuron loss caused by α-synuclein in animal models of PD (Cooper et al. 2006).

Mutations and changes in SNCA were suggested to impact mitochondrial function via a decrease in ATP production, mitochondrial fragmentation, and mitochondrial biogenesis. A study from Arias-Fuenzalida et al. showed that SNCA mutant neuroepithelial stem cells (NESCs) reduced energy performance including, lower ATP production and non-mitochondrial respiration, which indicates that SNCA mutant present in mitochondrial impairment (Arias-Fuenzalida et al. 2017). Another study by Nakamura et al. found that overexpression of SNCA in mammalian cells can cause mitochondrial fragmentation. The effect is specific to mitochondria, with no morphological changes in other intracellular organelles or mitochondrial membrane potential (Nakamura et al. 2011). The fragmentation does not rely on the major mitochondrial fission protein dynamin-related protein 1 (Drp1). Other than effects on mitochondrial morphology, a study from Ryan et al. showed that α-synuclein can reduce mitochondrial biogenesis by down-regulating peroxisome proliferation-activating receptor gamma coactivator 1-α (PGC1α) (Ryan et al. 2013). Furthermore, overexpression of α-synuclein binds to the inner mitochondria membrane (IMM), inhibiting the function of mitochondrial complexes I (MCI) and increasing the production of reactive oxygen species (ROS) (Devi et al. 2008). Consistent with these findings, the N-terminal structural domain of α-synuclein is associated with MCI and interferes with its functions (Devi et al. 2008; Borsche et al. 2021).

Another study showed that extracellular α-synuclein is involved in glycogen synthase kinase-3β (GSK-3β) -dependent Tau hyperphosphorylation, leading to microtubule destabilization. Further, this leads to impairment of cytoskeleton stability (Gąssowska et al. 2014). In addition, α-synuclein can affect cytoskeletal stability by inhibiting phospholipase D2 activity (Jenco et al. 1998) and binding to synphilin-1 (Engelender et al. 1999).

Apart from that, α-synuclein also can regulate vesicle release from synaptic membranes (Murphy et al. 2000; Cabin et al. 2002), and inhibit dopamine synthesis and the release of dopamine neurotransmitters (Masliah et al. 2000; Baptista et al. 2003). α-synuclein inhibits dopamine synthesis by suppressing tyrosine hydroxylase (TH) expression and activity, which may be achieved by reducing the phosphorylation state of TH and stabilizing dephosphorylated inactive TH (Lou et al. 2010; Wu et al. 2011).

In short, various pieces of evidence suggest that the misfolding and aggregation of α-synuclein interact with the abnormal function of various organelles, including mitochondrial dysfunction, lysosomal function, and ER stress, et al. Therefore, multiple cellular processes are suspected to be involved in PD via α-synuclein, as summarized in Figure 4.

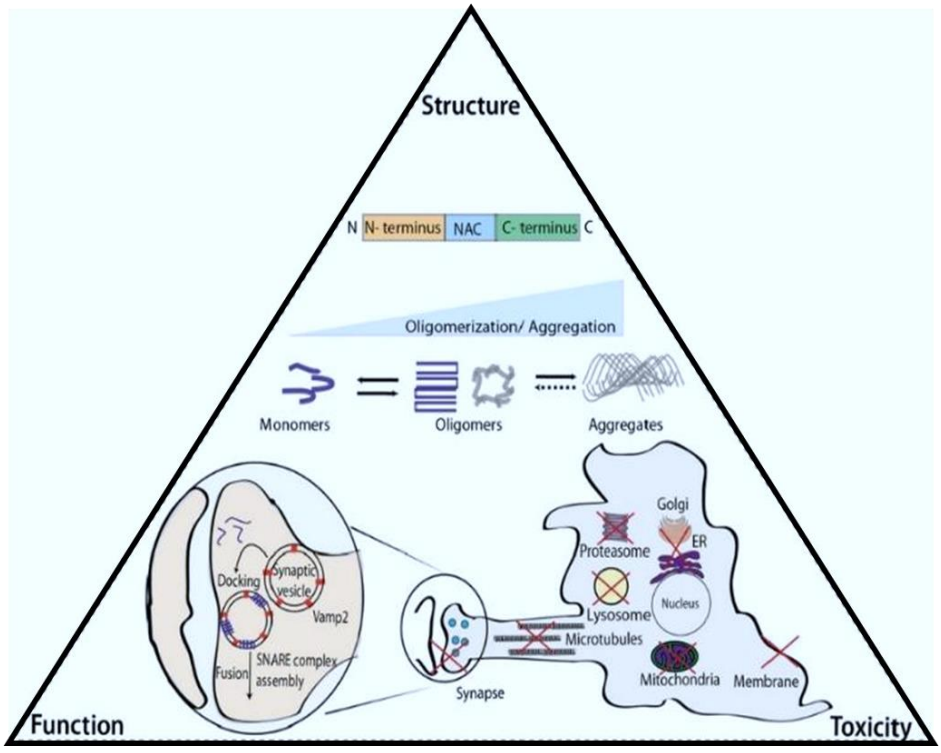

Figure 4. The triangle between a-syn structure, function, and toxicity. (from (Villar-Piqué, Lopes da Fonseca, and Outeiro 2016), with permission from Wiley)

1.4 Mitochondrial dysfunction in PD

Mitochondria are considered to be the 'powerhouse' of the cell (Franco-Iborra, Vila, and Perier 2016). Its primary function is to provide energy to the cell through adenosine triphosphate (ATP). It has been found that most inherited PD loci are directly linked to mitochondria, which implies that mitochondrial dysfunction is a central factor in the pathogenesis of both sporadic and familial PD (Borsche et al. 2021).

1.4.1 Oxidant stress and MCI dysfunction in PD

Mitochondria produce about 90% of cellular ROS, making oxidative stress closely related to mitochondrial function (Perfeito, Cunha-Oliveira, and Rego 2012). Loss of MCI in dopaminergic neurons is a hallmark of PD, which is mainly caused by the abnormal α-synuclein and toxins at the level of the electron transport chain (Wright 2022), and this, in turn, drives ROS production (Mullin and Schapira 2013). The auto-oxidation of dopamine can also produce free radicals and active quinones (LaVoie and Hastings 1999) that elevate mitochondrial oxidant stress. Studies have shown that inhibition of MCI by rotenone, 1-methyl-4-phenyl-1,2,3,6-tetrahydropyridine (MPTP), or paraquat poisoning leads to iron accumulation associated with PD (Muñoz et al. 2016). Similarly, inhibition of the UPS can lead to an imbalance in cellular iron homeostasis, which further induces positive feedback on ROS generation and α-synuclein aggregation (Le 2014).

Mitochondrial-derived ROS have been noted as significant contributors to inflammation by offloading danger signals into the intra- or extracellular compartments in response to stressors (Grazioli and Pugin 2018; Pérez-Treviño, Velásquez, and García 2020). These molecules that can cause inflammation are collectively referred to as damage-associated molecular patterns (DAMPs) and are sensed through pattern recognition receptors (PRRs) (Riley and Tait 2020). mtDNA can act as a DAMP molecule to trigger inflammation (West et al. 2015). Neuroinflammation and mitochondrial dysfunction are closely linked. Dysfunctional organelles may induce inflammation, leading to further mitochondrial damage and releasing of large amounts of mitochondrial DAMPs. Mitochondrial dysfunction may establish a vicious cycle through ROS signaling (Picca et al. 2020; Al Amir Dache et al. 2020).

1.4.2 Mitochondrial dynamics and mitophagy in PD

Many causal/risk mutations for PD occur in genes linked to mitochondrial dynamics and clearance (mitophagy), such as DJ-1, PARKIN, PINK1, etc.

Mitochondria are complex and highly dynamic cellular organelles that undergo frequent fission and fusion in a dynamically balanced manner within a cell. The repetitive cycles of fission and fusion regulate mitochondrial morphology, distribution, and function (X. Zhang et al. 2019). Mitochondrial fission occurs before mitophagy. Inhibiting mitochondrial fission can reduce mitophagy. Drp1 is a fission protein that can lead to mitochondrial fission when it is overexpressed. Studies show that inhibiting Drp1- mediated mitochondrial fission plays a neuroprotective role in the PD model (Losón et al. 2013; Osellame et al. 2016). Researches show that the VPS35 mutation can trigger mitochondrial fission, and the increase in mitochondrial fragmentation caused by the VPS35 mutation exhibited an impaired configuration of MCI (Zhou et al. 2017; Wang et al. 2016). Similarly, DJ-1, LRRK2, PARKIN, and PINK1 are all involved in regulating mitochondrial dynamics.

It is established that PARKIN is intimately involved in many aspects of mitochondria, such as it can affect mitochondrial homeostasis by regulating their biogenesis and degradation via mitophagy (Scarffe et al. 2014; Palacino et al. 2004). Similar to PARKIN, PINK1 also affects various aspects of mitochondrial function, including mitophagy, mitochondria morphology, trafficking, and diminished MCI activity (Morais et al. 2014; Geisler et al. 2010). Of all the functions of PINK1, the most studied is the function of mitophagy, promoting clearance of damaged mitochondria through the recruitment and activation of Parkin (Gladkova et al. 2018). Normally, Parkin is scattered in the cytosol. In the early stages of mitophagy, PINK1 bound to translocase of outer membrane (TOM) complex proteins and autophosphorylated to promote rapid recruitment of E3 ubiquitin ligase PARKIN from the cytosol to the damaged OMM, leading to the ubiquitination of OMM proteins and subsequent proteasomal degradation (Figure 5) (Shiba-Fukushima et al. 2012; Wauer et al. 2015).

Mitofusins (MFN1 and MFN2) are located in the outer mitochondrial membrane (OMM) and mediate OMM fusion (Frezza et al. 2006). PINK1-mediated phosphorylation of MFN2 may be involved in PINK1-PRKN-mediated mitophagy by directly recruiting PARKIN to mitochondria. Optic atrophy 1 (OPA1) is located in the IMM and mediates IMM fusion. OPA1 can protect from

apoptosis by decreasing the release of cytochrome c. (Stafa et al. 2014). The decreasing cytochrome c release further prevents mitochondrial dysfunction and reduces the loss of mitochondrial membrane potential.

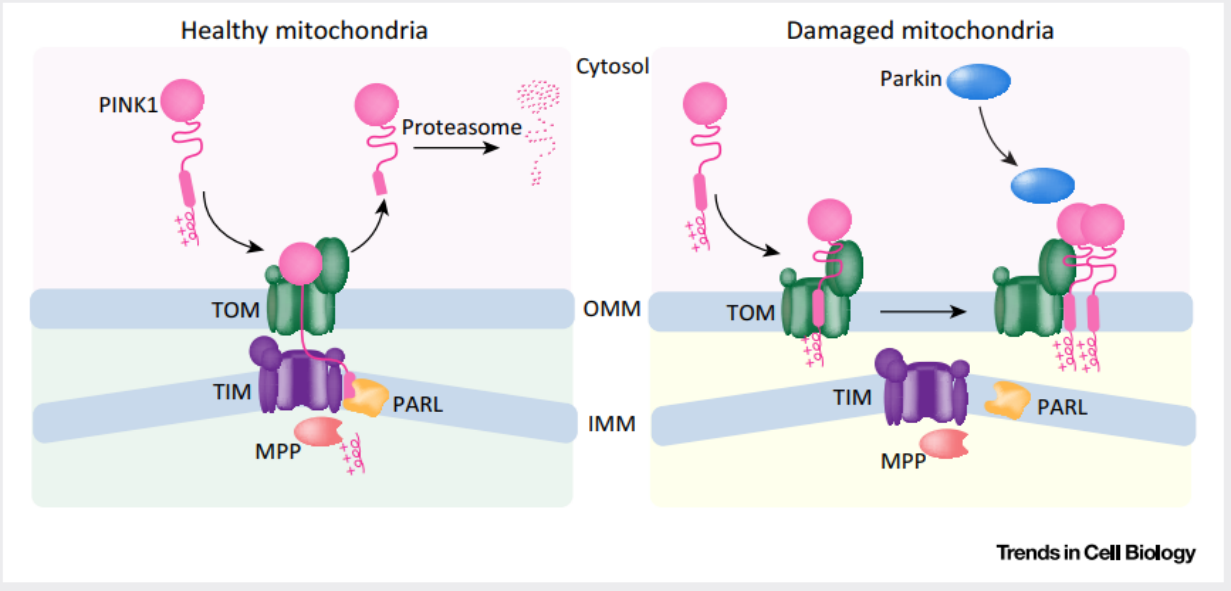

Figure 5. PINK1 imports mechanisms into healthy and damaged mitochondria. (from (Nguyen, Padman, and Lazarou 2016), with permission from Elsevier)

1.5 Lysosomal dysfunction in PD

Mutations in GBA, which encodes lysosomal hydrolase enzyme glucocerebrosidase (GCase) are the most important genetic risk factor for PD (Sidransky et al. 2009).

GBA mutations result in misfolded GCase proteins retained in the ER and fail to translocate to the lysosome. A persistent lack of GCase activity in the lysosome further leads to lysosomal dysfunction and subsequent impairment of the autophagy-lysosome pathway (ALP) (Blumenreich et al. 2020). The deficiency of GCase results in catalytic lipid substrate accumulation, thus hindering the transport of newly synthesized GCase from ER/Golgi to lysosomes, aggravating lysosomal dysfunction. As a result of the impairment of ALP, aggregation of α-synuclein may be induced. In addition, deficiency of GCase is also associated with oxidative stress, reduced ATP production, abnormal mitochondrial morphology, and neuroinflammation.

1.6 ER stress in PD

ER-to-mitochondrial calcium transport is vital for the pathology of PD. ER is considered the major calcium storage organelle in the metazoan cell. Alteration of Ca^{2+} homeostasis in ER can disrupt protein folding, accumulating misfolded proteins and initiating UPR. Evidence supports that misfolded protein in ER can cause Ca^{2+} release and transport to mitochondria (Kaufman and Malhotra 2014). Calcium transport from ER to mitochondrial results in the Ca^{2+} accumulation in mitochondrial, further stimulating mitochondrial respiration and ATP production and promoting ROS generation. The increased level of intracellular ATP inhibits the activation of AMP-activated kinase (AMPK). Inhibition of AMPK, in turn, increases the activity of the mammalian target of rapamycin (mTOR), which is a well-known autophagy inhibitor. In short, the Ca^{2+} accumulation in mitochondria suppressed autophagy in the end.

The degree of ER stress may correlate with the severity of PD. A growing body of evidence from cellular and animal models suggests that the accumulation of misfolded proteins in ER can induce ER stress, leading to unfolded protein response (UPR) (Fernandes et al. 2016). Studies from yeast show that ER stress can also induce autophagy. The possible mechanisms underlying the link between ER, lysosomal and mitochondrial dysfunction, α-synuclein, and PD are shown in Figure 6.

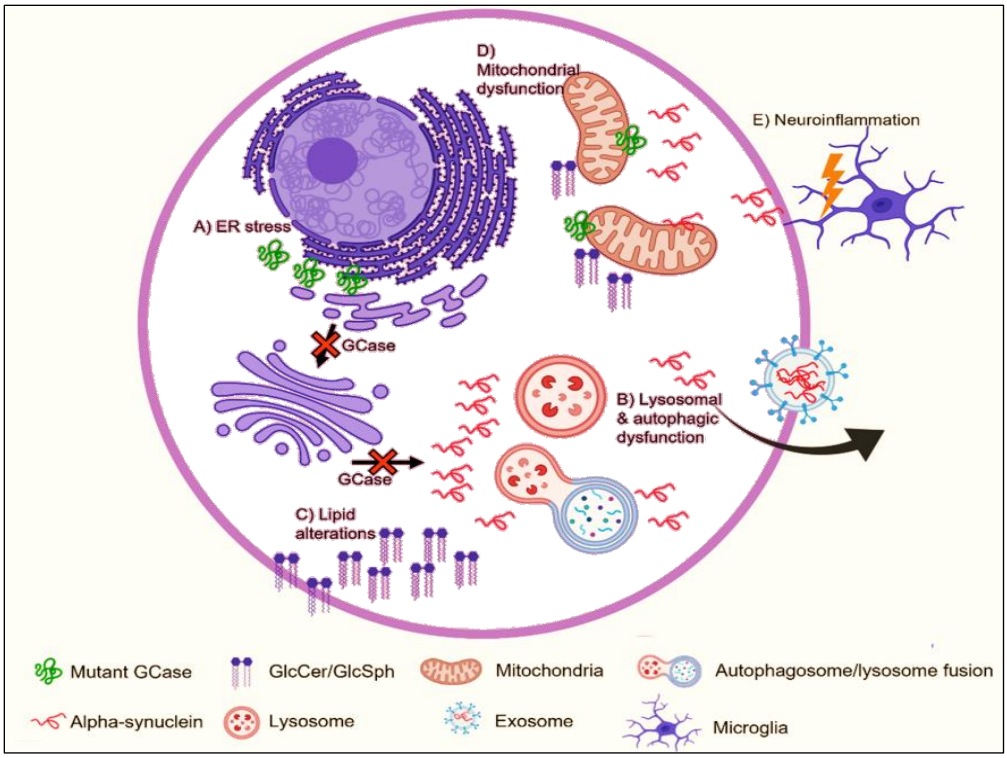

Figure 6. Possible mechanisms underlying the link between GCase, α-synuclein, and PD. ((Smith and Schapira 2022)(Smith and Schapira 2022)

1.7 Therapeutic strategies

As mentioned before, the symptoms of PD are mainly divided into motor symptoms and non-motor symptoms, so different therapy approaches are produced according to the different symptoms.

1.7.1 Treatment for motor symptoms

The mechanism of motor symptoms in PD is striatal dopamine depletion caused by the loss of dopaminergic neurons in the SNpc. The administration of levodopa to substitute striatal dopamine was a breakthrough in the treatment of PD, and since then, multiple additional targets for dopaminergic therapies have been identified (Radhakrishnan and Goyal 2018). Levodopa is considered a gold standard therapy, and most patients with PD require levodopa therapy within two years of symptom onset.

Although levodopa is the most efficient medicine for PD treatment, it also has some complications, such as levodopa-related motor complications. Concern about the complications, many patients

and doctors choose to start using levodopa therapy very carefully. There are also other disadvantages of levodopa, including erratic drug delivery due to the short half-life of levodopa, as well as variability in its absorption and blood-brain barrier transportation (Poewe and Antonini 2015). More effective oral formulations and innovative administration routes were developed to improve the absorption and bioavailability of levodopa. The research demonstrates that carbidopa being co-administered with levodopa can increase its bioavailability, prolong its efficacy, and promote levodopa's tolerability (Tambasco, Romoli, and Calabresi 2018). Oral levodopa inhibitors include IPX066, DM-1992, XP21279, ODM-101, et al. Levodopa-carbidopa intestinal gel (LCIG) is an intestinal-delivered drug approved for patients with advanced PD. It reduces L-dopa-plasma level fluctuations and decreases motor complications (Poewe and Antonini 2015).

To treat PD-related motor symptoms, many other types of medications are also available apart from levodopa. For instance, anticholinergics, amantadine, monoamine oxidase inhibitors (MAOIs), catechol-O-methyl transferase inhibitors (COMTIs), and dopamine agonists can be used.

Anticholinergics can antagonize acetylcholine to reduce the effect of muscarinic receptors postsynaptic to striatal interneurons. They are predominantly used to reduce tremors. However, anticholinergics have various adverse effects, such as cognitive impairment, confusion, blurred vision, and urinary retention, which limit their use in treating PD.

Amantadine, with both anti-glutamatergic and anti-cholinergic properties, has been shown to alleviate movement disorders. The most common side effects were visual hallucinations, peripheral edema, and dizziness. COMTIs include entacapone, tolcapone, and opicapone, which can block the peripheral degradation of dopamine. Thus, these drugs enhance the bioavailability of levodopa preparations.

Dopamine receptor agonists mainly target D2-like and D1-like dopamine receptor families. The most commonly used dopamine agonists in clinical practice are non-ergot dopamine agonists. The side effects of dopamine agonists are sleepiness, nausea, and hallucinations, making it essential to use the medication cautiously, especially in elderly patients.

1.7.2 Treatment for non-motor symptoms

The non-motor symptoms mainly include cognitive impairment, emotional problems such as depression, dementia, sleep disturbances, levodopa-induced dyskinesias, and so on. All these require treatment with non-dopaminergic agents.

Almost all types of antidepressant medications work on depression symptoms in patients with PD, for example, tricyclic antidepressants, mirtazapine, trazodone, and quetiapine. Antidepressant medications supplemented with hypnotics can be a strategy to improve sleep problems if needed. Dementia due to PD is caused by the degeneration of cholinergic neurons. Rivastigmine and Donepezil are cholinesterase inhibitors that can be used to treat PD-associated dementia. In addition to improving cognitive function, cholinesterase inhibitors may reduce hallucinations, improve postural stability, and even reduce the frequency of falls in some patients (Henderson et al. 2016).

1.7.3 Other treatment methods

Deep brain stimulation (DBS) is a well-known PD surgical treatment. The central role positions of DBS are the thalamus, globus pallidus, and subthalamic nucleus (STN) (Church 2021). The critical advantage of DBS is that the stimulation parameters can be adjusted as the disease progresses to optimize the benefits (Jankovic and Tan 2020). This treatment is mainly used for advanced PD patients.

Cell replacement therapy for PD initially used fetal tissue-derived cell transplants in 1987. The ethical concerns and limitations to cell survival after preservation restricted the clinical applicability of fetal transplantation. In 2010, human embryonic stem cells (hESCs) were first used to treat spinal cord injury (Lebkowski 2011)(Lebkowski 2011). Since then started stem cell-derived products therapy era. In 2018, the first human trial used induced pluripotent stem cells (iPSCs) as a cell source to treat PD (Doi et al. 2020). Compared to the previous cell therapy, iPSCs do not need to use human embryos, removing the ethical issues in stem cell therapy. Primate studies have already demonstrated significant improvements after transplanting human iPSCs-derived dopaminergic progenitors into the non-human primate model of PD (Kikuchi et al. 2017). However, we still have to look at iPSC therapy in a dialectical way. Although it has many advantages, problems such as possible tumor formation and the success rate of implantation still need to be studied in more depth. The steps required for patient-specific transplantation of iPSCs are outlined in Figure 7.

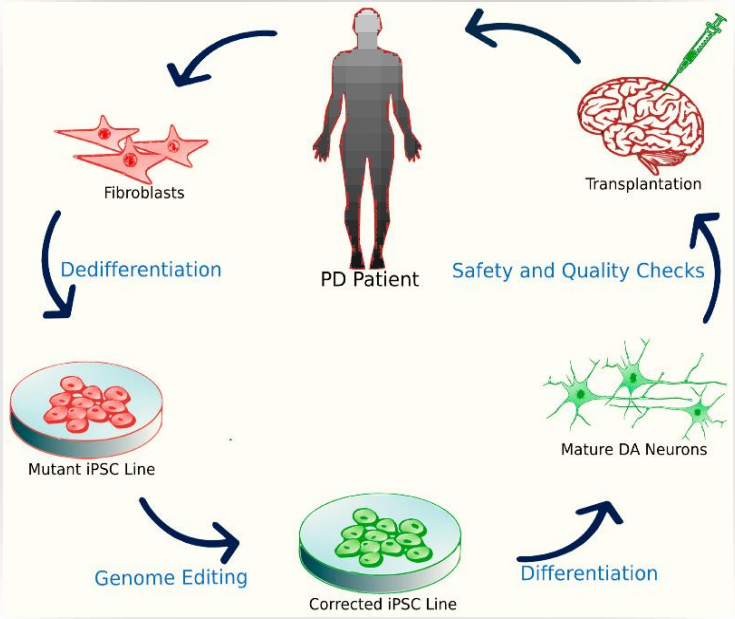

Figure 7. iPSC transplantation. First, fibroblasts are obtained from a patient afflicted with familial PD. Researchers express major reprogramming transcription factors to establish a mutant iPSC line. The significant mutation is corrected Using ZNF/TALEN or CRISPR/Cas9 technology, and then the line is differentiated into mature or progenitor DA neurons in xeno-free conditions. After sufficient quality assurance, the differentiated cells can be used for clinical trials. (from (Stoddard-Bennett and Reijo Pera 2019))

2. Objectives and background of this study

2.1 Objective of this study

With the development of genomics and its application in PD, more and more PD-related genetic studies are emerging. The familial PD pathogenic genes are now well established, but there is still no comprehensive study of the genes responsible for sporadic PD. Identifying risk loci associated with PD in the European and Asian populations is a breakthrough for studying sporadic PD. However, the associated SNPs from GWAS identify the genomic loci associated\linked with a genetic risk variant but do not identify the PD causal variants themselves. Under each association peak several genes can be located and considered candidate genes including coding and non-coding variants. Thus, the identification of the causal genes is challenging. For this reason, research into the causative genes of sporadic PD is essential.

A complete list of candidate genes was generated in our lab after determining the associated genomic region flanking the associated SNP based on linkage disequilibrium calculations, followed by determining the genes located in these 78 risk loci (Nalls et al. 2019; Foo et al. 2020). Our mission is to identify causal risk genes for sporadic PD and to demonstrate which changes in the function or regulation of these genes lead to altered disease risk by performing functional assays. The workflow of this study is shown in Figure 8.

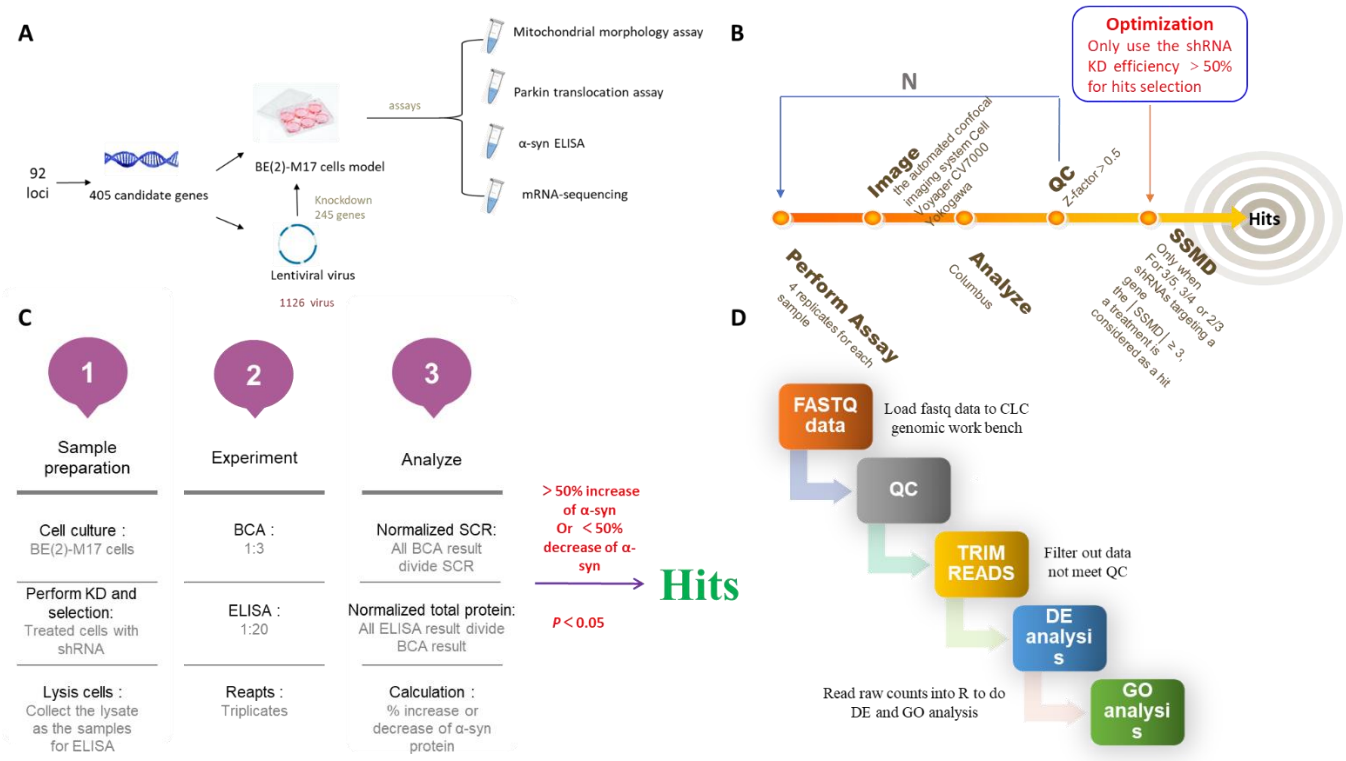

Figure 8. The experiment design and workflow. BE(2)-M17 cell model was used in this project. From 405 candidate genes associated with the 92 risk variants, 245 genes are expressed in BE(2)-M17. We designed 3 - 5 shRNA for each gene to perform knockdown (KD). After KD the 245 candidate genes one by one, the mRNA sequencing and the functional assays such as mitochondrial morphology assay, Parkin translocation assay, and α-synuclein ELISA were performed. The design flow of the experiment is shown schematically in Graph A. The experimental flow for mitochondrial morphology assay and Parkin translocation assay is shown in Graph B. The experimental flow for α-synuclein ELISA and mRNA sequencing are shown in Graphs C and D, respectively.

2.2 Background of this study

405 protein-coding and non-protein-coding elements had been identified as targets by using bioinformatics. We use BE(2)-M17 cells as the cellular model and a genome-wide lentiviral library for shRNA-based knockdowns. A total of 245 targets are expressed in BE(2)-M17 cells and have shRNAs available in our Mission shRNA library (from Sigma). After performing gene knockdown, several microscopic, biochemical, and transcriptomic assays were performed. According to the available literature, mitochondrial dysfunction, lysosomal dysfunction, and α-synuclein misfolding have an essential role in the pathogenesis of PD (Chen, Li, and Liu 2020). In this study, we investigated the effect of candidate genes on the change of mitochondrial dynamics on PD by

performing mitochondrial morphology assay and Parkin translocation assay, and the effect of candidate genes on α-synuclein proteins level by performing α-synuclein enzyme-linked immunosorbent assay (ELISA). In addition, we performed mRNA sequencing to determine the knockdown efficiency and the effect of gene knockdown on molecular pathways to learn more about potential novel PD-relevant pathways. Furthermore, we may be able to establish additional assays based on the findings we get from the mRNA sequencing.

Based on the 90 risk variants associated with PD in the European population and 2 risk variants from the Asian population identified by Nalls et al. and Foo et al. (Nalls et al. 2019; Foo et al. 2020). Linkage disequilibrium (LD) blocks were calculated based on the variant allele frequency of the 1000G project European population. The maximum R2 to be considered in LD with the sentinel SNP was 0.2. Coordinates of most left and most right SNPs were used to intersect with gene code annotation to obtain the final gene list.

Considering establishing a cell model to study the role of these 405 candidate genes for PD, we tried to find a cell line that was as suitable as possible for our experimental requirements. To accomplish this, we first selected three cell lines as candidate cell lines, which were BE(2)-M17 cell line, SH-SY5Y cell line, and HEK293T cell line. Among these candidate cell lines, we comprehensively considered the number of candidate genes expressed by each candidate cell line, whether there are available shRNAs for each candidate gene, whether they expressed SNCA, and whether their mitochondrial morphology was easy for image analysis. In the end, the BE(2)-M17 cell line was chosen as the cell model for this study due to expressing more candidate genes (245 genes) and having a mitochondrial morphology that was easier to image and analyze. A recent study showed that BE(2)-M17 was shown to have a better dopaminergic phenotype and was more suitable as a cellular model for *in vitro* studies of PD compared to the SH-SY5Y cell line (Carvajal-Oliveros et al. 2022).

After cell line selection, we designed 1126 shRNAs to perturb the expression of candidate genes, with a range of 3-5 shRNAs targeting each gene. In this experiment, the mitochondrial morphology assay and Parkin translocation assay were performed using all 1126 shRNAs targeting the 245 candidate genes. To know the knockdown (KD) efficiency, we design a real-time quantitative polymerase chain reaction (RT-qPCR) experiment. According to the result of RT-qPCR, we finally identified 195 candidate genes with a good KD efficiency (＞50%) and further focused on those.

In the end, we only include genes with good KD efficiency to do data analysis for mitochondrial morphology assay and Parkin translocation assay and use the most efficient KD shRNA to perform α-synuclein ELISA and mRNA sequencing. The research status of the identified 78 PD risk loci in this study is shown in Figure 9.

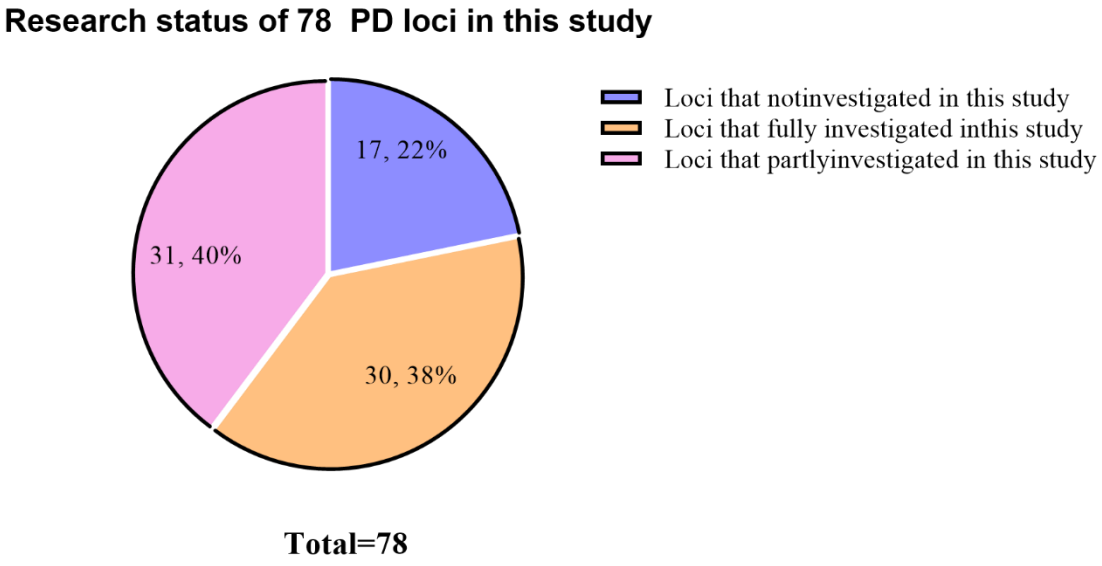

Figure 9. The overview of the research status of 78 PD loci in this study. Nalls et al. and Foo et al. identified 92 independent genome-wide significant risk variants across 78 loci. This study thoroughly investigated the candidate genes located in 30 loci. We partly investigated the candidate genes located in 31 loci, and 17 loci were not investigated because the candidate genes on these loci are not expressed in BE(2)-M17 cell model or no available shRNA library.

3. Materials and methods

3.1 Short hairpin ribonucleic acid (shRNA) virus production

3.1.1 Plasmid production

Bacterial glycerol stocks containing the shRNA vectors (Sigma, St. Louis, MO, USA; TRC1 and 1.5) were grown overnight in lysogeny broth (LB) (L3022, Sigma) media containing 100 μg/mL of ampicillin (AMP) (A9518, Sigma-Aldrich). At least three shRNA clones per gene were selected. Endotoxin-free shRNA plasmids were extracted according to the manufacturer's instructions (ZR Plasmid Miniprep Classic kit, Cat. No. D4054). For lentiviral production, the packaging plasmid (psPAX2, Addgene 12260) and envelope plasmid (PMD2.G, Addgene 12259) were prepared using the Giga prep instructions (Qiagen). EpMotion 5075 (Eppendorf) automated system was used to normalize the shRNAs plasmid preparations before they were used for virus production. All isolated plasmids were stored at −20 °C before use.

3.1.2 Lentivirus production

HEK293T (ATCC® CRL-11268™) packaging cells were seeded at a density of 2 - 2.5×10^5/mL (200 μL per well) in cell culture media Opti-MEM (Cat. No. 31985054, Thermo Fisher) containing 10% fetal bovine serum (FBS) in 96-well cell culture plates (Cat. No. 655180, Greiner bio one). Cells were incubated in the incubator (Thermo Fisher) for 24 h (37 °C, 5%CO_2) to ensure wells were 50% -70% confluent. For each transfection, the mixture was prepared with 100 ng of shRNA plasmid, 90 ng of packaging plasmid, and 10 ng of envelope plasmid combined with 0.6 μL of Fugene HD (E2312, Promega) in a total volume of 10 μL. Incubate the mixture for 5 min, add to well, and mix by tapping. Transfection efficiency was monitored using the green fluorescent protein (GFP) plasmid and had to be greater than 80% after 24 h transfection. Forty-eight hours after transfection, collect supernatant, store at 4°C, add fresh media (200 μL Opti-MEM + 10%FBS), and supernatant harvested after a further 24 h. Aliquot virus and freeze at −80 °C.

To ensure successful lentivirus production, HEK293T has been passaged at least twice before virus production and no more than 15 times, and cells were rapidly dividing and have not been passaged too densely or sparsely.

3.2 Neuroblastoma cell culture

BE(2)-M17 (ATCC® CRL-2267™) neuroblastoma cell line was cultured in cell culture media Dulbecco's Modified Eagle Medium F-12 Nutrient Mixture (DMEM/F-12), HEPES (Cat. No. 31330095, Thermo Fisher) supplemented with 10% FBS, and 1% penicillin/streptomycin (P/S) (Cat. No. 15140122, Thermo Fisher).

The genetically modified BE(2)-M17 line stably overexpressing N-terminally tagged eGFP-Parkin was used, which was created using the plasmid pLVX-TIGHT-PUR-EGFPnFusPARK2. The BE(2)-M17 eGFP-Parkin cell line was cultured in DMEM/F-12, HEPES -10% FBS media +1% P/S and 4 μg/mL puromycin (P8833, Sigma-Aldrich).

All cell lines were routinely tested for mycoplasma contamination. For lentivirus infection, 20 μL of the lentivirus and 8 μg/mL protamine sulfate (P-3369, Sigma-Aldrich) were added to each well of a 96-well plate.

3.3 Cell-based screening assays

3.3.1 Mitochondrial morphology assay

Mitochondrial morphology assay (Koopman et al. 2006) was performed with BE(2)-M17 cell line. Thaw cells in cell culture media DMEM/F-12, HEPES- 10% FBS media +1% P/S. Passage and bulk twice before using cells for screenings to allow the cells to recover. In this assay, eight replicates of the negative control and positive control groups were used. In the negative control group, the cells were treated with scramble shRNA. In the positive control group, the cells were treated with OPA1 shRNA. Each sample was repeated four times.

On day 1, seed 5 000 BE(2)-M17 cells in CellCarrier- 96 ultra microplates (6055302, PerkinElmer), 150 μL per well with DMEM/F-12, HEPES-10%FBS media + 8μg/mL of protamine sulfate, 1% of P/S. Incubate for 2-3 h and add 20 uL of lentivirus. On day 4, refresh cell culture media with DMEM/F-12, HEPES-10%FBS media +4 μg/mL of puromycin and 1% of P/S. On day 6, cells were labeled with 100 nM MitoTracker™ Red CMXros (M7512, Thermo Fisher), 100 nM MitoTracker™ DeepRed (M22426, Thermo Fisher), and 1 μg/mL Hoechst (H3570, Thermo Fisher) in DMEM/F12, HEPES-10%FBS media +4 μg/mL of puromycin and 1% of P/S and incubated 20 min (37 °C, 5%CO_2). Refresh media (DMEM/F-12, HEPES-10%FBS media +4 μg/mL of

puromycin and 1% of P/S) without dyes and incubate cells for a further 2 h, afterward wash with Dulbecco's Phosphate Buffered Saline (DPBS) (Cat. No.14190-094, Thermo fisher) and fix with 4% paraformaldehyde (PFA) (Cat. No. 28908, Thermo Fisher) for 20 min. After fixation, wash cells 3 times with DPBS, seal them, and store at 4°C until they are imaged.

3.3.2 Parkin translocation assay

The Parkin translocation assay was performed with the BE(2)-M17 eGFP-Parkin cell line (BE(2)-M17 neuroblastoma cells stably expressing Parkin-GFP). The stable cell line is a slow-growing cell line but can be passaged at least 6 times without loss of morphology and increased growth rate.

Thaw cells in DMEM/F-12, HEPES - 10% FBS media + 4 μg/mL of puromycin and 1% of P/S. Passage and bulk twice before using cells for screenings to allow the cells to recover. In this assay, eight replicates of the negative control and positive control groups were used. In the positive control group, cells were treated with scramble shRNA. In the negative control group, cells treated with carbonyl cyanide m-chlorophenyl hydrazine (CCCP) were transduced with scramble shRNA. Each sample was repeated four times.

On day 1, BE(2)-M17 eGFP-Parkin cells were plated out at a density of 1 × 10^5 cells/mL (100 μL per well) in DMEM/F-12, HEPES - 10% FBS media+ 4 μg/mL of puromycin + 8μg/mL of protamine sulfate and 1% of P/S in CellCarrier- 96 ultra microplates. Incubate the cells for 2 - 3 h to allow the cells to settle before transducing the cells with 20 μL of lentivirus. On day 3, replace with 200 μL media (DMEM/F-12, HEPES - 10% FBS media + 4 μg/mL of puromycin and 1% of P/S). On day 5, cells were incubated with 100 nM MitoTracker™ Red CMXros, 100 nM MitoTracker™ DeepRed, and 1 μg/mL Hoechst in DMEM/F12, HEPES-10%FBS media +4 μg/mL of puromycin and 1% of P/S and incubated 20 min. After 20 min, refreshed media (DMEM/F-12, HEPES - 10% FBS media + 4 μg/mL of puromycin and 1% of P/S) containing 15 μM CCCP. Cells were incubated for 5 h with CCCP. Five hours later, fix cells with 4% PFA and incubate for 20 min. Wash Cells afterward 3 times with DPBS, seal, and store at 4°C until they are imaged.

3.3.3 Data processing and analysis

Cell-based screening mitochondrial morphology assay and Parkin translocation assay were carried out on the automated confocal imaging system Cell Voyager CV7000 (Yokogawa, Tokyo, Japan).

In the mitochondrial morphology assay, 82 fields per well were captured using the 60X water immersion objective lens for higher resolution. The 405 nm laser was used for image nuclei, the 561 nm laser was used for image MitoTracker™ Red CMXros. In the Parkin translocation assay, 25 fields per well were captured using the 20X objective lens. The 405 nm laser was used for image nuclei, the 488 nm laser was used for image Parkin-GFP, and the 561 nm laser was used for image MitoTracker™ Red CMXros.

Columbus Image Data storage (PerkinElmer, Waltham, MA, USA) ("Updated Version of Image Data Storage and Analysis System. - Free Online Library" n.d.) was used for storing and analyzing the images. The criteria for image quality control are as follows: only include well-segmented cells, exclude poorly segmented, apoptotic, out-of-focus cells, incompletely captured cells, for example, cells touching the border of the image as well as exclude the strong perturbation decreased cell number wells. Cell nuclei were segmented based on the Hoechst staining using "Find nuclei" method C. Segmented nuclei were classified into four sub-populations based on nuclear size and roundness, allowing to differentiate between single nuclei and multiple nuclei being too close to each other impairing successful segmentation of single nuclei. This resulted in a more precise nuclei count. For analyzing the mitochondrial morphology assay, the mean of axial length ratio was calculated to quantify mitochondrial morphology. For analyzing the Parkin translocation assay, the nuclei were segmented as described above, the spots in these cells were detected using method C, and the number of spots formed on mitochondrial was calculated to distinguish between CCCP-treated cells, and untreated cells, cells containing 2 or more than 2 sports were considered positive for Parkin translocation. The ratio of cells positive for translocation versus the number of cells negative for translocation was calculated per well to give a cell number independent measure of Parkin translocation. All results are exported to Excel for analysis. Data was normalized against the negative controls on a per-plate basis to minimize variation between plates.

3.3.4 Hit selection and statistical analysis

Plate-to-plate quality control (QC) for each assay was assessed by calculating the Z-factor using the normalized values for the controls from all plates. The Z-factor is defined in terms of four parameters: the mean (μ) and standard deviations (SD, σ) of both the positive (p) and negative (n)

controls (μ_p, σ_p, μ_n, σ_n). The formula of Z-factor is Z-factor$=1-\frac{3(\sigma p+\sigma n)}{|\mu p-\mu n|}$. The interpretations for the Z-factor are shown in Table 1 (J. H. Zhang, Chung, and Oldenburg 1999). The cut-off for Z-factor is 0.5. Plates with a Z-factor $\geqslant$0.5 were included for further analysis. For each of the shRNA screenings, data were analyzed using T-tests with false discovery rate (FDR) correction ($P<0.05$, FDR$<$0.05).

For each of the shRNA screenings, each assay plate was completed with 4 replicates to enable the detection of subtle effects and minimize false negatives. For each shRNA, the robust strictly standardized median difference (SSMD) (X. D. Zhang 2011) was calculated for hit selection. SSMD is the mean of differences divided by the standard deviation of the differences between a KD sample and a negative reference. The interpretations for the SSMD are shown in Table 2.

We used the following criteria for hit selection:

- The effects of the shRNAs can be positive or negative, but the effects of the shRNAs targeting the same gene fulfilling the criteria below have to be in the same direction.

- Three out of five shRNAs, or two out of three shRNAs, or both shRNAs, if only two shRNA were used for screening, must have very high effects (SSMD $\geqslant$ 3 or $\leqslant$-3).

Effects were considered significant when the SSMD normalized effect of shRNA treatment satisfied the criteria above.

Table 1. The interpretation of Z-factor.

Z-factor	Interpretation
1.0	Ideal. Z-factors can never exceed 1.
0.5-1.0	An excellent assay.
0-0.5	A marginal assay.
less than 0	There is too much overlap between the positive and negative controls for the assay to be useful.

Table 2. The interpretation of SSMD.

SSMD	Interpretation
$\lvert SSMD \rvert \geq 5$	extremely strong
$5 > \lvert SSMD \rvert \geq 3$	very strong
$3 > \lvert SSMD \rvert \geq 2$	strong
$2 > \lvert SSMD \rvert \geq 1.645$	fairly strong
$1.645 > \lvert SSMD \rvert \geq 1.28$	moderate
$1.28 > \lvert SSMD \rvert \geq 1$	fairly moderate
$1 > \lvert SSMD \rvert \geq 0.75$	fairly weak
$0.75 > \lvert SSMD \rvert \geq 0.5$	weak
$0.5 > \lvert SSMD \rvert \geq 0.25$	very weak
$\lvert SSMD \rvert \leq 0.25$	extremely weak effects

3.4 RNA isolation

3.4.1 Sample preparation for RNA isolation

BE(2)-M17 cell line was used for the sample preparation of RNA isolation. Thaw and passage cells with the same method as mitochondrial morphology assay. Each sample was prepared in triplicates.

On day 1, seed 1 × 10^5 cells/mL (100 µL per well) in DMEM/F-12, HEPES - 10% FBS media + 8µg/mL of protamine sulfate and 1% of P/S in 96 well cell culture plates. Incubate the cells for 2 - 3 h to allow the cells to settle before transducing the cells with 20 µL of lentivirus. On day 4, Change media with DMEM/F-12, HEPES-10%FBS media +4 µg/mL of puromycin, and 1% of P/S. On day 6, wash the cells once with 200 µL of DPBS and then add 100 µL of RNA lysis buffer (from ZYMO Quick-RNA 96 Kit, R1053) to each well. Store the plate directly at -80°C until use. To reduce the batch effect, all samples were completed in one go using the cell culture framework and Hamilton system (Microlab Star).

3.4.2 RNA isolation and quantification

RNA was extracted following the ZYMO Quick-RNA 96 Kit (R1053) instruction. Once RNA isolation was performed for all the samples, RNA content in each sample was measured following

the instruction of QuantiFluor® RNA System (E3310). Agilent RNA ScreenTape (5067-5576, Agilent) on an Agilent 4200 TapeStation System (G2991A) was used to determine the RNA quality. Only RNA samples with an RNA integrity number (RIN) ⩾7.0 were used for experiments. The extracted RNA plates were stored at -80°C until used for RT-qPCR and mRNA sequencing.

3.5 RT- qPCR for shRNA knockdown validation

3.5.1 Design primers

The most important thing to design a primer is to make sure the primer can specifically detect mRNA and not DNA. Therefore, the primers have to be designed in 2 different exons. If primers are designed in different exons and the intron separated by both exons is quite large (>1000 bp), there is no risk of amplifying DNA. When designing the primers, we also need to try to design a primer specific for all transcripts of a given gene with the amplified product being of the same size. If that is not possible, remove transcripts with lower confidence.

The genome browser ensemble (www.ensembl.org) was used for identifying common exons in a gene. Moreover, the website of NCBI (https://www.ncbi.nlm.nih.gov/tools/primer-blast/) was used for primer design. The following parameters were used to design the primers. Firstly, make sure that the melting temperature is in a similar range, the optimal is about 55°-60°C. Secondly, the length of the primer should be between 18 to 24 bp. Thirdly, the length of the product should be between 75 to 200 bp. Fourthly, the GC content should be between 50% to 65%. Fifthly, avoid having too many G/C at the 3' end. Sixthly, avoid regions containing variants for primer design and self-complementary regions. And avoid palindromic regions and more than 4 repeats of the same nucleotide. The information on the primer used in this project please find in the supplementary material Table 1 (https://github.com/Weiping123/PD-GWAS-project).

3.5.2 cDNA synthesis

The cDNA synthesis was done according to a 96-well plate. Took out the RNA plate from -80°C and thaw on ice. Use the Integra 8-channel electronic pipette to take 12 µL of sample into a 96-well PCR plate, farblos, and ABI sequencer 3100/30 (710879, Biozym) for cDNA synthesis. Prepare the reaction system according to the manufacturer's specifications in Table 3. The mixture

of the reaction system was dispensed using the MANTIS® Liquid Handler (FORMULATRIX). After cDNA synthesis, the cDNA plates were stored at -80°C until used for RT-qPCR.

Table 3. Reaction system for cDNA synthesis.

Reagent	**Amount**
oligo dT 0.4µg/µL (79237, Qiagen)	0.5 µL
Random decamers 50µM (AM5722G, Thermo Fisher)	0.5 µL
dNTPs 10mM (11814362001, Roche)	1.0 µL
RNA	12 µL
65 °C 5 min, 2 min on ice	
Buffer 5X (18080085, Invitrogen)	4.0 µL
DTT 100 mM (18080085, Invitrogen)	1.0 µL
RnaseOut 40u/µl (10777019, Invitrogen)	0.5µL
SuperScript® III Reverse Transcriptase 200u/ µL (18080085, Invitrogen)	0.5µL
Final volume	20 µL
25 °C 5 min, 50 °C 1 h, 70 °C 15 min	

3.5.3 RT-qPCR

Before performing RT-qPCR, the cDNA was diluted using RNase-free water at a ratio of 1:4. Then, the reaction system was prepared according to the manufacturer's specifications in Table 4. RT-qPCR was carried out in a MicroAmp® Optical 384 well reaction plate (4309849, Applied Biosystems) in triplicates on Applied Biosystems® ViiA7 Real-Time PCR system using SYBR Green PCR master mix (Life Technologies). Each sample had triplicates of scrambled control and 2 housekeeping (HK) genes (HMBS and B2M) with triplicates of each HK gene.

Table 4. Reaction system for RT-qPCR.

Reagent	Amount
SYBR® Select Master Mix 2X (4472919, Applied Biosystems)	5.0 µL
Forward + Reverse primers (pro primer 100 µM, Metabion)	2 µL
cDNA	3 µL
Final volume	10 µL

3.5.4 Data processing and analysis

Normalized relative quantities were calculated with HMBS and B2M as housekeeping genes by using the online tool (https://apps.thermofisher.com/apps/spa/#/dashboard). The KD efficiencies per clone were calculated using scrambled control as a reference.

3.6 α-synuclein ELISA

3.6.1 Protocol for sample preparation and ELISA

BE(2)-M17 cell line was used for extracting proteins. Thaw cells with the same method as mitochondrial morphology assay. Passage and bulk twice before using cells for screenings to allow the cells to recover. In this assay, four replicates of the negative control were used. In the negative control group, cells were transduced with scramble shRNA. Each sample was treated only with the most efficient shRNA selected by the result of RT-qPCR and repeated three times.

On day 1, seed 13000 BE(2)-M17 cells, 150µL per well in 96-well cell culture plates with DMEM/F-12, HEPES -10%FBS media + 8µg/mL of protamine sulfate, 1% of P/S. Incubate for 2-3 h and add 20 uL of lentivirus. On day 4, refresh media with DMEM/F-12, HEPES-10%FBS media +4 µg/mL of puromycin, and 1% of P/S. On day 6, wash the cells twice with cold DPBS, then add 50µL of lysis buffer (Table 5) to each well, incubate 5 min on ice, then centrifuge at 4 000 rpm, 4°C for 35 min. Take the supernatant and store it at -80°C until use.

According to the manufacturer's instructions, the SensoLyte™ Anti-alpha-Synuclein Quantitative ELISA Kit (AS-55550, AnaSpec) was used to measure the α-synuclein protein concentration. The

total protein concentration was determined by the Pierce BCA protein assay kit (Cat. No. 23225, Thermo Fisher).

Table 5. 5× RIPA (radio immunoprecipitation assay) buffer recipe for 100mL.

Reagent	Amount
250 mM Tris-HCL (pH 8.0) (Sigma)	3.03 g
750 mM NaCl (Sigma)	4.39 g
5% NP-40 (11596671, Thermo Fisher)	5 mL
25 mM EDTA (25300054, Thermo Fisher)	5 mL (500 mM)
2.5% Sodium deoxycholate (30970, Sigma)	2.5 g
0.5% SDS (Sigma)	5 mL (10% solution)

*Tris-HCL: TRIS hydrochloride; NP-40: nonidet P-40 Substitute; EDTA: Ethylenediaminetetraacetic acid; SDS: Sodium dodecyl sulfate.

To prepare the lysis buffer, add 250 µL of 10× protease inhibitor cocktail (S8820, Sigma-Aldrich) and 50 µL of 0.1M phenylmethanesulfonyl fluoride (PMSF) freshly (Cat. No. 93482, Sigma-Aldrich) for each 5mL of 1× RIPA.

3.6.2 Data processing and analysis

Normalized relative quantities were calculated by dividing the total protein (BCA result) of each KD sample. The percentage of increase or decrease of α-synuclein protein per sample was calculated using negative control as a reference. For each of the shRNA screens, data were analyzed using T-tests with the FDR correction ($P < 0.05$, FDR < 0.05).

Effects were considered significant when the percentage of increase of α-synuclein protein is equal to or more than 50% of negative control, or the decrease of α-synuclein protein is equal to or more than 50% of negative control for each treatment.

3.7 mRNA-sequencing

3.7.1 Library preparation and sequencing

For mRNA sequencing, we only use the RNA produced by transducing with the most efficient shRNA based on the result of RT-qPCR. Samples were normalized and plated out in two 96-well plates in two batches before preparing the library. The library was generated following the reference guide of Illumina Stranded mRNA Prep, Ligation (96 Samples) Kit (20040534, Illumina). For batch one, the library was pooled in two tubes based on the sample plates. The ready-to-load libraries were sequenced in a high-quality sequencing format on NovaSeq 6000 (Illumina) at a depth of 10 – 102 million reads by CeGat in Tübingen (https://www.cegat.de/). For batch two, the samples have been sequenced on a SR Flowcell with 1X50 bp and Dual-Index on the Illumina HiSeq4000 at a depth of 2 – 27 million reads by CeGat in Tübingen.

3.7.2 Data processing and analysis

For mRNA sequencing data analysis, we only use the data of hits from functional assays (mitochondrial morphology assay, Parkin translocation assay, and α-synuclein ELISA) to improve the efficiency and accuracy of the analysis.

The quality of the FASTQ files was analyzed with FastQC (version 0.11.5-cegat) ((de Sena Brandine and Smith 2019)). After FASTQ quality checking, the FASTQ files were loaded into the QIAGEN CLC genomic workbench 22.0.2 (QIAGEN, Aarhus, Denmark) (Liu and Di 2020)for further analysis. Data was trimmed based on the following criteria: trim using the quality limit 0.05, a maximum number of trim ambiguous nucleotides is 2, removing one nucleotide from both 5’ terminal and 3’ terminal. The trimmed data was used for RNA-seq analysis. The reference genome version used in this analysis was hg38 without alternative contigs (“Homo_sapiens_sequence_hg38_no_alt_analysis_set" option), using Ensembl gene annotation (Cunningham et al. 2022) (“Homo_sapiens_ensembl_v99_hg38_ no_alt_analysis_set_Genes” and “Homo_sapiens_ensembl_v99_hg38_ no_alt_analysis_set_mRNA” specifically for mRNA subset). A principal component analysis (PCA) plot was done for controls (samples transduced with scramble) from two batches to extrapolate the batch effect. The differential gene expression analysis was done separately for each batch due to the large batch effect size, the samples of each batch were compared with their corresponding controls separately. The fold change for each KD sample was calculated after this step to evaluate the gene KD efficiency. Samples with fold change $\leqslant$-1 were considered to have good KD.

Then, the gene set test was performed separately based on each batch to get the Gene Ontology (GO) terms ("goa_human_20190201_ no_alt_analysis_set" used for annotation). The GO terms of hits from functional assays were exported from CLC genomic workbench and loaded into R (R Core Team (2022), RStudio Team (2022)) for further analysis. GO terms from both batches were analyzed together from this step on. For each sample, only the top 10 enriched GO terms were included. Base functions in R were further used to get the frequency of each GO term. The GO terms with frequency $\geqslant 3$ were prioritized as the most interesting GO terms most likely related to multiple risk variants for PD (samples sharing the enriched GO term). The priority genes were further screened by searching references to obtain information on the pathways they may be involved in, as well as SNP information of samples (KD genes) and functional assays information. For cases where there are multiple candidate genes on a SNP, searching for the function of each gene and comparing the results of the functional assay of this study helps to filter out the more significant genes on each SNP for the following priority study, thus further reducing the number of candidate genes.

4. Results

4.1 Result of RT-qPCR

Relative quantification (Rq) is the fold change compared to the negative control. The Rq of the negative control is 1. All samples (treated with shRNAs) were compared to the negative control. When Rq is less than 1, it indicates that this gene is less expressed in this sample compared to the negative control. When Rq is more than 1, it indicates that this gene is more expressed in this sample compared to the negative control.

The result of RT-qPCR showed that 195 candidate genes (targets) have a good KD ($Rq < 0.5$), and for each target, we selected the most efficient KD shRNA for performing ELISA and mRNA sequencing experiments. The Rq of each shRNA is shown in Figure 10. The KD efficiency ranking of shRNAs corresponding to each target is shown in Table 6.

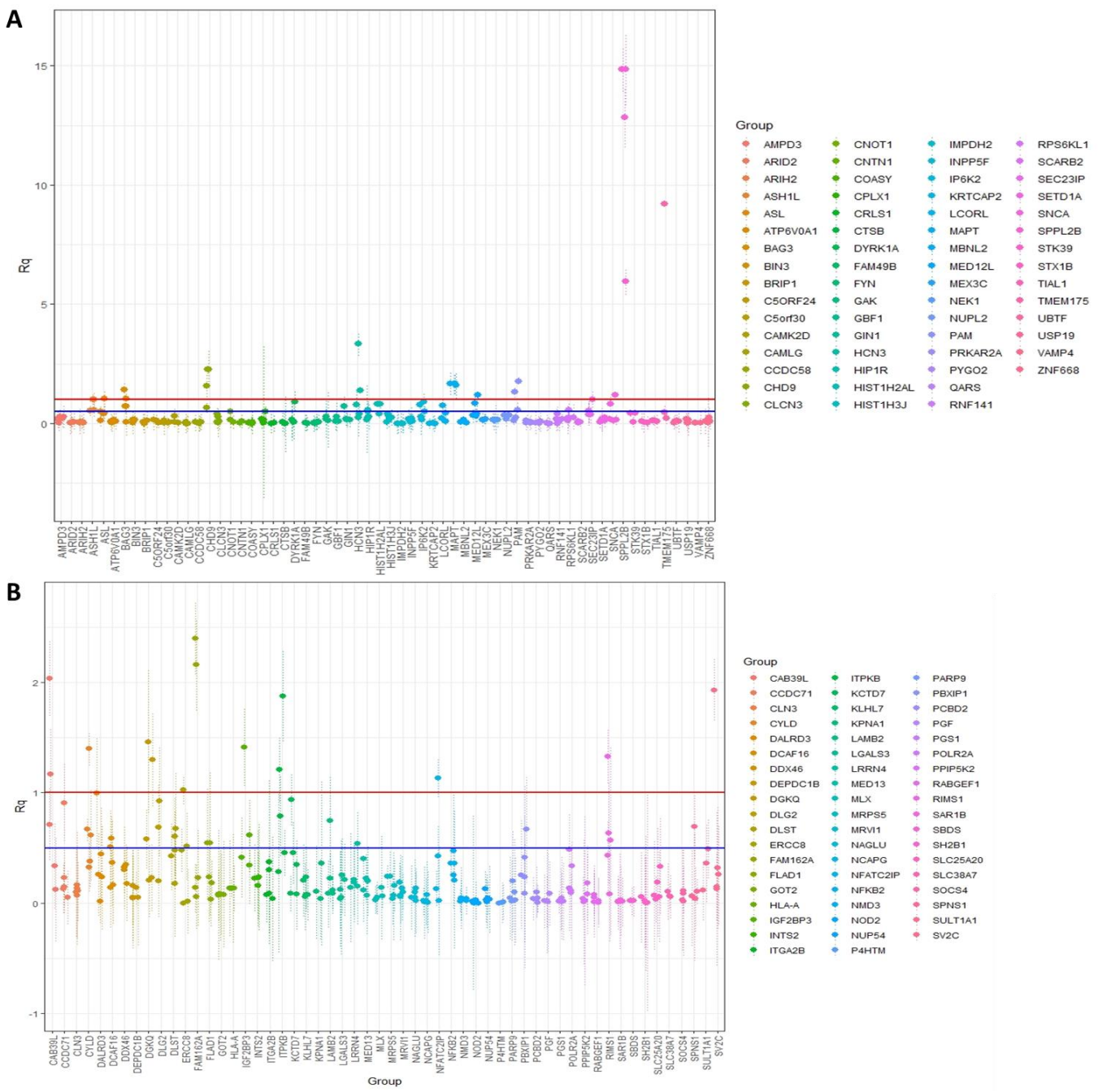

Figure 10. The result of RT-qPCR. In this figure, each color represents a candidate gene. For each gene, there are several spots, and each spot represents the mean of Rq for one shRNA that targets this gene. The red line represents the negative control. Samples below the blue line (Rq=0.5) were considered significant Rq, which indicates a good KD.

Table 6. The KD efficiency ranking of shRNAs corresponding to each target based on the RT-qPCR results.

targets	most efficient shRNA	2nd efficient	3rd efficient	4th efficient	5th efficient
DGKQ	DGKQ-3	DGKQ-5	DGKQ-4	DGKQ-1	DGKQ-2
DALRD3	DALRD3-3	DALRD3-2	DALRD3-4	DALRD3-1	DALRD3-5
CAB39L	CAB39L-3	CAB39L-4	CAB39L-2	CAB39L-5	CAB39L-1
SV2C	SV2C-4	SV2C-3	SV2C-2	SV2C-1	SV2C-5
DLG2	DLG2-1	DLG2-5	DLG2-4		
RIMS1	RIMS1-3	RIMS1-4	RIMS1-1	RIMS1-2	RIMS1-5
ITPKB	ITPKB-2	ITPKB-4	ITPKB-7	ITPKB-1	ITPKB-3
LGALS3	LGALS3-2	LGALS3-1	LGALS3-3	LGALS3-4	LGALS3-5
BAG3	BAG3-5				
BIN3	BIN3-3	BIN3-7	BIN3-6		
BRIP1	BRIP1-2	BRIP1-4	BRIP1-3		
CLCN3	CLCN3-3	CLCN3-2	CLCN3-4	CLCN3-1	CLCN3-5
CPLX1	CPLX1-4	CPLX1-3	CPLX1-6	CPLX1-2	CPLX1-1
CNOT1	CNOT1-4	CNOT1-2	CNOT1-1		
CTSB	CTSB-4	CTSB-3	CTSB-2		
FYN	FYN-4	FYN-1	FYN-3	FYN-5	FYN-2
GIN1	GIN1-3	GIN1-2	GIN1-4	GIN1-5	
KRTCAP2	KRTCAP2-1	KRTCAP2-5	KRTCAP2-4	KRTCAP2-3	KRTCAP2-2
INPP5F	INPP5F-4	INPP5F-3	INPP5F-5	INPP5F-2	INPP5F-1
DYRK1A	DYRK1A-4	DYRK1A-1	DYRK1A-7	DYRK1A-5	DYRK1A-3
IP6K2	IP6K2-6	IP6K2-4	IP6K2-5		
NEK1	NEK1-2	NEK1-5	NEK1-1	NEK1-3	NEK1-4
PAM	PAM-5	PAM-1	PAM-4		
CRLS1	CRLS1-4	CRLS1-5	CRLS1-3		
CAMK2D	CAMK2D-10	CAMK2D-7	CAMK2D-1		
FAM49B	FAM49B-4	FAM49B-8	FAM49B-3		
GAK	GAK-6	GAK-7	GAK-8		
GBF1	GBF1-8	GBF1-6	GBF1-5		
HCN3	HCN3-3	HCN3-1			
HIST1H3J	HIST1H3J-5	HIST1H3J-1	HIST1H3J-4	HIST1H3J-2	HIST1H3J-3
MED12L	MED12L-2	MED12L-3	MED12L-5		
NUPL2	NUPL2-2	NUPL2-3	NUPL2-4	NUPL2-1	NUPL2-5
RNF141	RNF141-4	RNF141-5	RNF141-2	RNF141-3	RNF141-1
RPS6KL1	RPS6KL1-1	RPS6KL1-2	RPS6KL1-3	RPS6KL1-4	RPS6KL1-5
SEC23IP	SEC23IP-3	SEC23IP-5	SEC23IP-2	SEC23IP-4	
SETD1A	SETD1A-1	SETD1A-4	SETD1A-2	SETD1A-3	SETD1A-5
LCORL	LCORL-2	LCORL-3	LCORL-5		

MBNL2	MBNL2-5	MBNL2-3	MBNL2-4		
MEX3C	MEX3C-4	MEX3C-3	MEX3C-5		
HIP1R	HIP1R-1	HIP1R-3	HIP1R-5	HIP1R-4	HIP1R-2
HIST1H2AL	HIST1H2AL-1				
SNCA	SNCA-3	SNCA-4	SNCA-5	SNCA-1	SNCA-2
TIAL1	TIAL1-1	TIAL1-2	TIAL1-5	TIAL1-4	TIAL1-3
SPPL2B	SPPL2B-1	SPPL2B-3	SPPL2B-2	SPPL2B-4	SPPL2B-5
C5ORF24	C5ORF24-12	C5ORF24-9	C5ORF24-6		
CNTN1	CNTN1-1	CNTN1-2	CNTN1-5		
SCARB2	SCARB2-2	SCARB2-3	SCARB2-1		
STK39	STK39-11	STK39-2	STK39-3		
TMEM175	TMEM175-1	TMEM175-3			
ARIH2	ARIH2-4	ARIH2-1	ARIH2-2	ARIH2-5	ARIH2-3
COASY	COASY-2	COASY-5	COASY-3	COASY-1	COASY-4
IMPDH2	IMPDH2-5	IMPDH2-3	IMPDH2-2	IMPDH2-1	IMPDH2-4
PRKAR2A	PRKAR2A-5	PRKAR2A-4	PRKAR2A-3	PRKAR2A-1	PRKAR2A-2
PYGO2	PYGO2-2	PYGO2-4	PYGO2-3	PYGO2-5	PYGO2-1
USP19	USP19-5	USP19-1	USP19-4	USP19-3	USP19-2
ZNF668	ZNF668-2	ZNF668-3	ZNF668-1	ZNF668-5	ZNF668-4
UBTF	UBTF-2	UBTF-5	UBTF-4	UBTF-3	
STX1B	STX1B-3	STX1B-2	STX1B-4	STX1B-1	
QARS	QARS-3	QARS-4	QARS-1	QARS-2	
VAMP4	VAMP4-4	VAMP4-1	VAMP4-2		
AMPD3	AMPD3-2	AMPD3-5	AMPD3-1	AMPD3-3	AMPD3-4
ARID2	ARID2-3	ARID2-4	ARID2-1	ARID2-5	ARID2-2
ASL	ASL-3	ASL-1	ASL-2	ASL-5	
ATP6V0A1	ATP6V0A1-5	ATP6V0A1-1	ATP6V0A1-4	ATP6V0A1-2	ATP6V0A1-3
CAMLG	CAMLG-2	CAMLG-5	CAMLG-3	CAMLG-4	CAMLG-1
CCDC58	CCDC58-6	CCDC58-1	CCDC58-5	CCDC58-7	CCDC58-3
CCDC71	CCDC71-5	CCDC71-3	CCDC71-2	CCDC71-4	
CLN3	CLN3-2	CLN3-4	CLN3-5	CLN3-1	CLN3-3
C5orf30	C5orf30-2	C5orf30-3	C5orf30-4	C5orf30-1	
CYLD	CYLD-5	CYLD-3	CYLD-2		
DCAF16	DCAF16-5	DCAF16-4	DCAF16-2	DCAF16-7	
DEPDC1B	DEPDC1B-3	DEPDC1B-5	DEPDC1B-1	DEPDC1B-2	DEPDC1B-4
DLST	DLST-5	DLST-1	DLST-2	DLST-3	DLST-4
ERCC8	ERCC8-3	ERCC8-1	ERCC8-5	ERCC8-4	ERCC8-2
FAM162A	FAM162A-3	FAM162A-2	FAM162A-6		

FLAD1	FLAD1-1	FLAD1-5	FLAD1-2	FLAD1-4	FLAD1-3
GOT2	GOT2-1	GOT2-4	GOT2-5	GOT2-3	GOT2-2
HLA-A	HLA-A-4	HLA-A-3	HLA-A-5	HLA-A-2	HLA-A-1
DDX46	DDX46-3	DDX46-2	DDX46-1	DDX46-4	
IGF2BP3	IGF2BP3-5	IGF2BP3-1	IGF2BP3-4		
ITGA2B	ITGA2B-4	ITGA2B-5	ITGA2B-3	ITGA2B-1	ITGA2B-2
KCTD7	KCTD7-4	KCTD7-2	KCTD7-3	KCTD7-5	
KLHL7	KLHL7-5	KLHL7-6	KLHL7-2	KLHL7-3	KLHL7-4
LAMB2	LAMB2-4	LAMB2-1	LAMB2-5	LAMB2-3	
LRRN4	LRRN4-2	LRRN4-1	LRRN4-3	LRRN4-5	LRRN4-4
MED13	MED13-1	MED13-3	MED13-2	MED13-5	MED13-4
MLX	MLX-1	MLX-2	MLX-3	MLX-5	MLX-4
MRPS5	MRPS5-4	MRPS5-1	MRPS5-3	MRPS5-2	MRPS5-5
MRVI1	MRVI1-3	MRVI1-1	MRVI1-4	MRVI1-2	MRVI1-5
NAGLU	NAGLU-2	NAGLU-1	NAGLU-4	NAGLU-3	NAGLU-5
INTS2	INTS2-4	INTS2-1	INTS2-2	INTS2-3	
KPNA1	KPNA1-4	KPNA1-5	KPNA1-1		
NCAPG	NCAPG-5	NCAPG-1	NCAPG-2	NCAPG-3	NCAPG-4
NFKB2	NFKB2-4	NFKB2-2	NFKB2-1	NFKB2-5	NFKB2-3
NMD3	NMD3-2	NMD3-6	NMD3-1	NMD3-3	NMD3-5
NOD2	NOD2-1	NOD2-4	NOD2-5	NOD2-3	NOD2-2
NUP54	NUP54-5	NUP54-1	NUP54-4	NUP54-3	NUP54-2
PARP9	PARP9-2	PARP9-3	PARP9-1	PARP9-5	PARP9-4
PBXIP1	PBXIP1-3	PBXIP1-5	PBXIP1-1	PBXIP1-2	PBXIP1-4
PCBD2	PCBD2-6	PCBD2-9	PCBD2-10	PCBD2-8	PCBD2-7
PGF	PGF-1	PGF-2	PGF-3	PGF-4	PGF-5
PGS1	PGS1-4	PGS1-2	PGS1-3	PGS1-1	PGS1-5
NFATC2IP	NFATC2IP-3	NFATC2IP-1	NFATC2IP-2		
P4HTM	P4HTM-3	P4HTM-4	P4HTM-5		
POLR2A	POLR2A-5	POLR2A-4	POLR2A-3	POLR2A-1	POLR2A-2
PPIP5K2	PPIP5K2-5	PPIP5K2-4	PPIP5K2-3	PPIP5K2-2	PPIP5K2-1
RABGEF1	RABGEF1-1	RABGEF1-2	RABGEF1-5	RABGEF1-4	RABGEF1-3
SAR1B	SAR1B-2	SAR1B-4	SAR1B-1	SAR1B-5	SAR1B-3
SH2B1	SH2B1-1	SH2B1-4	SH2B1-2	SH2B1-3	
SLC25A20	SLC25A20-1	SLC25A20-5	SLC25A20-4	SLC25A20-3	SLC25A20-2
SPNS1	SPNS1-4	SPNS1-5	SPNS1-3	SPNS1-1	
SOCS4	SOCS4-2	SOCS4-4	SOCS4-1	SOCS4-3	
SLC38A7	SLC38A7-1	SLC38A7-3	SLC38A7-2		
SBDS	SBDS-1	SBDS-3	SBDS-4		
SULT1A1	SULT1A1-4	SULT1A1-1	SULT1A1-2		

TPST1	TPST1-5	TPST1-1	TPST1-3	TPST1-2	TPST1-4
TUFM	TUFM-5				
C4orf27	C4orf27-1	C4orf27-4	C4orf27-7	C4orf27-2	C4orf27-6
FAM134C	FAM134C-4	FAM134C-3	FAM134C-2	FAM134C-1	FAM134C-5
SFRS2IP	SFRS2IP-2	SFRS2IP-5	SFRS2IP-3	SFRS2IP-1	SFRS2IP-4
CCDC101	CCDC101-1	CCDC101-6	CCDC101-4	CCDC101-5	CCDC101-2
C6orf192	C6orf192-4	C6orf192-1			
ZNF192	ZNF192-5	ZNF192-3	ZNF192-4	ZNF192-1	ZNF192-2
CRCP	CRCP-2	CRCP-3	CRCP-1	CRCP-4	CRCP-5
RPP21	RPP21-5	RPP21-4	RPP21-2	RPP21-3	RPP21-1
PPP1R11	PPP1R11-5	PPP1R11-3			
B3GALNT1	B3GALNT1-5	B3GALNT1-4	B3GALNT1-1	B3GALNT1-2	B3GALNT1-3
BCL7C	BCL7C-1	BCL7C-3	BCL7C-4	BCL7C-5	
DCUN1D1	DCUN1D1-1	DCUN1D1-5			
DLGAP5	DLGAP5-1	DLGAP5-5	DLGAP5-4	DLGAP5-3	DLGAP5-2
EFNA1	EFNA1-1	EFNA1-3	EFNA1-4	EFNA1-5	
KCNN3	KCNN3-4	KCNN3-1	KCNN3-5	KCNN3-2	
NDUFAF3	NDUFAF3-1	NDUFAF3-5	NDUFAF3-3	NDUFAF3-4	NDUFAF3-2
PPM1L	PPM1L-2				
PRSS3	PRSS3-2	PRSS3-3	PRSS3-5	PRSS3-1	PRSS3-4
QRICH1	QRICH1-2	QRICH1-1	QRICH1-4	QRICH1-5	QRICH1-3
HIST1H2BN	HIST1H2BN-1	HIST1H2BN-5	HIST1H2BN-4	HIST1H2BN-3	
DPM3	DPM3-2	DPM3-1	DPM3-3		
SLC41A1	SLC41A1-2	SLC41A1-4	SLC41A1-3	SLC41A1-5	SLC41A1-1
TXNDC15	TXNDC15-3	TXNDC15-2	TXNDC15-5	TXNDC15-1	TXNDC15-4
TYW1	TYW1-1	TYW1-3	TYW1-5		
UBE2R2	UBE2R2-3	UBE2R2-5	UBE2R2-2	UBE2R2-4	UBE2R2-1
WDR5B	WDR5B-2				
ZBTB4	ZBTB4-4	ZBTB4-2	ZBTB4-5	ZBTB4-3	
ZBTB7B	ZBTB7B- 3	ZBTB7B-5	ZBTB7B-2	ZBTB7B-1	ZBTB7B-4
ZNF646	ZNF646-5	ZNF646-1	ZNF646-2	ZNF646-3	ZNF646-4
ZNRD1	ZNRD1-1	ZNRD1-3	ZNRD1-2	ZNRD1-4	ZNRD1-5
ZSCAN16	ZSCAN16-4	ZSCAN16-5	ZSCAN16-2	ZSCAN16-1	ZSCAN16-3
UBAP2	UBAP2-1	UBAP2-4	UBAP2-3		
ZNF514	ZNF514-1	ZNF514-4	ZNF514-2		
KIAA1967	KIAA1967-5	KIAA1967-2	KIAA1967-1	KIAA1967-3	KIAA1967-4
RAG1AP	RAG1AP1-2	RAG1AP1-5	RAG1AP1-3	RAG1AP1-4	

1					
CLK2	CLK2-6	CLK2-2	CLK2-5	CLK2-1	CLK2-9
KIAA1267	KIAA1267-6	KIAA1267-3	KIAA1267-5	KIAA1267-2	KIAA1267-1
EFNA3	EFNA3-4	EFNA3-5	EFNA3-3	EFNA3-2	EFNA3-1
WNT3	WNT3-3	WNT3-4	WNT3-1	WNT3-5	WNT3-2
SCAMP3	SCAMP3-4	SCAMP3-2	SCAMP3-1	SCAMP3-3	
GBA	GBA-1	GBA-4	GBA-5	GBA-2	
KIAA0317	KIAA0317-4	KIAA0317-2	KIAA0317-1	KIAA0317-3	
C7orf30	C7orf30-2	C7orf30-3	C7orf30-1	C7orf30-4	
VKORC1	VKORC1-2	VKORC1-1	VKORC1-5		
ATXN2L	ATXN2L-4	ATXN2L-3	ATXN2L-6	ATXN2L-5	ATXN2L-2
DTX3L	DTX3L-3	DTX3L-4	DTX3L-1	DTX3L-5	DTX3L-2
FBXL19	FBXL19-5	FBXL19-4	FBXL19-1	FBXL19-2	FBXL19-3
FBXO34	FBXO34-3	FBXO34-4	FBXO34-2	FBXO34-5	FBXO34-1
GRN	GRN-5	GRN-2	GRN-3	GRN-4	GRN-1
MAPK1IP1L	MAPK1IP1L-2	MAPK1IP1L-3	MAPK1IP1L-5	MAPK1IP1L-4	MAPK1IP1L-1
NDUFAF2	NDUFAF2-4	NDUFAF2-3	NDUFAF2-5	NDUFAF2-2	NDUFAF2-1
NOL4	NOL4-1	NOL4-3	NOL4-5	NOL4-2	NOL4-4
PDLIM2	PDLIM2-4	PDLIM2-2	PDLIM2-1	PDLIM2-5	PDLIM2-3
SLC45A3	SLC45A3-3	SLC45A3-5	SLC45A3-1	SLC45A3-2	SLC45A3-4
C8orf58	C8orf58-2	C8orf58-4			
TUBG1	TUBG1-1	TUBG1-4	TUBG1-3	TUBG1-2	TUBG1-5
ZNF165	ZNF165-1	ZNF165-5	ZNF165-4	ZNF165-3	
C7orf42	C7orf42-3				
SYT17	SYT17-5	SYT17-3			
ADAM15	ADAM15-1	ADAM15-2			
BST1	BST1-2	BST1-3			
CKS1B	CKS1B-7	CKS1B-2			
FDFT1	FDFT1-5	FDFT1-4	FDFT1-2		
FDPS	FDPS-5	FDPS-3			
GALC	GALC-4	GALC-1			
GCH1	GCH1-5	GCH1-4			
ITGA8	ITGA8-3	ITGA8-2			
MAP4K4	MAP4K4-1	MAP4K4-3	MAP4K4-2		
MCCC1	MCCC1-2	MCCC1-1			
MTX1	MTX1-3	MTX1-1			
NUCKS1	NUCKS1-4	NUCKS1-1			
PMVK	PMVK-1	PMVK-6			
RUSC1	RUSC1-3	RUSC1-2			

SHC1	SHC1-8	SHC1-7			
STX4	STX4-1	STX4-2			
THBS3	THBS3-4	THBS3-3			
WDHD1	WDHD1-1	WDHD1-3			
WDR6	WDR6-1	WDR6-5			

4.2 Result of mitochondrial morphology assay

4.2.1 The plate-to-plate QC for mitochondrial morphology assay

The Z-factor was calculated to evaluate the quality of this assay. In mitochondrial morphology assay, the Z-factors for all the plates are greater than 0.5 (Figure 11), and the average Z-factor for all the plates is 0.69, meaning that the quality of this assay is excellent.

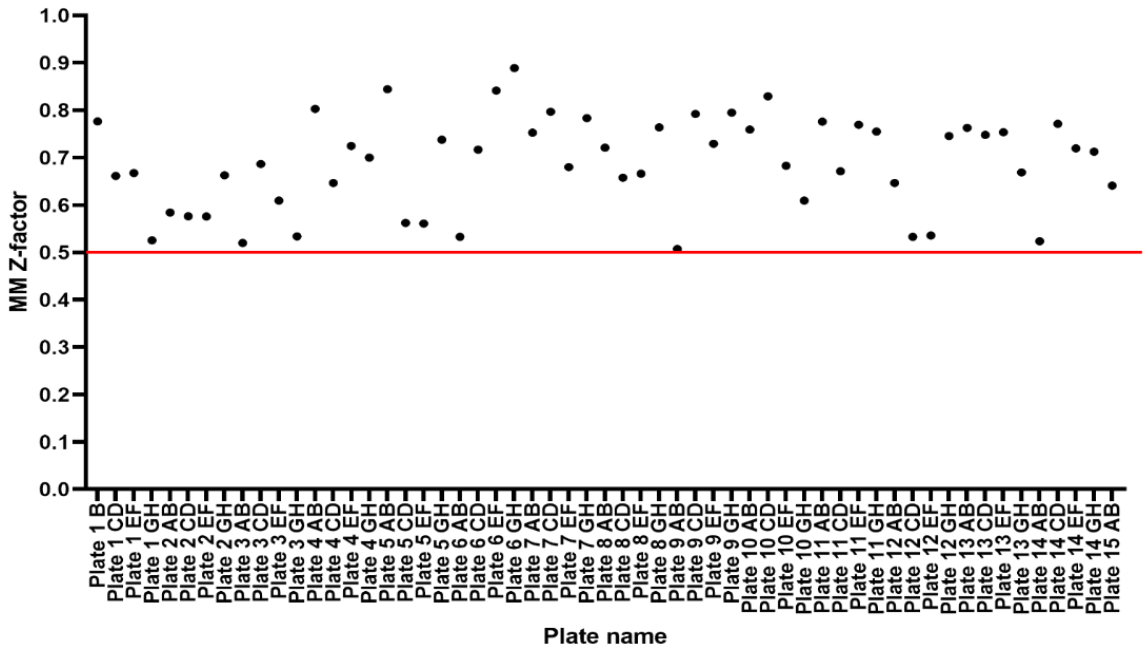

Figure 11. The Z-factor for all the plates of the mitochondrial morphology assay. In this figure, each spot represents the Z-factor for each plate.

4.2.2 Hits from mitochondrial morphology assay

In this assay, the axial length ratio of mitochondrial from each sample (treated with shRNA) was calculated and normalized by the negative control group. The SSMD was calculated for hit selection.

Based on the hit selection criteria according to SSMD, 49 hits were selected in this assay. For all the hits, the SSMDs of 48 hits are less than -3, and only the SSMD of CCDC101 is greater than 3 (Figure 12). This means that KD CCDC101 has the opposite effect on the axial length ratio of mitochondrial compared to the other 48 hits. The detailed hits information is shown in Table 7.

The normalized axial length ratio of mitochondrial morphology assay hits is shown in Figure 13A. Figure 13B is a schematic diagram showing the effect of the axial length ratio on mitochondrial morphology and possible functions. Compared to the negative control group, a decrease in the axial length ratio represents a more rounded mitochondrial morphology, which may indicate mitochondrial fission. In contrast, an increase in the axial length ratio represents elongated mitochondria, which may indicate mitochondrial fusion. Compared to the negative control group (Figure 14A), CCDC101-KD shows a significant increase in axial length ratio (Figure 14B, 14C), Compared to the negative control group (Figure 13A), KD each of the other 48 hits shows a significant decrease in axial length ratio, and SFRS2IP-KD shows the most significant decrease in axial length ratio (Figure 15).

Table 7. The information of mitochondrial morphology hits.

The Column "Suggested_gene" means if this gene was suggested as a priority test gene under this locus. The Column "Average Axial Length Ratio_1st" means the average Axial Length Ratio of the 4 replicates of the most efficient shRNA, and the Column "Average Axial Length Ratio_2nd" means the average Axial Length Ratio of the 4 replicates of the second efficient shRNA, same reasoning below. NA means no efficient shRNA data for its corresponding target. The average Axial Length Ratio of the negative control is 1.

Targets	Locus Number	rsID	BrainExp	Population	Sugested_gene	Average Axial Length Ratio_1st	Average Axial Length Ratio_2nd	Average Axial Length Ratio_3rd	Average Axial Length Ratio_4th	Average Axial Length Ratio_5th
MTX1	1	rs35749011	Yes	European	Y	0.939	0.918	NA	NA	NA
THBS3	1	rs35749011	Yes	European	Y	0.978	0.937	NA	NA	NA
RUSC1	1	rs35749011	Yes	European	Y	0.987	0.967	NA	NA	NA
SLC50A1	1	rs35749011	Yes	European	No	1.008	0.946	0.961	0.955	NA

KRTCAP2	1	rs35749011	Yes	European	No	0.959	0.983	0.972	0.939	0.953
THBS3	1	rs76763715	Yes	European	Y	0.978	0.937	NA	NA	NA
MTX1	1	rs76763715	Yes	European	No	0.939	0.918	NA	NA	NA
RUSC1	1	rs76763715	Yes	European	Y	0.987	0.967	NA	NA	NA
KRTCAP2	1	rs76763715	Yes	European	Y	0.959	0.983	0.972	0.939	0.953
SLC50A1	1	rs76763715	Yes	European	No	NA	NA	NA	NA	NA
SLC41A1	4	rs823118	Yes	European	No	0.983	0.929	1.022	0.943	0.961
MRPS5	8	rs2042477	Yes	European	No	0.955	0.965	0.966	0.958	0.977
ZNF514	8	rs2042477	Yes	European	Y	0.948	0.970	0.959	NA	NA
NDUFAF3	14	rs12497850	Yes	European	Y	0.966	1.003	0.933	0.983	0.941
PRKAR2A	14	rs12497850	Yes	European	Y	0.965	0.937	0.979	0.909	1.040
ARIH2	14	rs12497850	Yes	European	Y	0.981	0.947	0.895	0.961	1.021
LAMB2	14	rs12497850	Yes	European	Y	0.971	0.995	0.965	0.949	NA
PARP9	15	rs55961674	Yes	European	No	0.955	0.998	0.961	0.922	0.972
KPNA1	15	rs55961674	Yes	European	No	0.982	0.999	0.947	NA	NA
MCCC1	18	rs10513789	Yes	European	Y	0.980	0.933	NA	NA	NA
DGKQ	19	rs34311866	Yes	European	Y	0.929	0.981	0.968	0.994	0.927
LCORL	21	rs34025766	Yes	European	Y	0.971	0.976	0.995	NA	NA
NCAPG	21	rs34025766	Yes	European	No	0.946	0.958	0.978	0.968	0.994

NUP54	22	rs6825004	Yes	European	Y	0.960	0.968	0.998	0.935	0.972
SNCA	23	rs356182	Yes	European	Y	0.952	1.032	0.955	0.891	1.060
SNCA	23	rs5019538	Yes	European	Y	0.952	1.032	0.955	0.891	1.060
CLCN3	25	rs62333164	Yes	European	Y	1.001	1.023	0.950	0.946	0.931
HPF1	25	rs62333164	Yes	European	No	0.967	1.001	1.011	0.953	0.966
ERCC8	26	rs1867598	Yes	European	No	0.954	0.971	0.993	0.939	0.941
NDUFAF2	26	rs1867598	Yes	European	Y	1.029	0.966	0.971	0.964	1.067
SAR1B	28	rs11950533	Yes	European	No	0.976	0.959	0.972	1.001	1.005
RPP21	30	rs9261484	Yes	European	Y	0.983	0.951	0.935	1.027	0.963
ZNRD1	30	rs9261484	Yes	European	Y	0.959	0.943	0.989	0.932	0.969
FYN	33	rs997368	Yes	European	Y	0.932	0.956	0.986	0.929	0.969
IGF2BP3	35	rs199351	Yes	European	No	0.920	0.987	0.950	NA	NA
KLHL7	35	rs199351	Yes	European	Y	0.965	0.967	0.950	0.975	0.981
NUP42	35	rs199351	Yes	European	No	NA	NA	NA	NA	NA
FAM49B	40	rs2086641	Yes	European	Y	0.963	0.980	0.965	NA	NA
MRVI1	46	rs7938782	Yes	European	Y	1.021	0.979	0.944	0.992	0.974
ARID2	50	rs7134559	Yes	European	Y	0.974	0.947	0.965	1.021	1.020
SFRS2IP	50	rs7134559	Yes	European	Y	0.955	0.922	0.950	1.052	0.901
MBNL2	54	rs4771268	Yes	European	Y	0.945	1.014	0.969	NA	NA

MAPK1IP1L	56	rs11158026	Yes	European	No	0.958	0.972	1.020	0.954	0.932
DLGAP5	56	rs11158026	Yes	European	Y	0.965	0.996	0.971	0.969	0.930
SOCS4	56	rs11158026	Yes	European	Y	0.974	0.948	0.938	0.966	NA
RPS6KL1	57	rs3742785	Yes	European	No	0.995	0.999	0.963	0.978	0.956
SGF29	61	rs2904880	Yes	European	Y	1.020	1.007	1.037	1.028	1.025
POLR2A	66	rs12600861	Yes	European	Y	0.951	0.945	0.956	1.035	0.993
TUBG1	67	rs12951632	Yes	European	No	0.989	0.977	0.945	1.020	0.980
NAGLU	67	rs12951632	Yes	European	Y	0.943	0.994	0.945	1.013	0.973
MLX	67	rs12951632	Yes	European	No	0.935	0.958	0.952	0.962	0.969
GRN	68	rs850738	Yes	European	Y	1.004	0.970	1.060	0.972	0.972
MEX3C	75	rs8087969	Yes	European	Y	0.981	0.961	0.970	NA	NA
CRLS1	77	rs77351827	Yes	European	Y	0.961	0.985	0.969	NA	NA
DYRK1A	78	rs2248244	Yes	European	Y	0.941	0.983	0.976	0.956	0.926

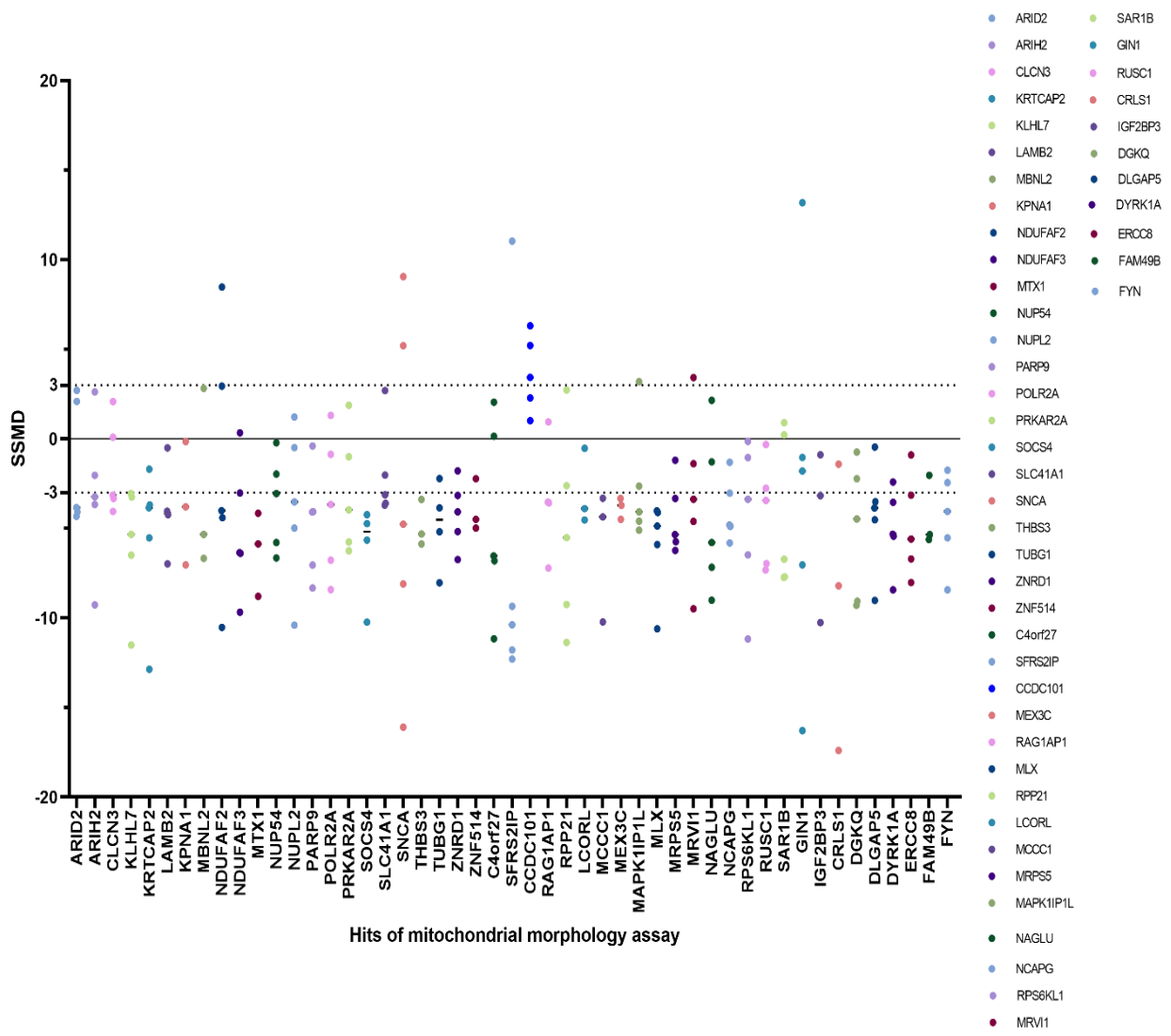

Figure 12. The SSMD of mitochondrial morphology assay hits. In this figure, each color represents the SSMD of each hit of mitochondrial morphology based on the criteria of hit selection. For each hit, there are 3 to 5 shRNA targeting it. For each hit, most of the shRNA targeting is either less than -3 or greater than 3. Most of the SSMD for the shRNAs targeting CCDC101 are greater than 3 (shown in blue).

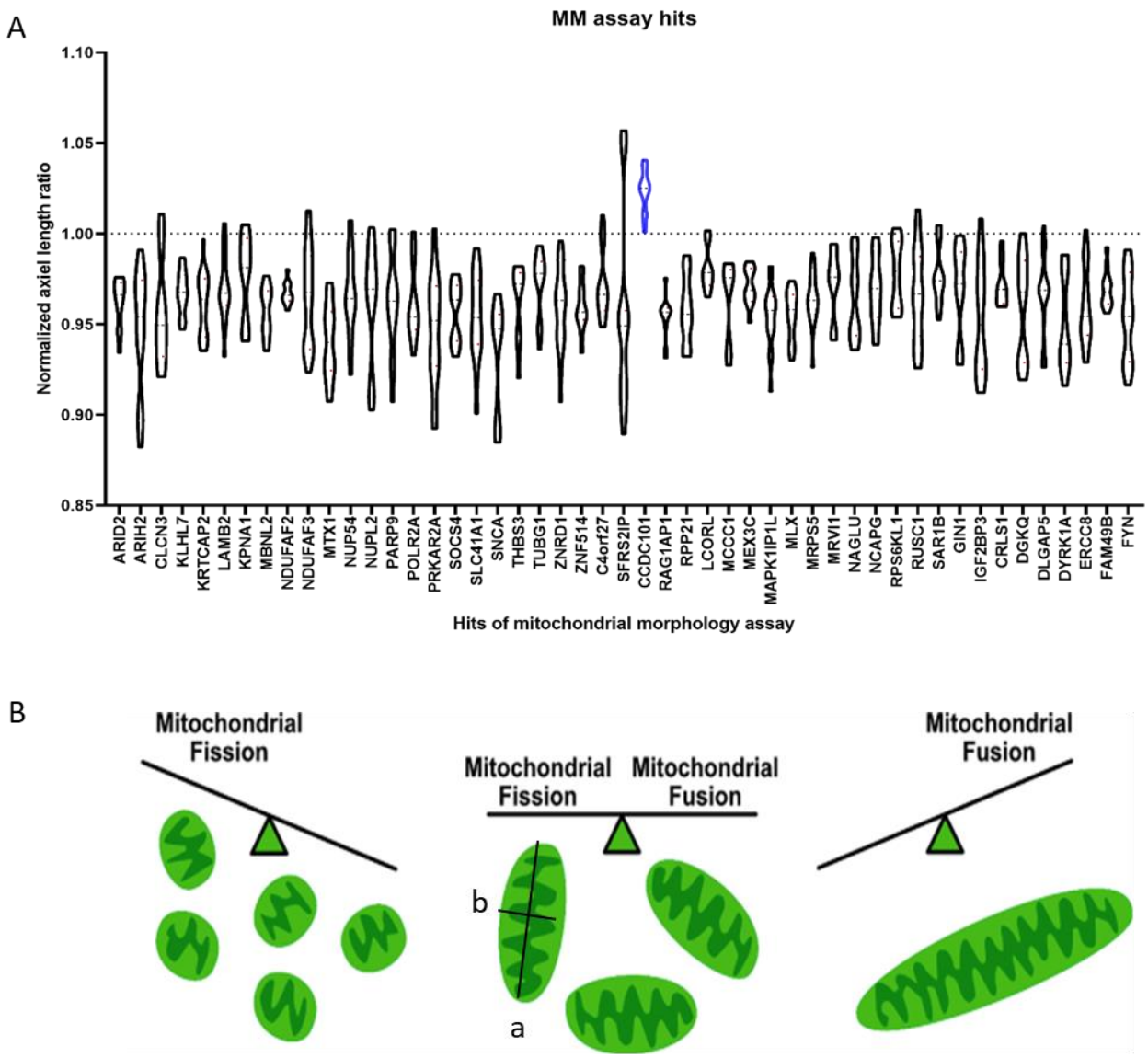

Figure 13. The normalized axial length ratio of mitochondrial morphology assay hits. In Graph A, there are 4 replicates for each sample. The data was normalized by negative control. After normalization, the axial length ratio of the negative control is 1. Compared to the negative control, KD CCDC101 increases the axial length ratio, and KD others decrease the axial length ratio. Graph B is a schematic diagram of the mitochondrial morphology. When b divided by a equals 1, it represents the normal state of mitochondria, corresponding to the normalized axial length ratio of 1 in Graph A. When b divided by a is greater than 1, it represents more rounded mitochondria, corresponding to the part above the dashed line in Graph A. When b divided by a is less than 1, it represents elongated mitochondria, corresponding to the part below the dashed line in Graph A.

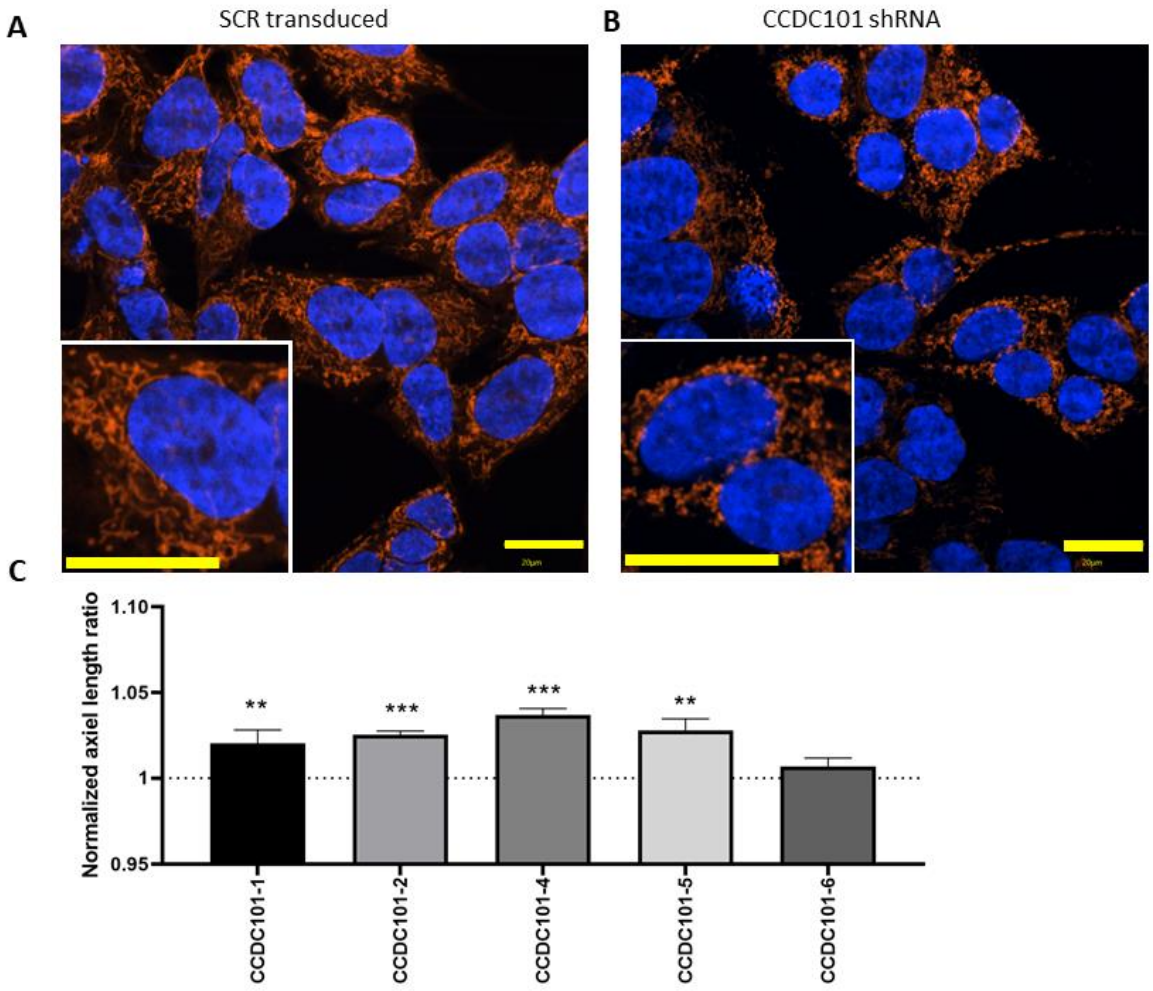

Figure 14. The most increased axial length ratio of mitochondrial from mitochondrial morphology assay. Cells are labeled for nuclei (blue, Hoechst) and mitochondria (red, MitoTracker CMXros). The negative control that cells transduced with scrambled is shown in Graph A. Compared to the negative control, cells infected with CCDC101 shRNA increase the axial length ratio of mitochondrial (B). Graph C displays the normalized axial length ratio of mitochondria. All the data were normalized to the negative control. Error bars are the standard deviation (SD) of the mean. For each group, n = 4. *P < 0.05, **P < 0.01, ***P < 0.001 for T-test with FDR correction. The scale bar for A and B is 20 μm.

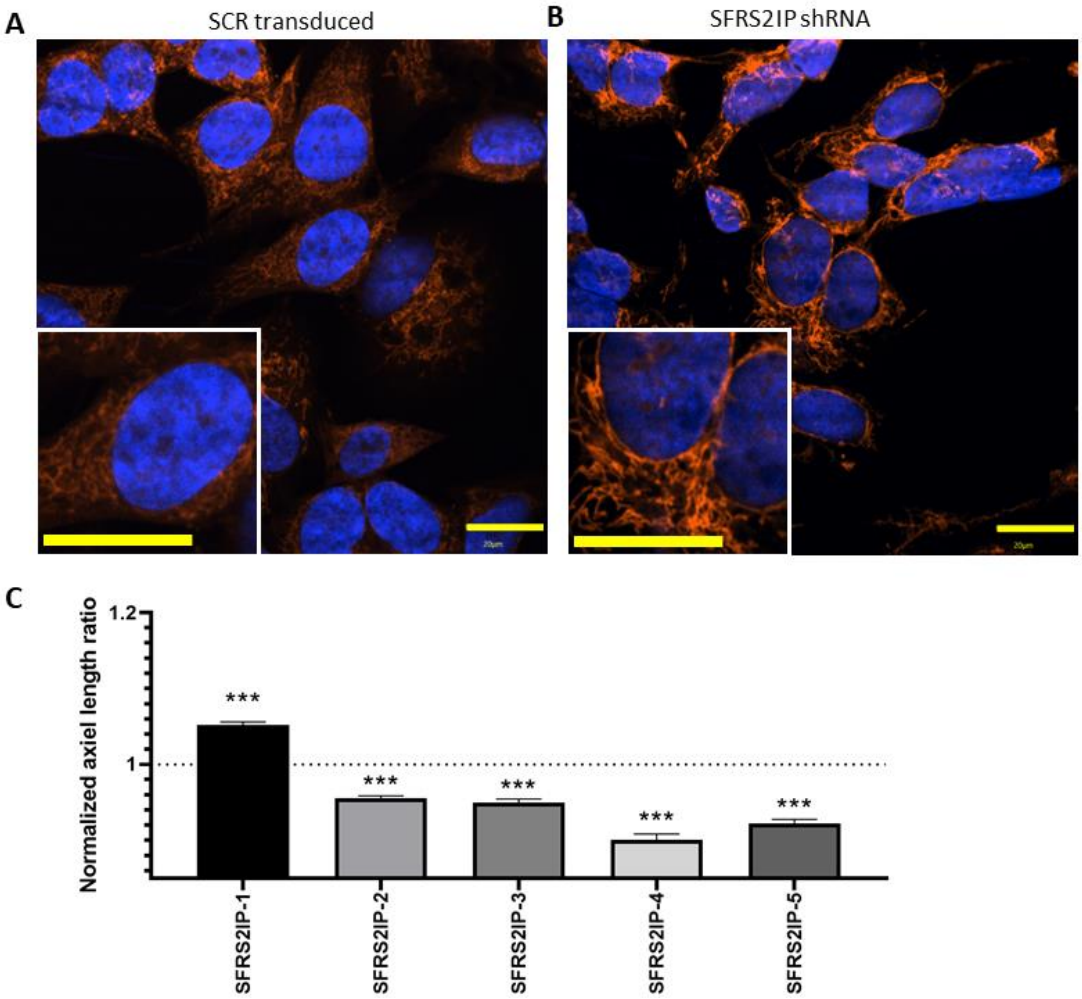

Figure 15. The most decreased axial length ratio of mitochondrial from mitochondrial morphology assay. Cells are labeled for nuclei (blue, Hoechst) and mitochondria (red, MitoTracker CMXros). The negative control that cells transduced with scrambled is shown in Graph A. Compared to the negative control, cells infected with SFRS2IP shRNA decrease the axial length ratio of mitochondria (B). Graph C displays the normalized axial length ratio of mitochondria. All the data were normalized to the negative control. Error bars are the standard deviation (SD) of the mean. For each group, n = 4. *P < 0.05, **P < 0.01, ***P < 0.001 for T-test with FDR correction. The scale bar for A and B is 20 µm.

4.3 Result of Parkin translocation assay

4.3.1 The plate-to-plate QC for Parkin translocation assay

The Z-factors for all the plates of the Parkin translocation assay are greater than 0.5 (Figure 16), and the average Z-factor for all the plates is 0.67, meaning that the quality of this assay is excellent.

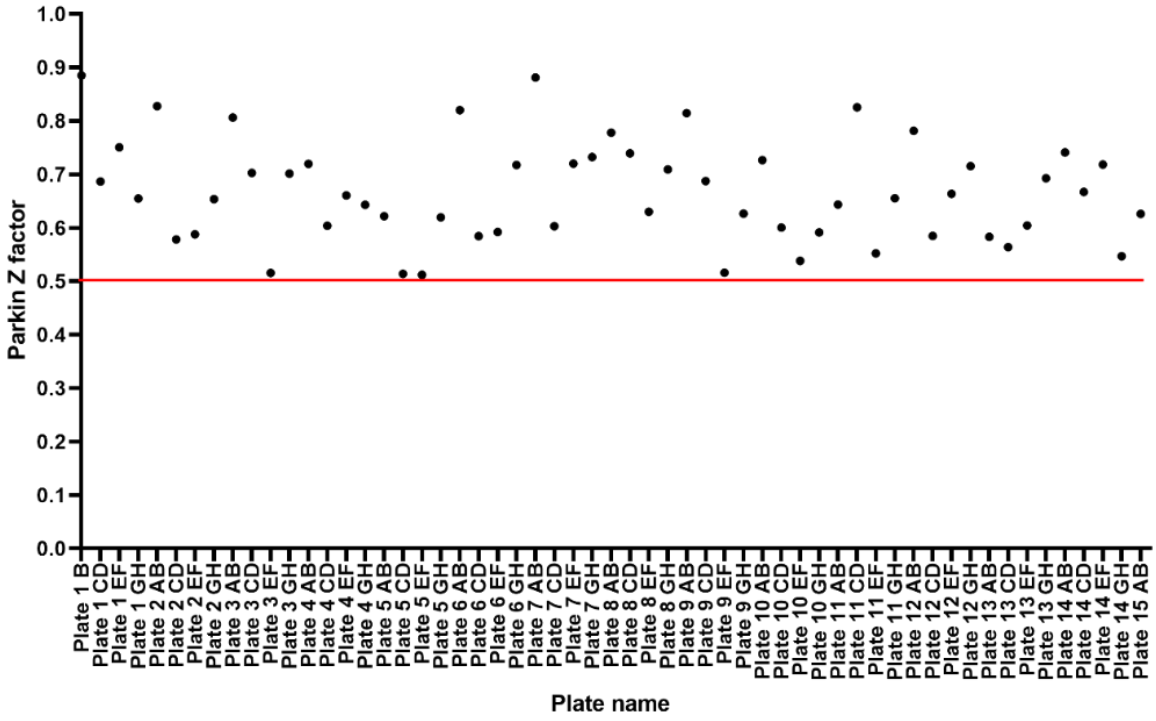

Figure 16. The Z-factor for all the plates of the Parkin translocation assay. In this figure, each spot represents the Z-factor for each plate.

4.3.2 Hits from Parkin translocation assay

In this assay, the ratio of positive Parkin translocation cells from each sample (treated with shRNA) was calculated and normalized by the negative control group. The SSMD was calculated for hit selection.

Based on the hit selection criteria according to SSMD, 29 hits were selected in this assay. For all the hits, the SSMDs of 27 hits are less than -3, and only the SSMD of SFRS2IP and MED12L are greater than 3 (Figure 17). This means that KD SFRS2IP and MED12L has the opposite effect on the ratio of positive Parkin translocation cells compared to the other 27 hits. The detailed hits information is shown in Table 8.

The normalized ratio of positive Parkin translocation cells of Parkin translocation assay hits is shown in Figure 18. Normally, Parkin scattered in the cell, when BE(2)-M17 eGFP-Parkin cells are exposed to mitochondrial toxicity and the electron transport chain uncoupler, CCCP, Parkin-GFP is translocated from the cytoplasm to the mitochondrial membrane. Compared to the negative control group, SFRS2IP-KD, and MED12L-KD show a significant increase in this ratio, and KD

the other 27 hits shows a significant decrease in this ratio (Figure 18). Compared to the negative control group (Figure 19A), SFRS2IP-KD shows the largest increase in positive Parkin translocation cells (Figure 19B, 19C), and CRLS1-KD shows the largest decrease in positive Parkin translocation cells (Figure 20).

Table 8. The information of Parkin translocation hits.

The Column "Suggested_gene" means if this gene was suggested as a priority test gene under this locus. The Column "Average Translocation_1st" means the average ratio of positive Parkin translocation cells of the 4 replicates of the most efficient shRNA, and the Column "Average Translocation_2nd" means the average ratio of positive Parkin translocation cells of the second efficient shRNA, same reasoning below. NA means no efficient shRNA data for its corresponding target. The average ratio of positive Parkin translocation cells of the negative control is 1.

Targets	**Locus Number**	**rsID**	**Brain Exp**	**Population**	**Sugested_gene**	**Average Translocation_1st**	**Average Translocation_2nd**	**Average Translocation_3rd**	**Average Translocation_4th**	**Average Translocation_5th**
NUCKS1	4	rs11557080	Yes	European	Y	0.495	NA	NA	NA	NA
NUCKS1	4	rs823118	Yes	European	Y	0.495	NA	NA	NA	NA
STK39	11	rs1474055	Yes	European	Y	0.756	0.439	0.426	NA	NA
NDUFAF3	14	rs12497850	Yes	European	Y	0.795	0.642	0.582	0.808	0.551
SLC25A20	14	rs12497850	Yes	European	Y	0.522	0.132	0.333	0.438	1.097
CCDC71	14	rs12497850	Yes	European	No	0.482	0.968	0.344	0.371	NA
MED12L	16	rs11707416	Yes	European	Y	0.757	1.496	1.627	NA	NA
B3GALNT1	17	rs1450522	Yes	European	Y	0.196	0.587	0.924	1.376	0.691

MCCC1	18	rs10513789	Yes	European	Y	0.627	1.285	NA	NA	NA
TMEM175	19	rs34311866	Yes	European	Y	0.353	0.573	NA	NA	NA
TMEM175	19	rs873786	Yes	European	Y	0.353	0.573	NA	NA	NA
CAMLG	28	rs11950533	Yes	European	Y	0.556	0.368	0.743	0.515	0.857
DDX46	28	rs11950533	Yes	European	No	0.438	0.325	0.312	1.033	NA
ZSCAN16	29	rs4140646	Yes	European	No	1.068	1.234	0.233	0.612	0.602
ZKSCAN8	29	rs4140646	Yes	European	No	0.313	0.503	0.316	0.777	0.772
ZNRD1	30	rs9261484	Yes	European	Y	0.307	0.634	1.381	1.516	0.514
CRCP	36	rs76949143	Yes	European	Y	0.373	0.552	0.865	0.439	0.872
BIN3	39	rs2280104	Yes	European	Y	0.275	0.315	0.473	NA	NA
UBAP2	42	rs6476434	Yes	European	No	0.814	0.470	0.535	NA	NA
SFRS2IP	50	rs7134559	Yes	European	Y	1.515	2.405	0.801	0.511	1.774
MBNL2	54	rs4771268	Yes	European	Y	1.254	0.426	0.662	NA	NA
RPS6KL1	57	rs3742785	Yes	European	No	0.316	0.492	0.476	0.266	0.571
PGF	57	rs3742785	Yes	European	Y	1.043	0.358	0.381	0.289	1.328

SULT1A1	61	rs2904880	Yes	European	Y	0.535	1.007	0.650	NA	NA
ZNF646	62	rs11150601	Yes	European	No	0.290	0.331	0.637	0.546	0.553
POLR2A	66	rs12600861	Yes	European	Y	1.044	0.451	0.558	1.148	0.295
WNT3	70	rs11658976	Yes	European	Y	0.973	0.437	0.386	1.683	0.372
INTS2	71	rs61169879	Yes	European	No	0.463	0.463	1.307	0.378	NA
CRLS1	77	rs77351827	Yes	European	Y	0.321	0.383	0.250	NA	NA
LRRN4	77	rs77351827	Yes	European	No	0.894	0.712	0.735	0.491	0.687

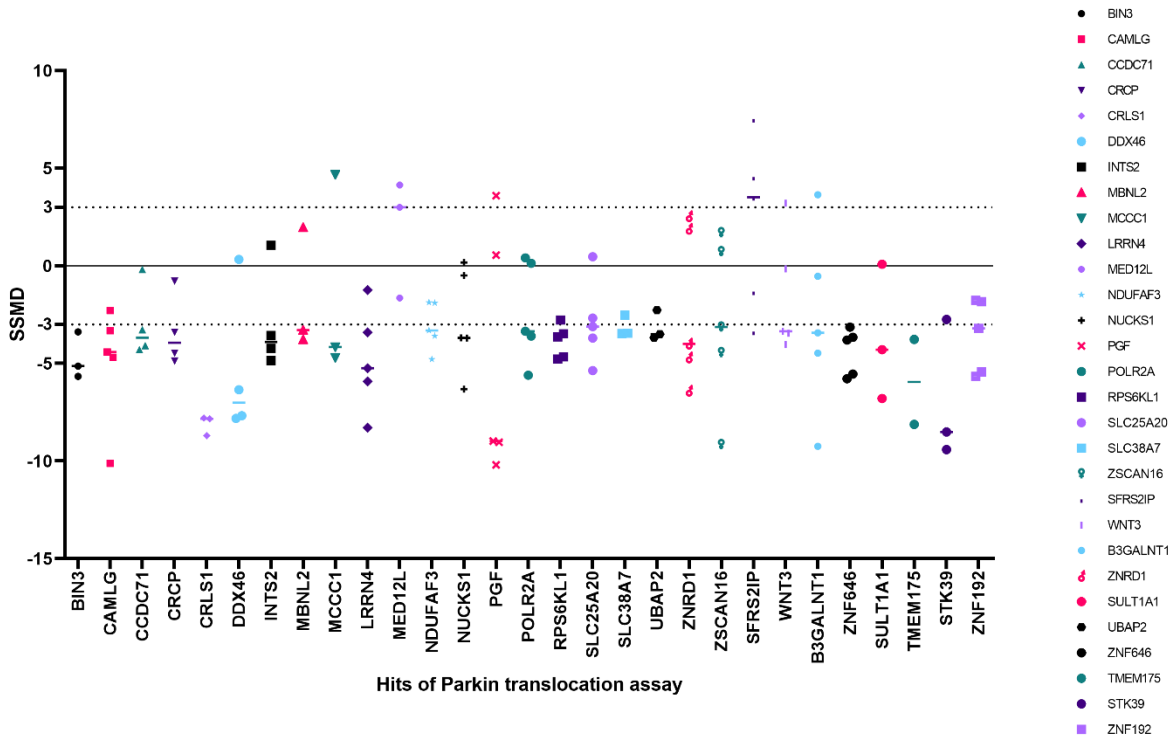

Figure 17. The SSMD of Parkin translocation assay hits. In this figure, each color represents the SSMD of each hit of the Parkin translocation assay based on the hit selection criteria. For each hit, there are 3 to 5 shRNA targeting it. For each hit, most of the shRNA targeting is either less than -3 or greater than 3.

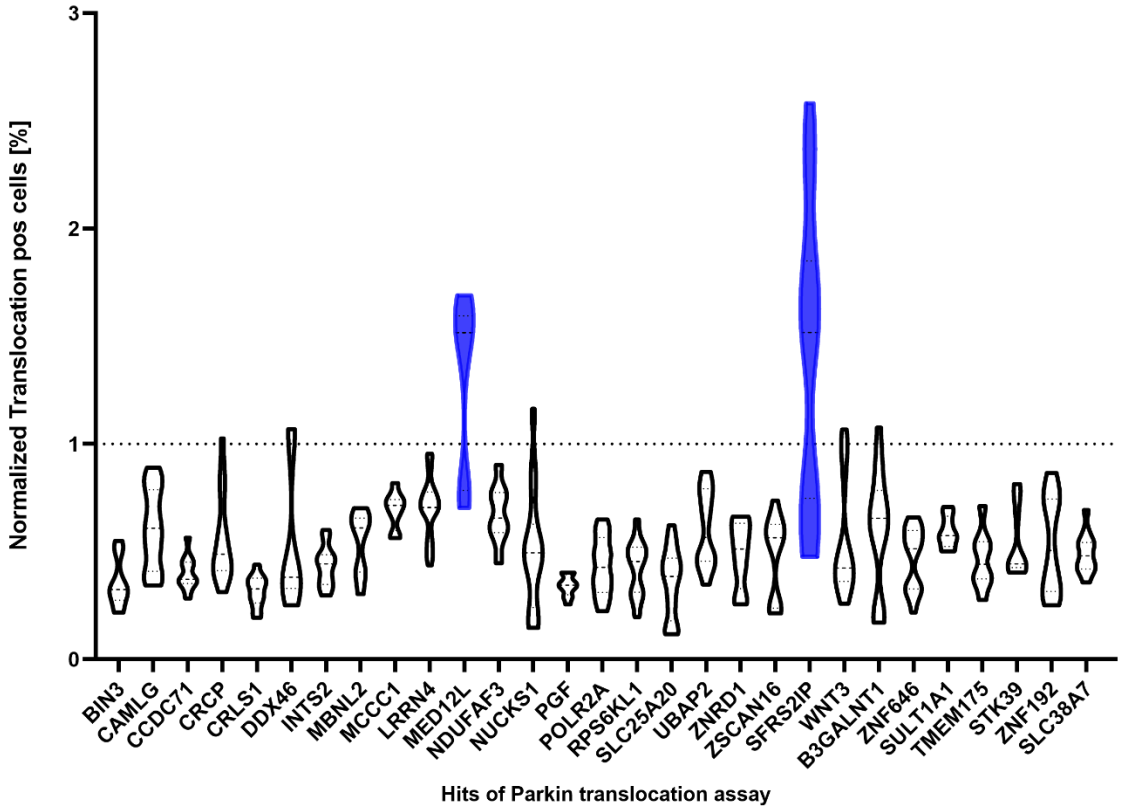

Figure 18. The normalized ratio of positive Parkin translocation cells from Parkin translocation assay hits. There are 4 replicates for each sample. The data was normalized by negative control. After normalization, the ratio of positive Parkin translocation cells of negative control is 1. Compared to the negative control, KD MED12L and SFRS2IP increase this ratio, while KD others decrease this ratio.

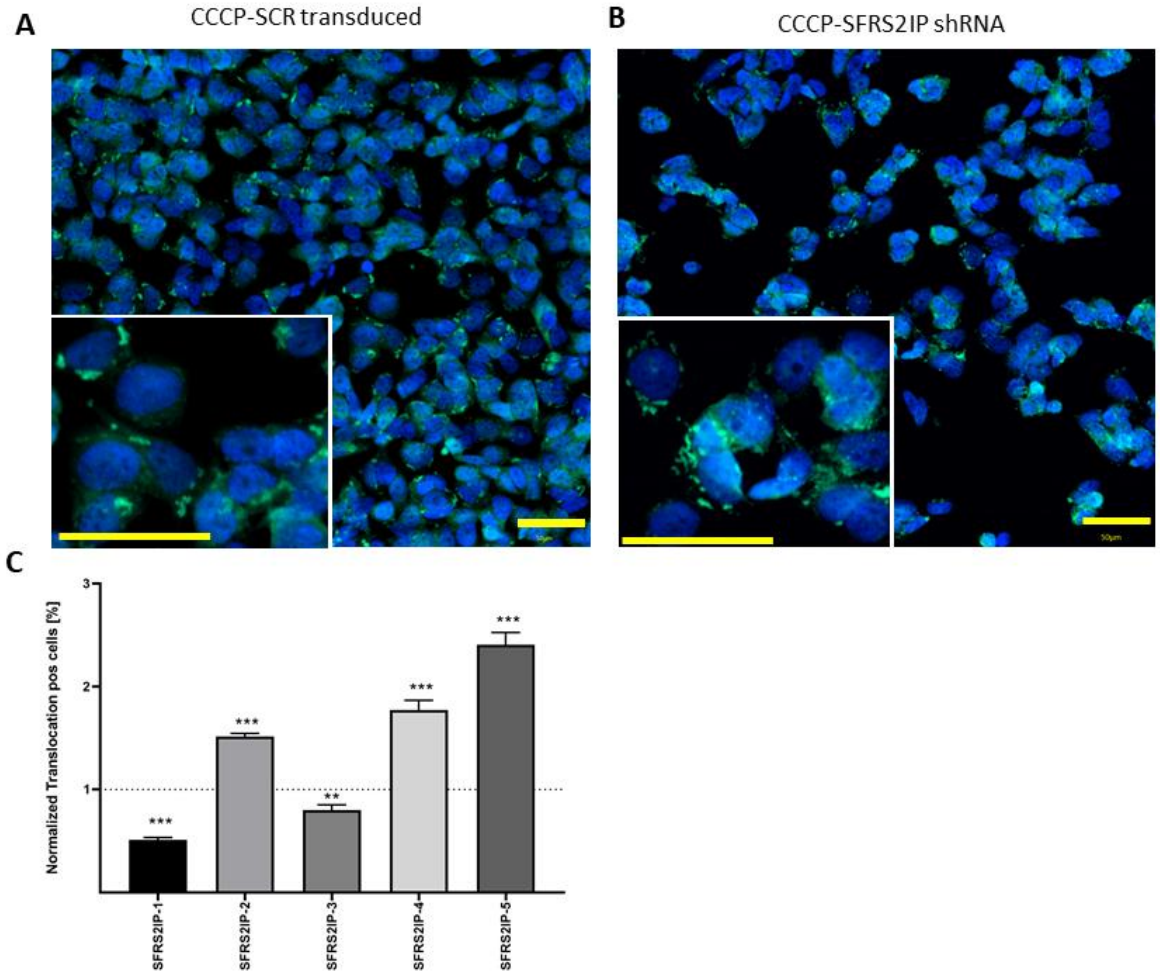

Figure 19. The most increased positive Parkin translocation cells from Parkin translocation assay. Cells are labeled for nuclei (blue, Hoechst), and Parkin-GFP (green). Cells transduced with scrambled and treated with CCCP (negative control) show a significant increase in spot formation (A). Cells infected with SFRS2IP shRNA increase the accumulation of spots (B). Graph C displays the normalized ratio of cells positive for parkin translocation and cells negative for translocation. All the data were normalized to the negative control. Error bars are the standard deviation (SD) of the mean. For each group, n = 4. *P < 0.05, **P < 0.01, ***P < 0.001 for T-test with FDR correction. The scale bar for A and B is 50 µm.

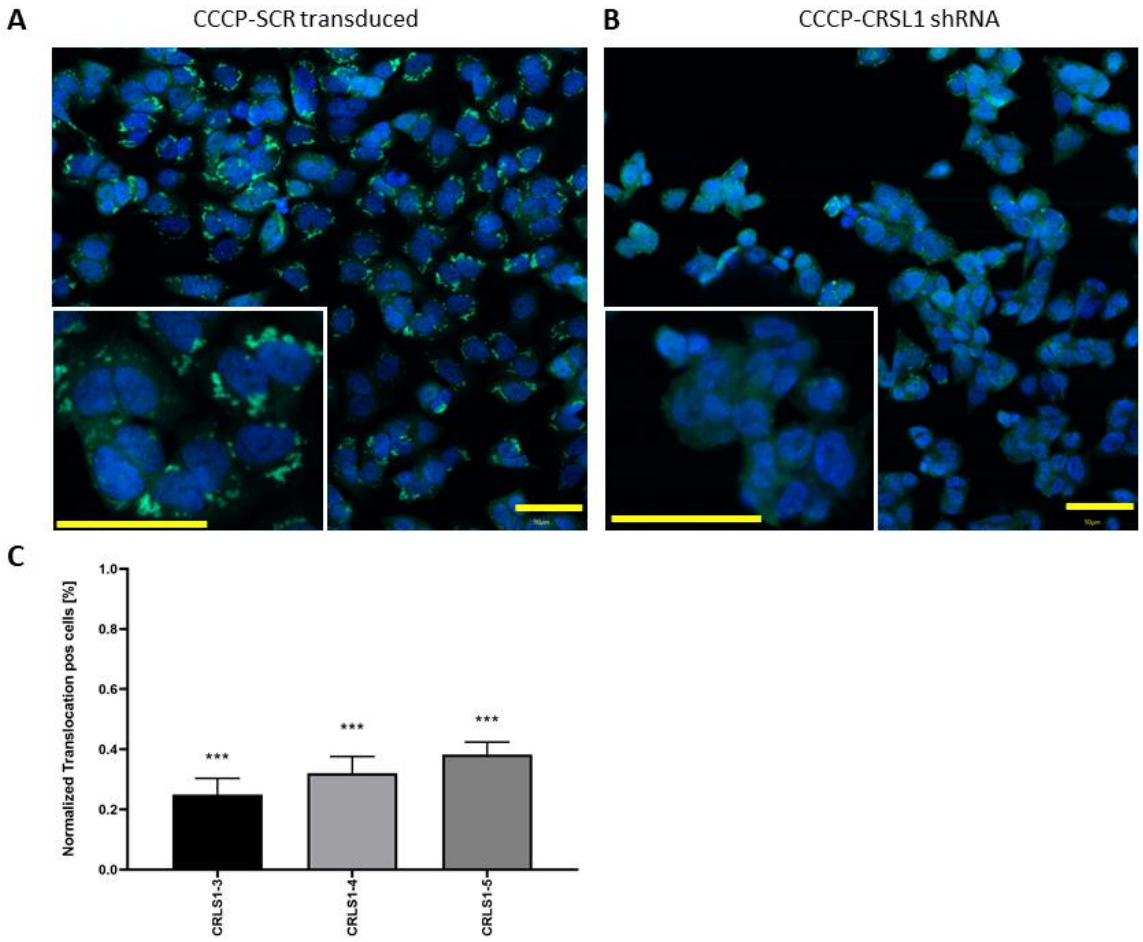

Figure 20. The most decreased positive Parkin translocation cells from Parkin translocation assay. Cells are labeled for nuclei (blue, Hoechst), Parkin-GFP (green). Cells transduced with scrambled and treated with CCCP (negative control) show a significant increase in spot formation (A). Cells infected with CRLS1 shRNA prevent the accumulation of spots (B). Graph C displays the normalized ratio of cells positive for parkin translocation and cells negative for translocation. All the data were normalized to the negative control. Error bars are the standard deviation (SD) of the mean. For each group, n = 4. *P < 0.05, **P < 0.01, ***P < 0.001 for T-test with FDR correction. The scale bar for A and B is 50 µm.

4.4 Result of α-synuclein ELISA

There are 8 experiment plates in this assay, with a negative control group treated with Scramble shRNA in each plate. For each plate, the α-synuclein (pg/µg) content normalized by total protein is shown in Figure 21. The percentage of α-synuclein increase or decrease per sample after normalization using the negative control group are shown in Figure 22A and Table 9.

Compare to the negative control group, the amount of α-synuclein increased by at least 50% in 39 targets (Table 9, Figure 22B). Among them, compare to the negative control group, CAMK2D-KD shows the largest increase of α-synuclein.

Compare to the negative control group, the amount of α-synuclein decreased at least 50% in 53 targets (Table 9, Figure 22B). Among them, compare to the negative control group, AMPD3-KD shows the largest decrease of α-synuclein. These samples, which increase or decrease 50% of α-synuclein were selected as hits.

Table 9. The information of α-synuclein ELISA hits.

The Column "Suggested_gene" means if this gene was suggested as a priority test gene under this locus. The Column "%increase of α-syn _1st" means the percentage of increase or decrease of α-synuclein protein level of the most efficient shRNA compared to the negative control.

Targets	Locus Number	rsID	Brain Exp	Population	MM hits	PT hits	ELISA hits	sugested_gene	%increase of α-syn _1st	T-test_1st
PBXIP1	1	rs114138760	Yes	European	N	N	decrease	No	-65.092	0.006273
PYGO2	1	rs114138760	Yes	European	N	N	decrease	Y	-61.152	0.007566
CKS1B	1	rs114138760	Yes	European	N	N	decrease	Y	-56.950	0.000842
PBXIP1	1	rs35749011	Yes	European	N	N	decrease	No	-65.092	0.006273
PYGO2	1	rs35749011	Yes	European	N	N	decrease	Y	-61.152	0.007566
ADAM15	1	rs35749011	Yes	European	N	N	decrease	No	-87.646	0.000029
HCN3	1	rs35749011	Yes	European	N	N	decrease	Y	-82.603	0.000041
CKS1B	1	rs35749011	Yes	European	N	N	decrease	No	-56.950	0.000842

ADAM15	1	rs76763715	Yes	European	N	N	decrease	Y	-87.646	0.000029
PYGO2	1	rs76763715	Yes	European	N	N	decrease	Y	-61.152	0.007566
PBXIP1	1	rs76763715	Yes	European	N	N	decrease	No	-65.092	0.006273
HCN3	1	rs76763715	Yes	European	N	N	decrease	Y	-82.603	0.000041
CKS1B	1	rs76763715	Yes	European	N	N	decrease	Y	-56.950	0.000842
NDUFAF3	14	rs12497850	Yes	European	Y	Y	decrease	Y	-53.882	0.013298
SLC25A20	14	rs12497850	Yes	European	N	Y	decrease	Y	-85.692	0.000358
ARIH2	14	rs12497850	Yes	European	Y	N	decrease	Y	-73.865	0.000091
P4HTM	14	rs12497850	Yes	European	N	N	decrease	No	-82.587	0.002111
CCDC71	14	rs12497850	Yes	European	N	Y	decrease	No	-67.752	0.000313
CCDC58	15	rs55961674	Yes	European	N	N	decrease	Y	-71.166	0.000242
PPM1L	17	rs1450522	Yes	European	N	N	decrease	Y	-54.582	0.012002
B3GALNT1	17	rs1450522	Yes	European	N	Y	decrease	Y	-81.710	0.000042
TMEM175	19	rs34311866	Yes	European	N	Y	decrease	Y	-61.874	0.000024
TMEM175	19	rs873786	Yes	European	N	Y	decrease	Y	-61.874	0.000024

CPLX1	19	rs873786	Yes	European	N	N	decrease	Y	-67.616	0.000291
BST1	20	rs4698412	Yes	European	N	N	decrease	Y	-82.392	0.000039
NUP54	22	rs6825004	Yes	European	Y	N	decrease	Y	-51.677	0.016191
SCARB2	22	rs6825004	Yes	European	N	N	decrease	No	-53.094	0.014144
GIN1	27	rs26431	Yes	European	N	N	decrease	No	-73.350	0.000068
PAM	27	rs26431	Yes	European	N	N	decrease	Y	-65.869	0.005411
PPIP5K2	27	rs26431	Yes	European	N	N	decrease	Y	-51.808	0.015739
C5orf30	27	rs26431	Yes	European	N	N	decrease	Y	-87.043	0.000032
PCBD2	28	rs11950533	Yes	European	N	N	decrease	No	-66.997	0.005199
DDX46	28	rs11950533	Yes	European	N	Y	decrease	No	-60.284	0.000118
SAR1B	28	rs11950533	Yes	European	Y	N	decrease	No	-50.262	0.008912
H3C12	29	rs4140646	Yes	European	N	N	decrease	Y	-54.278	0.000384
H2AC16	29	rs4140646	Yes	European	N	N	decrease	No	-89.372	0.000026
IGF2BP3	35	rs199351	Yes	European	Y	N	decrease	No	-64.894	0.000517
TMEM248	36	rs769491 43	Yes	European	N	N	decrease	No	-52.922	0.003385

SBDS	36	rs7694 9143	Yes	European	N	N	decrease	No	-52.987	0.01442 7
ASL	36	rs7694 9143	Yes	European	N	N	decrease	No	-89.604	0.00002 8
CCAR2	39	rs2280 104	Yes	European	N	N	decrease	Y	-54.240	0.00263 2
C8orf58	39	rs2280 104	Yes	European	N	N	decrease	No	-82.216	0.00004 0
BIN3	39	rs2280 104	Yes	European	N	Y	decrease	Y	-84.837	0.00003 6
PRSS3	42	rs6476 434	Yes	European	N	N	decrease	Y	-74.551	0.00321 0
BAG3	45	rs1178 96735	Yes	European	N	N	decrease	Y	-85.548	0.00003 3
BAG3	45	rs7284 0788	Yes	European	N	N	decrease	Y	-85.548	0.00003 3
AMPD3	46	rs7938 782	Yes	European	N	N	decrease	No	-91.003	0.00002 4
ARID2	50	rs7134 559	Yes	European	Y	N	decrease	Y	-90.123	0.00002 5
HIP1R	51	rs1084 7864	Yes	European	N	N	decrease	Y	-71.795	0.00008 2
GCH1	56	rs1115 8026	Yes	European	N	N	decrease	Y	-89.780	0.00002 6
DLST	57	rs3742 785	Yes	European	N	N	decrease	No	-86.258	0.00009 1
PGF	57	rs3742 785	Yes	European	N	Y	decrease	Y	-52.501	0.01517 1
ATXN2L	61	rs2904 880	Yes	European	N	N	decrease	Y	-78.638	0.00005 1

SULT1A1	61	rs2904880	Yes	European	N	Y	decrease	Y	-63.306	0.001730
NFATC2IP	61	rs2904880	Yes	European	N	N	decrease	Y	-84.038	0.001913
SETD1A	62	rs11150601	Yes	European	N	N	decrease	Y	-56.259	0.002730
ZNF646	62	rs11150601	Yes	European	N	Y	decrease	No	-74.659	0.000009
BCL7C	62	rs11150601	Yes	European	N	N	decrease	Y	-86.559	0.000031
CYLD	63	rs6500328	Yes	European	N	N	decrease	Y	-56.601	0.000681
ATP6V0A1	67	rs12951632	Yes	European	N	N	decrease	No	-89.581	0.000029
KANSL1	69	rs117615688	Yes	European	N	N	decrease	Y	-67.681	0.001575
KANSL1	69	rs62053943	Yes	European	N	N	decrease	Y	-67.681	0.001575
BRIP1	71	rs61169879	Yes	European	N	N	decrease	No	-77.944	0.000056
FLAD1	1	rs114138760	Yes	European	N	N	increase	No	294.584	0.013557
EFNA1	1	rs35749011	Yes	European	N	N	increase	Y	98.969	0.100116
FLAD1	1	rs35749011	Yes	European	N	N	increase	No	294.584	0.013557
FDPS	1	rs35749011	Yes	European	N	N	increase	Y	80.163	0.001601
SCAMP3	1	rs35749011	Yes	European	N	N	increase	No	62.422	0.003720

KRTCAP2	1	rs35749011	Yes	European	Y	N	increase	No	100.611	0.010958
SCAMP3	1	rs76763715	Yes	European	N	N	increase	Y	62.422	0.003720
EFNA1	1	rs76763715	Yes	European	N	N	increase	No	98.969	0.100116
FLAD1	1	rs76763715	Yes	European	N	N	increase	No	294.584	0.013557
KRTCAP2	1	rs76763715	Yes	European	Y	N	increase	Y	100.611	0.010958
FDPS	1	rs76763715	Yes	European	N	N	increase	Y	80.163	0.001601
VAMP4	3	rs11578699	Yes	European	N	N	increase	Y	69.260	0.000057
ITPKB	5	rs4653767	Yes	European	N	N	increase	Y	122.476	0.001313
MRPS5	8	rs2042477	Yes	European	Y	N	increase	No	285.577	0.001377
IP6K2	14	rs12497850	Yes	European	N	N	increase	No	84.241	0.007380
LAMB2	14	rs12497850	Yes	European	Y	N	increase	Y	151.893	0.000080
WDR6	14	rs12497850	Yes	European	N	N	increase	Y	184.594	0.0000013
PARP9	15	rs55961674	Yes	European	Y	N	increase	No	94.243	0.000014
GAK	19	rs34311866	Yes	European	N	N	increase	Y	70.231	0.000025
GAK	19	rs873786	Yes	European	N	N	increase	Y	70.231	0.000025

CAMK2D	24	rs13117519	Yes	European	N	N	increase	Y	399.624	0.000004
CLCN3	25	rs62333164	Yes	European	Y	N	increase	Y	52.515	0.003751
ERCC8	26	rs1867598	Yes	European	Y	N	increase	No	52.481	0.011385
NDUFAF2	26	rs1867598	Yes	European	Y	N	increase	Y	70.106	0.000026
CAMLG	28	rs11950533	Yes	European	N	Y	increase	Y	256.326	0.000000
RPP21	30	rs9261484	Yes	European	Y	N	increase	Y	90.160	0.003613
ZNRD1	30	rs9261484	Yes	European	Y	Y	increase	Y	97.027	0.000138
FYN	33	rs997368	Yes	European	Y	N	increase	Y	151.958	0.005998
SLC18B1	34	rs75859381	Yes	European	N	N	increase	Y	129.360	0.004508
KCTD7	36	rs76949143	Yes	European	N	N	increase	No	139.583	0.000200
RABGEF1	36	rs76949143	Yes	European	N	N	increase	Y	89.330	0.014548
ITGA8	43	rs896435	Yes	European	N	N	increase	Y	192.538	0.000050
INPP5F	45	rs11789735	Yes	European	N	N	increase	Y	75.609	0.004644
RNF141	46	rs7938782	Yes	European	N	N	increase	No	60.337	0.006836
SFRS2IP	50	rs7134559	Yes	European	Y	Y	increase	Y	69.630	0.002216

TUFM	61	rs2904880	Yes	European	N	N	increase	Y	90.638	0.000296
STX1B	62	rs11150601	Yes	European	N	N	increase	No	62.883	0.002641
ZBTB4	66	rs12600861	Yes	European	N	N	increase	Y	161.916	0.000011
POLR2A	66	rs12600861	Yes	European	Y	Y	increase	Y	82.612	0.002216
RETREG3	67	rs12951632	Yes	European	N	N	increase	Y	104.532	0.003195
WNT3	70	rs11658976	Yes	European	N	Y	increase	Y	134.460	0.000618
MED13	71	rs61169879	Yes	European	N	N	increase	Y	76.903	0.002798
NOL4	73	rs1941685	Yes	European	N	N	increase	Y	131.534	0.000073
MEX3C	75	rs8087969	Yes	European	Y	N	increase	Y	100.994	0.001064
SPPL2B	76	rs55818311	Yes	European	N	N	increase	Y	103.608	0.003040
DYRK1A	78	rs2248244	Yes	European	Y	N	increase	Y	110.106	0.000304

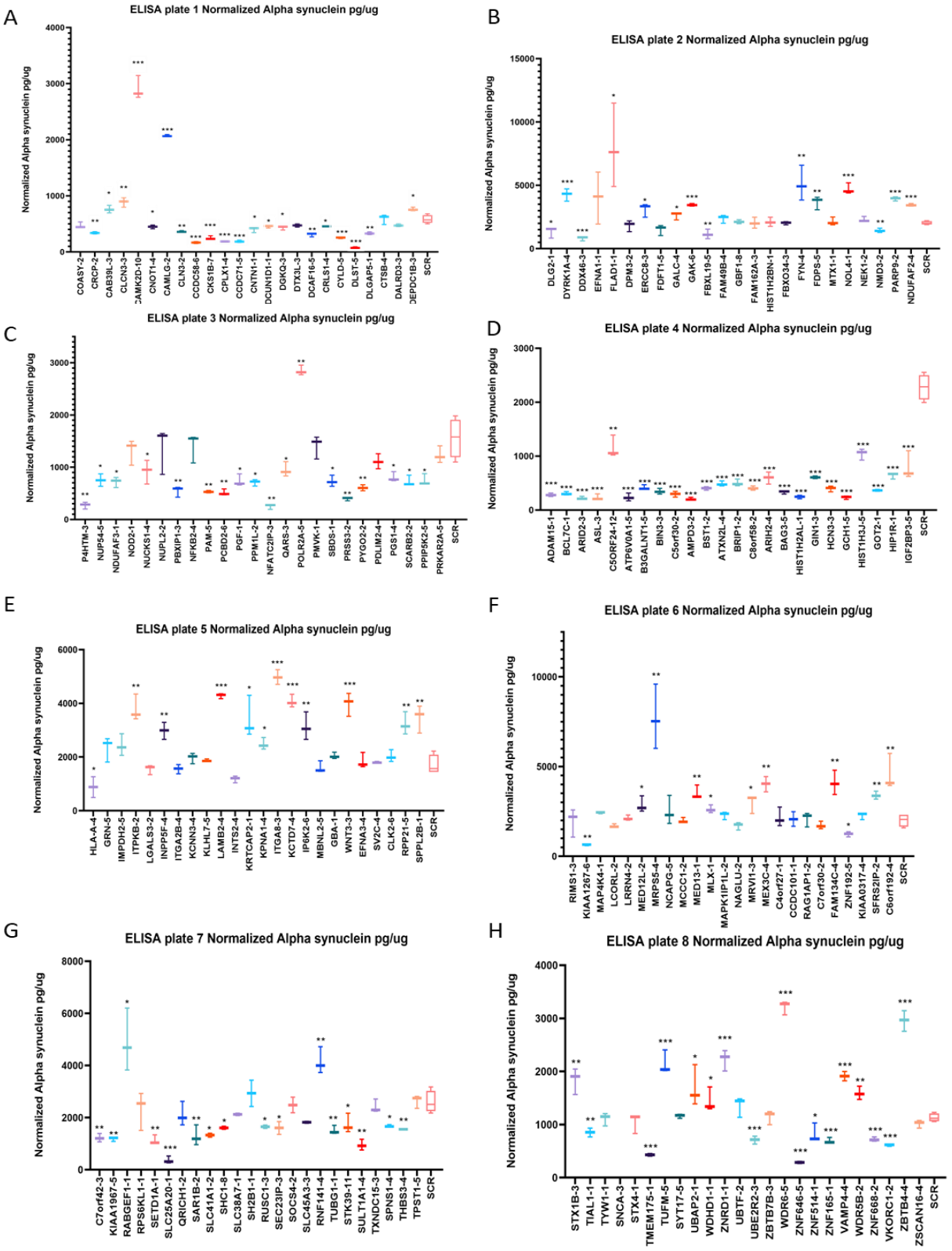

Figure 21. The normalized α-synuclein content in each experiment plate. A - H represents different plates. Each plate has 4 replicates for negative control (cells were transduced with scramble shRNA) and triplicates for each

experimental group. For each sample, α-synuclein content (pg) was normalized by using its total protein content (μg). *P < 0.05, **P < 0.01, ***P < 0.001 for T-test with FDR correction.

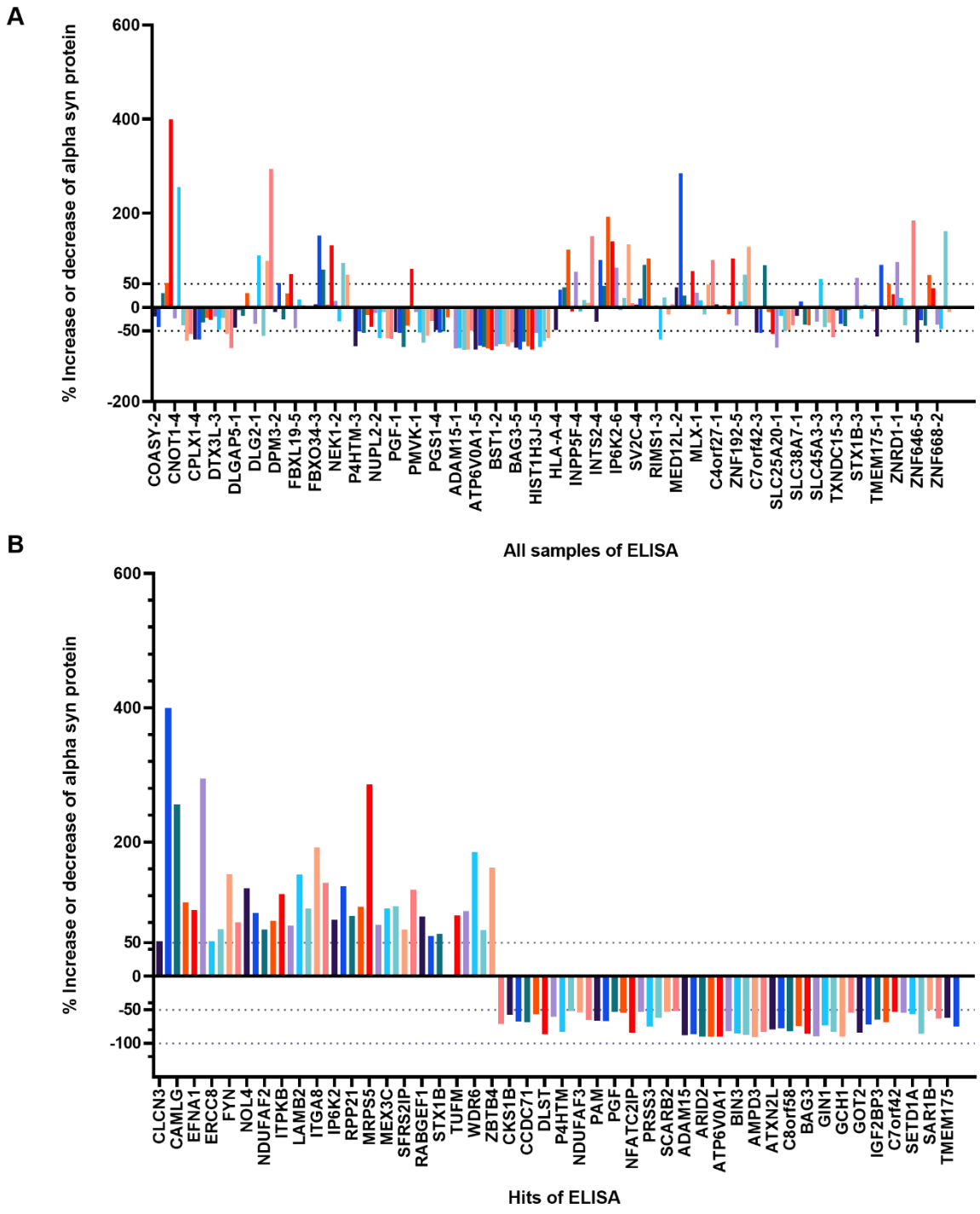

Figure 22. The percentage of increase or decrease of α-synuclein compared to negative control. After α-synuclein content (pg) was normalized by its total protein (μg), we calculated the increase or decrease percentage of α-synuclein

compared to negative control. In Graph A shows the increase or decrease percentage of α-synuclein for all the samples. In Graph B, the selected hits have at least 50% increase or decrease of α-synuclein.

4.5 Result of mRNA sequencing

4.5.1 The fold change result

The fold change was calculated to evaluate the KD efficiency for each sample. Only samples with a good KD efficiency (fold change less than -1) were included for further analysis. For samples with extremely low fold change (< -100), other parameters (e.g. gene expression levels, FDR) were examined to exclude abnormal values (Figure 23). For more details about mRNA sequencing QC results, please see supplementary material file 1 (https://github.com/Weiping123/PD-GWAS-project).

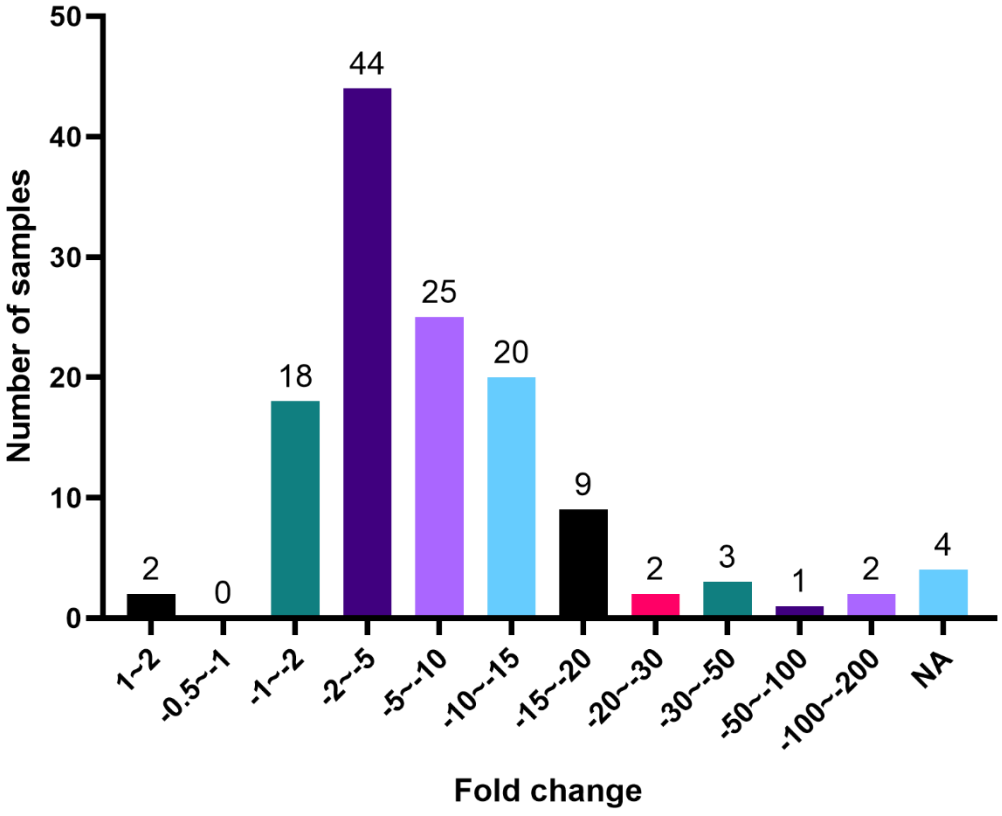

Figure 23. The fold change for mRNA sequencing samples. This figure shows the fold change for most of the samples is less than -1. This indicates that the majority of samples have a good KD effect. Samples with NA fold change, have 0 reads mapping to the target in both KD samples and the scramble controls. Samples with fold change over than one and NA were excluded from further data analysis.

4.5.2 The GO result

Since KD experiments were performed in a neuroblastoma cell line, the top 10 most frequent GO terms were all related to the cell cycle (Figure 24). These GO terms were GO:1903047 (mitotic cell cycle process), GO:0022402 (cell cycle process), GO:0051726 (regulation of cell cycle), GO:0006260 (DNA replication), GO:0010564 (regulation of cell cycle process), GO:0007346 (regulation of mitotic cell cycle), GO:0044770 (cell cycle phase transition), GO:0006259 (DNA metabolic process), GO:0007049 (cell cycle), GO:0044772 (mitotic cell cycle phase transition), respectively.

19 PD-related GO terms were prioritized based on their frequency of enrichment in the candidate KD samples. In these 19 GO terms, there are 4 GO terms related to protein targeting to ER (GO:0006614, GO:0072599, GO:0045047, GO:0070972), 5 GO terms related to mitogen-activated protein kinase (MAPK) activity (GO:1902949, GO:0000188, GO:0043407, GO:0043405, GO:1902947). The rest GO terms are related to organelle organization (GO:0033043), unfolded protein response (GO:0036499), apoptotic process (GO:0042981), programmed cell death (GO:0043067), neuron death (GO:1901214), neurogenesis (GO:0050767), cellular response to hypoxia (GO:0071456, GO:1900038), glucose metabolic process (GO:0006006) and catecholamine transport (GO:0051937), respectively. For more details about the GO terms of each sample, please see the supplementary material Table 2 (https://github.com/Weiping123/PD-GWAS-project).

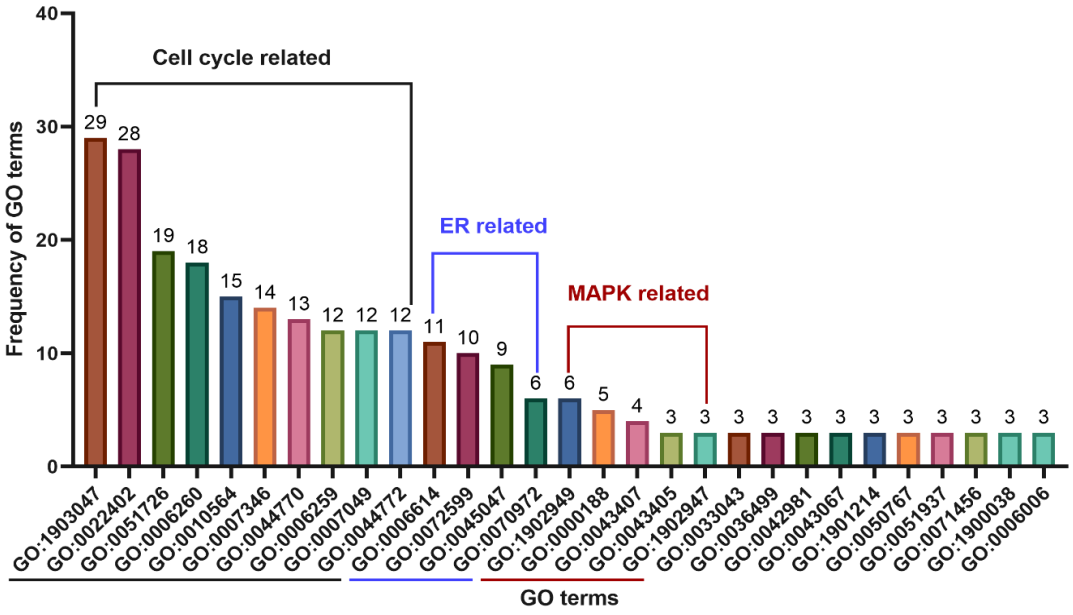

Figure 24. The frequency of the enriched GO terms across all KD samples. The top 10 most frequent GO terms are all cell circle-related (marked with black lines in the figure), probably due to the cell model used in this study. GO terms that might be associated with the onset of PD were selected among those with a frequency ⩾3. Two groups of related terms are marked with a square bracket, which are ER-related and MAPK-related. The remaining ungrouped GO terms are PERK-mediated unfolded protein response, regulation of the apoptotic process, cellular response to hypoxia, etc. The numbers on top of each GO term represent the number of samples in which the GO term is enriched.

After obtaining the priority GO terms, samples enriched for each prioritized GO term and the differentially expressed gene sets driving the terms were analyzed. There were 9 samples enriched for the term GO:0072599 (establishment of protein localization to endoplasmic reticulum, sample HIST1H3J was excluded due to fold change over 1, which signified the failure of KD). Knocking down samples ZBTB4 and ITPKB were enriched for this GO term via overexpression of the term-contributor genes; the rest of the KD samples were enriched for the GO term due to downregulation of the gene expression within a pathway (Figure 25). Interestingly, INPP5F and BAG3, both enriched for this GO term, are associated with the same SNP.

The research showed that KD of sample ZBTB4 resulted in upregulation of the apoptosis-inhibiting P21CiP, which in turn inhibited cyclin-dependent kinases (CDK) 2 and pro-apoptotic kinases apoptosis signal-regulating kinase 1 (ASK1) and c-Jun-N-terminale Kinase (JNK), ultimately leading to apoptosis inhibition (Blue et al. 2018; Weber et al. 2008). KD of sample ITPKB leads to the accumulation of Ca^{2+} in mitochondria. The accumulation of Ca^{2+} in

mitochondria triggers several responses, such as activation of respiration, accumulation of ROS, and activation of inhibitor of autophagy initiation mTOR, all of which ultimately lead to inhibition of autophagy (Apicco et al. 2021). The publication shows that upregulation of BAG3 mediates the disposal of damaged mitochondria and enhances autophagy. The overexpression of BAG3 mediates the initiation of the autophagy-lysosomal degradation pathway (Y.-L. Cao et al. 2017; Ying et al. 2022; Tahrir et al. 2017). INPP5F shares the same SNP (rs117896735) with BAG3, loss of function of INPP5F can lead to PD-related symptoms (M. Cao et al. 2020). However, INPP5F-KD did not affect the expression of BAG3, so both of them play a role in the pathogenesis of PD, but they might work independently. The other genes that drove this GO term were also checked to know the PD pathways they might be involved in. In this GO term (GO:0072599), KLHL7, FDPS, and CRCP could be good priority genes based on their molecular functions.

In addition to looking at the function of these genes that drove the GO terms, I also looked at the SNPs of these genes, as well as information on other candidate gene(s) located at the same SNP, to obtain more meaningful information to help us identify the causative gene for PD. POLR2A shares the same SNP (rs12600861) with ZBTB4, and inhibition of phosphorylation of POLR2A reduces PINK1-PRKM-mediated mitophagy (Yao et al. 2022). On the same SNP (rs76763715) with FDPS, there are also other candidate genes like EFNA1, KRTCAP2, ADAM15, HCN3, MTX1, RAG1AP1, RUSC1, SCAMP3, THBS3, CKS1B, PYGO2, PBXIP1. Among these genes, EFNA1 is involved in the MAPK signaling pathway, Ras signaling pathway, and PI3K-Akt signaling pathway, which all can contribute to PD. HCN3 regulates ion channel HCN3 as a likely contributor to altered neuronal excitability. MTX1 encodes a protein located in the OMM. Homozygosity for the MTX1 alteration induces an earlier onset of PD in affected patients. RUSC1 is involved in SNARE-associated proteins, and its encoding protein plays a role in neuronal differentiation. THBS3 shares a joint promoter with MTX1, and it can mediate ER stress and ER vesicular expansion through the transcription factor ATF6α. PYGO2 is involved in signal transduction through the Wnt pathway. There is no evidence of an association with PD for other genes on this SNP (rs76763715).

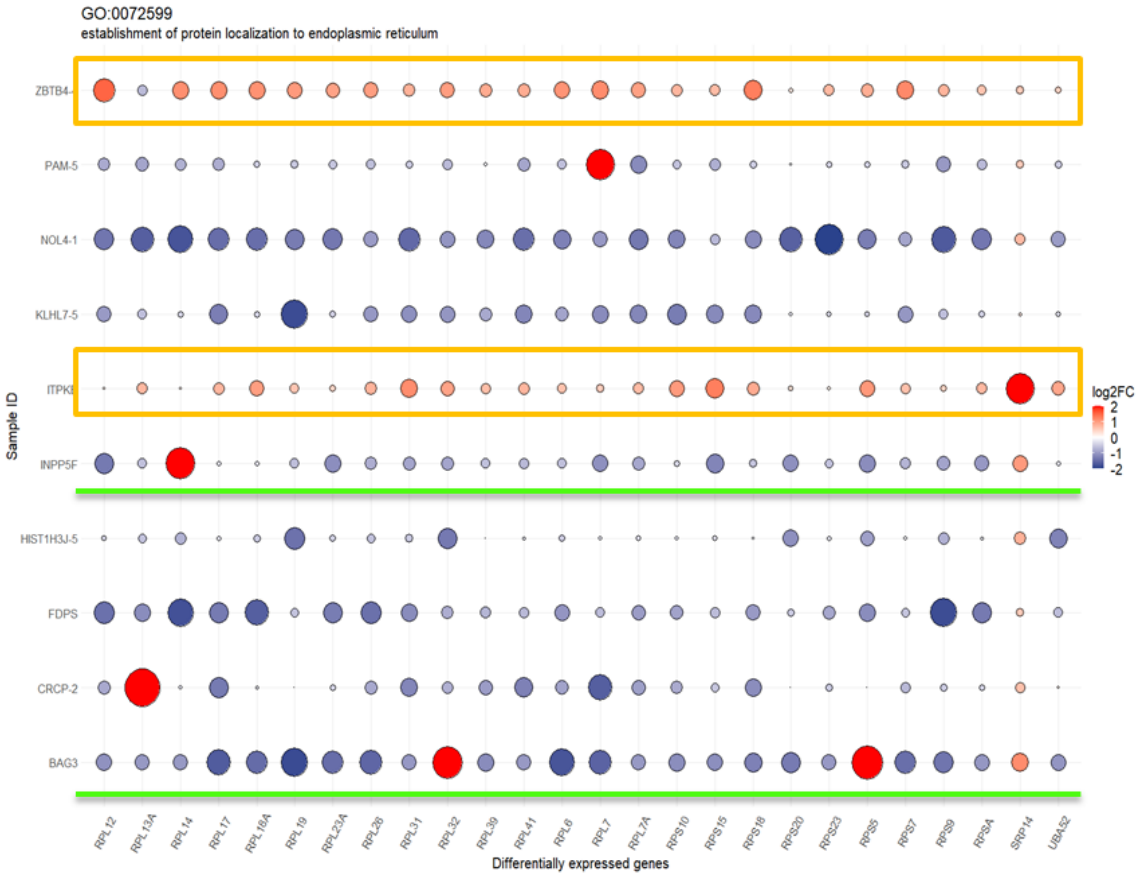

Figure 25. The bubble plot of GO:0072599. The genes on the X-axis represent the differentially expressed genes driving the GO term in specific KD samples annotated on the Y-axis. The color of the bubbles represents the value of log_2FC, red represents an increase in the gene expression ($log_2FC > 0$), and blue represents the down-regulation of gene expression ($log_2FC < 0$). Color brightness represents the effect size of log_2FC. The size of the bubbles represents the effect size. The bigger the bubble, the bigger the effect size.

5. Discussion

This study was based on 92 risk variants across 78 genomic regions (loci) identified by the GWAS. Of these 78 loci, 61 loci were included in the study, with all of the candidate genes located on 30 loci were included in the study, and some of the candidate genes located on 31 loci were included in the study. This study has screened some of the more critical loci (e.g. locus 17, locus 19, locus 33, locus 57, etc.) for us based on known PD risk loci by investigating mitochondrial morphology and function, α-synuclein protein content, etc., as well as suggesting priority genes to test for each locus (Supplementary Table 3, https://github.com/Weiping123/PD-GWAS-project).

The priority test genes suggested under each locus need to be given extra attention. The experimental data of this study suggests a link between certain genes with the known pathways affected in PD, including the effects on mitochondrial function and α-synuclein-mediated neuronal injury, as well as the PD-related pathways involved in the GO term by the KD of each gene. This information provides a substantial research base and reference material for subsequent studies. For the genes not selected for priority tests in this study, we cannot rule out the possibility that they may play a role in the pathogenesis of PD.

All these data generated in the functional assays, as well as mRNA sequencing data, will be made public for future PD risk variant investigations.

5.1 Hits from functional assays

5.1.1 Discussion of mitochondrial-related assays result

A large body of evidence suggests that mitochondrial morphology and mitophagy are implicated in the risk and pathological process of PD (Cookson 2012; Eldeeb et al. 2022; Park, Davis, and Sue 2018). Following shRNA-mediated KD, 49 genes (hits) showed the effect on mitochondrial morphology, 29 genes showed the effect on Parkin translocation to mitochondria in our cell model and 8 genes showed the effect on both assays, which are more likely to contribute to PD. I take 3 genes (CCDC101, SFRS2IP, CRLS1) for further discussion. CCDC101 is a prioritized candidate gene based on mitochondrial morphology assay. Its KD increased mitochondrial axial length ratio, potentially connected to mitochondrial fragmentation. The protein encoded by CCDC101 is a component of the chromatin-modifying SAGA complex (Guelman et al. 2009). Recent studies

have shown that the CCDC101-associated SAGA complex is a potent inhibitor of mTORC1, which is comprised of mTOR (Long et al. 2021; Z. Zhu et al. 2019). It is well known that mTOR plays an important role in many diseases, such as diabetes, obesity, depression, certain cancers, and aging (Beevers et al. 2006; Kennedy and Lamming 2016). The biological processes in which mTOR is involved include autophagy, clearance of damaged mitochondria and lysosomes, and response to ROS, which are all closely related to PD. Another study showed that CCDC101 plays a dual role in responding to ER stress. Before ER stress, CCDC101-encoded protein that coordinates tri-methylated lysine-4 of histone H3 (H3K4me3) levels, maintaining a "ready" chromatin state on the promoters of ER stress target genes. Following the induction of ER stress, CCDC101 is required to increase H3K14 acetylation on these genes, which leads to full transcriptional activation, thereby promoting cell survival (Schram et al. 2013). The mRNA sequencing results of this study showed that the downregulation of CCDC101 is associated with the upregulation of genes associated with glial cell differentiation (GO:0045687) as well as expression changes of the genes involved in the regulation of membrane fusion (GO:0061025). Under this SNP (rs2904880) of CCDC101, there are also other candidate genes, IL27, NUPR1, SULT1A1, MIR6862-2, TUFM, MIR4721, ATP2A1-AS1, MIR4517, SPNS1, CLN3, APOBR, SULT1A2, NPIPB8, EIF3C, NPIPB9, SH2B1, ATP2A1, RABEP2, CD19, LAT, ATXN2L, NFATC2IP, we tested 12 out of these candidate genes (SULT1A1, TUFM, SPNS1, CLN3, SULT1A2, EIF3C, SH2B1, ATP2A1, RABEP2, LAT, ATXN2L, NFATC2IP). Based on the literature and our experimental results, we suggest that CCDC101 may influence PD pathogenesis by affecting morphological changes in mitochondria and thus triggering a series of responses. Under this SNP, we also suggest further investigating SULT1A1, TUFM, ATXN2L, and NFATC2IP candidate genes as the PD risk factor.

SFRS2IP is another promising gene. It was selected based on the results of the mitochondrial morphology assay, Parkin translocation assay, and α-synuclein ELISA assay. SFRS2IP-KD significantly increased the axial length ratio and positive Parkin translocation cells, as well as increased α-synuclein protein level. It is well known that there is a close relationship between mitochondrial morphological changes and mitochondrial function (McCarron et al. 2013; MacVicar and Lane 2014; Galloway, Lee, and Yoon 2012; Picard et al. 2013). The increased axial length ratio can be interpreted as an observation of mitochondrial fission (Viana et al. 2020). Mitochondrial fission and fusion are thought to be associated with apoptosis and mitochondrial

quality control via autophagy (mitophagy), but there is a wealth of conflicting data. MacVicar and Lane suggested that the shift towards increased fission and decreased fusion promotes autophagy and degradation of the damaged mitochondria (MacVicar and Lane 2014). Other studies show that enhanced mitochondrial fission did not induce but protect against apoptosis (James and Martinou 2008; Perfettini, Roumier, and Kroemer 2005). Our experimental results show that downregulation leads to mitochondrial elongation and fusion increase, which in turn results in increased mitophagy. The results of this study, as well as published literature, both suggest the involvement of this gene in mitophagy. However, the previous research on this gene was limited, so there is a great need for additional functional testing and characterization in the future. Under this SNP (rs7134559), another candidate gene, ARID2, shows the effect on mitochondrial and α-synuclein protein level after downregulation. Taking together, under this SNP (rs7134559), we suggest that both SFRS2IP and ARID2 are priority genes for further investigation.

CRLS1-KD leads to mitochondrial effects, which decrease the mitochondrial axial length ratio and impaire Parkin translocation. CRLS1 encodes a protein that catalyzes the synthesis of cardiolipin, an essential phospholipid in the mitochondrial membrane that plays a vital role in maintaining the functional integrity and dynamics of mitochondria under stress. A recent study shows that CRLS1 defects impair mitochondrial morphology and biogenesis, which ultimately cause mitochondrial disease (Lee et al. 2022). Knockout of CRLS1 leads to mitochondrial fragmentation, which further causes mitochondrial and ER stress. This finding is consistent with our experimental result that knocking down CRLS1 reduces the axial length ratio. In addition, the degree of CRLS1 defect correlates with the degree of mitochondrial damage, with mild mitochondrial dysfunction manifested by activation of stress responses to rescue or compensate for defects. In contrast, severe mitochondrial dysfunction leads to organismal decline (Ren et al. 2023). There are also MCM8-AS1 and LRRN4 as candidate genes under this SNP (rs77351827). LRRN4 was included in this study, but downregulated it caused a decrease in Parkin-positive cells. We suggest CRLS1 and LRRN4 as priority test genes under this SNP (rs77351827).

5.1.2 Discussion of α-synuclein expression result

In addition to mitochondrial dysfunction, the aggregation of α-synuclein plays an essential role in the pathogenesis of PD. Based on the findings of this study and supported by information from the available literature, I will focus on two genes (CAMK2D, ZNRD1) in this section. CAMK2D is a

member of the Ca^{2+}/calmodulin-dependent protein kinase (CAMK) class of enzymes. CAMKII is a Ser/Thr kinase highly expressed in the striatum (Klug et al. 2012). It is involved in many biological processes, such as neuroplasticity regulation and brain damage repair(Lobo et al. 2015). CAMK2D was also linked to several pathways, such as the cAMP signaling pathway, Wnt signaling pathway, and more importantly, dopaminergic synapse, pathways of neurodegeneration (H. Zhang et al. 2020; Cong et al. 2014). All the information indicates that CAMK2D plays an important role in the development of PD. However, there are few studies on its specific pathways of action and pathogenic mechanisms. CAMK2D is the only candidate gene under this SNP (rs13117519), so there is no doubt that it is the priority gene for this SNP.

According to the experimental data of this study, ZNRD1 plays an important role in maintaining mitochondrial morphology, influencing Parkin translocation and the level of α-synuclein protein. KD of ZNRD1 reduces mitochondrial axial length ratio and Parkin translocation, increasing the aggregation of α-synuclein proteins. The mRNA sequencing results showed that the KD of ZNRD1 could drive negative regulation of mitochondrial fission. This result is consistent with the results of the mitochondrial morphology assay. However, most of the few available papers are about the role of ZNRD1 in cancer. ZNRD1 promotes the activation of the Wnt/β-catenin signaling pathway in hepatocellular carcinoma (Hu et al. 2019). No search was done for functional studies related to its involvement in PD. There is still much room for research on this gene. There are also HCP5B, HLA-H, HCG4B, HLA-A, HCG9, HLA-J, ZNRD1ASP, PPP1R11, RNF39, TRIM31, TRIM10, TRIM15, RPP21, TRIM31-AS1, TRIM40, TRIM26, HLA-L, TRIM39, TRIM39-RPP21, HCG17, HCG18 as candidate genes share the same SNP (rs9261484) with ZNRD1, HLA-A, PPP1R11 and RPP21 were included in this study. Considering the results of this study, we suggested ZNRD1 as the priority test gene under this SNP (rs9261484).

5.2 Data from mRNA sequencing

Despite RT-qPCR showing an efficient KD effect, we could not confirm it for 6 genes using mRNA sequencing analysis (HIST1H3J, RPP21, ITGA8, WNT3, BST1, KIAA1267) because of the abnormal fold change. Therefore, the mRNA sequencing data from these samples were unnecessary for subsequent analysis and excluded. In addition to these fold change abnormal genes, some genes such as LRRN4, PGF, CRCP, and SULT1A1 are expressed at very low levels in neuroblastoma cell lines, so extra attention should be paid to analyzing these genes.

We focused on the top 10 GO terms of each sample for subsequent analysis. In the analysis of GO terms, we prioritize the analysis of those GO terms with frequency ⩾ 3 samples and could be related to PD. Although we prioritized some GO terms with higher frequency of occurrence, low frequency GO terms with functional relevance allowed for the prioritization of the additional KD gene candidates. For example, both GO:0061025 (membrane fusion) and GO:0090258 (negative regulation of mitochondrial fission) are directly shown to be associated with membrane fusion and mitochondrial fragmentation. The enriched genes of those two GO terms are CCDC101 and ZNRD1, respectively, and as I mentioned in the above discussion, their GO terms are mutually supported by the experimental data of this study. In addition, other PD-related GO terms are enriched in only one sample (frequency＝1), such as GO:1903298 (negative regulation of hypoxia-induced intrinsic apoptotic signaling pathway), GO:0006986 (response to unfolded protein), GO:0051084 ('de novo' posttranslational protein folding), GO:0051085 (chaperone mediated protein folding requiring cofactor). The enriched genes corresponding to these GO terms are FAM49B, TUFM, GAK, and GAK.

FAM49B is a mitochondria-localized protein. It inhibits the activity of the small GTPase RAC1 and negatively regulates RAC1-driven cytoskeletal remodeling (Yuki et al. 2019; Fort et al. 2018; Shang et al. 2018). It has also been shown that FAM49B is associated with mitochondrial dynamics and oxidative stress (Chattaragada et al. 2018). Results from studies in pancreatic ductal adenocarcinoma cells show that silencing FAM49B leads to increased fission and mitochondrial ROS production (Chattaragada et al. 2018). Another study on diabetes showed that high glucose caused increased calcium levels. Elevated calcium levels act as an upstream signal for mitochondrial fragmentation causing mitochondrial fission and ROS accumulation (Yu, Jhun, and Yoon 2011; Yu, Robotham, and Yoon 2006). FAM49B, as a hit selected from the mitochondrial morphology assay, when down-regulated its expression can lead to a reduction in the axial length ratio of mitochondria, resulting in fragmentation of mitochondria, which is consistent with the findings of the above literature. Based on published literature and the experimental data, the downregulation of FAM49B led to mitochondria fragmentation and ROS accumulation, which caused oxidative stress and associated apoptosis.

TUFM is nuclear-encoded and plays a role in protein translation in mitochondria (Ling et al. 1997). It mediates the GTP-dependent binding of aminoacyl-tRNA to ribosomal A sites during protein

biosynthesis. According to available studies, TUFM functions also include recognition and translocation of co-translationally impaired proteins to the proteasome (Chuang et al. 2005), rearrangement of cytoskeletal components (Shiina et al. 1994; Gross and Kinzy 2005), and regulation of cell survival (Tong et al. 2005). It has also been shown that mutations in the TUFM gene are associated with defects in oxidative phosphorylation and can lead to fatal encephalopathy (Valente et al. 2007). A study on Alzheimer's disease (AD) demonstrated that KD of TUFM resulted in increased levels of cellular ROS and increased protein levels of β-amyloid protein (Aβ) and β-amyloid converting enzyme 1 (BACE1). TUFM is involved in AD by regulating BACE1 translation, apoptosis, and Tau phosphorylation (Zhong et al. 2021). However, there are no studies on the role of TUFM in the pathological process of PD. The results of α-synuclein ELISA showed that downregulation of TUFM resulted in elevated α-synuclein protein. In addition, mRNA sequencing results showed that this gene is involved in response to unfolded protein. These suggest that TUFM may be involved in the misfolding of α-synuclein proteins and the accumulation of misfolded α-synuclein proteins, further triggering PD.

GAK is a 160 kDa serine/threonine kinase, as well as a member of the J-domain-containing protein family, which can bind to heat shock 70kD proteins (HSP70s) and act as co-chaperones in a universal process that includes protein folding and degradation (Lin et al. 2018; Kampinga and Craig 2010). The above study is consistent with the experimental results of mRNA sequencing of this study. Another study showed that the clathrin-binding C-terminal domain of GAK can bind to pre-cathepsin D (CTSD), which is a major lysosomal enzyme involved in α-synuclein degradation (Tseng et al. 2013; Sevlever, Jiang, and Yen 2008). Mutation in CTSD can induce the aggregation of α-synuclein. Based on these findings, a study showed that downregulation of GAK enhances α-synuclein mediated toxicity (Dumitriu et al. 2011). This result is also consistent with the results of α-synuclein ELISA experiment of this study. Therefore, both the results of existing studies and the experimental results of this study demonstrate the close relationship between GAK and the development of PD.

Mentioning GAK, we also consider another gene, TMEM175, which shares the same SNP (rs873786, rs34311866) and promoter with GAK. However, it has the opposite biological role to GAK in the pathogenesis of PD. TMEM175 is the central potassium selective channel on endosomes and lysosomes, which regulates lysosomal pH, autophagosome turnover, and organelle

fusion (Cang et al. 2015; Wie et al. 2021). Dysregulation of TMEM175 caused the deficiency in autophagosome clearance is presumably causative for the aggregation of α-synuclein (Brunner et al. 2020). In addition to that, TMEM175 dysfunction also impairs lysosome-mediated mitophagy, leading to energy homeostasis deficiency (Jinn et al. 2017; Oh, Paknejad, and Hite 2020). Another study in cellular models found that KD of TMEM175 decreased GCase activity (Krohn et al. 2020). All these effects of TMEM175 demonstrate a tight link to the primary neuropathology of PD. In this study, KD of TMEM175 showed a decrease in Parkin translocated cells and a decrease of α-syn protein level in α-synuclein ELISA experiments. Data from mRNA sequencing showed that downregulated TMEM175 can cause inactivation of MAPK activity, positive regulation of tau-protein kinase activity, and regulation of neuron death. These experimental results all point to the potential importance of TMEM175 in the pathogenesis of PD. However, the experimental data of α-synuclein ELISA in this study differs from the available literature, this might be because of the different PD models we adopted or might be caused by the activation of other pathways. On the other hand, GAK and TMEM175 do have opposite effects at the level of α-synuclein protein.

Considering the molecular function and locus information of GAK and TMEM175 together with the shared SNP, how they act in PD is a point of ongoing interest for scientists. It has been suggested that TMEM175 is a plausible and more important cause of PD by the variation of the locus (rs34311866) it is located in (Jinn et al. 2019). TMEM175 has two PD-associated variants, rs34311866 and rs873786. The literature mentions that at variant rs34311866, TMEM175 is the more significant PD-causing gene. And TMEM175 shares with GAK is variant rs873786. Taking this information together, we lean toward the view that both GAK and TMEM175 play an important role in the pathogenesis of PD and that both likely act independently. However, the specific mode of action and pathways of the two genes still need to be explored by more in-depth studies.

5.3 Limitations and outlooks of this study

Ideally, it would be best to find a cell line that expresses all the candidate genes and has the corresponding shRNAs available for KD of individual genes. However, after comprehensively comparing the number of candidate genes expressed in different cell lines, the availability of shRNAs, the resolution of mitochondrial morphology for image analysis, and whether SNCA is expressed. We finally chose BE(2)-M17 cell line, which expresses 245 candidate genes as the cell

model for this study. If one wants to study the effect of expression of all candidate genes on PD in the same cell line it is unlikely to be possible. Screening all candidate genes individually can only be achieved using different cell lines. If so, the rigor of the experiments and the comparability of the results are necessarily reduced. Another option, which might allow all genes to be studied in the same way, is to use iPSCs-induced neurons or microglia (Miller et al. 2013). However, this method is technically demanding, complex and expensive to perform experimentally. In practice, the feasibility of this option remains to be explored.

In this study, the shRNAs were used to interfere with gene expression when establishing the cell model to study the effect of downregulated genes on PD pathogenesis. RNAi temporarily reduces gene expression at the mRNA level and has highly consistent results between experiments. However, RNAi has an off-target effect, and incomplete silencing may not produce a strong signal to be detected in assays. To reduce the impact of off-target effects, we designed at least 3 shRNAs for each gene. Beyond that, another thing we should consider is that some genes act on PD not by loss-of-function but by gain-of-function, such as LRRK2, SNCA, etc. (Somayaji et al. 2021; Blanca Ramírez et al. 2017). Thus, genes that affect the pathological process of PD through upregulation of gene expression might be missed. In this regard, the CRISPR technology can be used to fill this gap. CRISPR can cause permanent mutations at the DNA level. Compared to RNAi, CRISPR is more efficient, robust, specific and has fewer off-target effects. What is more, we can achieve gene activation (CRISPRa) and gene ablation (CRISPR ko), gene interference (CRISPRi), and epigenetic silencing (CRISPR off) by CRISPR. Overall, the application of CRISPR will be more comprehensive and efficient in studying the effect of activation or ablation of each gene on PD. The latest research from Yin has constructed available arrayed CRISPR libraries, which makes it even easier to carry out further experiments (Yin et al. 2022).

To more comprehensively study the effects on different organelles after the down-regulation of candidate genes, the inclusion of more targeted assays can be considered when designing assays. For example, the lysosomal enzyme activity assay could be used to assess lysosomal function, and the MPP+ neuronal cell death assay could be used to assess neuronal death. Seahorse assay could be used to assess cellular energy metabolism. Cell painting can also be used to characterize the morphology features of multiple organelles simultaneously.

In conclusion, this study provides a good research strategy for experiments on the type of pathogenic gene screening. It also provides us with a subset of priority genes for further investigation. Based on the results of this study, we can use different cell types such as iPS-induced neurons or glial cells, applying methods, such as CRISPRa or CRISPR off to achieve individual candidate gene perturbation and use more comprehensive assays for multifaceted validation analyses. All in all, the results of this study are exciting, and we are one step closer to figuring out the PD genetic landscape.

Statement of personal contributions

The idea for this project came from Prof. Dr. Peter Heutink. The 92 PD-associated SNPs across 78 risk loci were derived from literature reports, and the list of candidate genes derived from the 92 SNPs was completed by Anastasia Illarionova. Based on the expression levels of candidate genes in cellular models and shRNAs available in our Mission shRNA library (from Sigma), Joachim Taeger selected 245 genes for the list of genes studied in this study. Below, I will list each part of the experiment in detail, with the participation of each person.

Idea and study design: Prof. Dr. Peter Heutink.

Plasmid production and lentivirus production: The vast majority of plasmid production and lentivirus production was done by Joachim Taeger. I produced a small percentage of specific plasmid and lentiviral shortages.

Functional assays (mitochondrial morphology assay, Parkin translocation assay, α-synuclein ELISA): All pre-experiments and practical experiments were done by myself. Joachim Taeger gave pre-experimental guidance at the beginning of the mitochondria morphology assay and Parkin translocation assay. Salvador Rodriguez-Nieto gave advice and guidance in terms of trouble shooting of α-synuclein ELISA pre-experiments.

Sample preparation for RNA isolation: I was in charge of cell culture and treated the cells with shRNA to perform gene knockdown. On the last day of sample collection, Joachim Taeger helped me with collecting the samples using the Hamilton system.

RT-qPCR: All experimental operations are done by myself. These include RNA isolation, cDNA synthesis, primer design, etc. Melissa Castillo Lizardo helped me with RNA quantification.

Library preparation for mRNA sequencing: Melissa Castillo Lizardo.

Data analysis: The data analysis for functional assays was done by myself. The mRNA sequencing data analysis was done with the help of Mohammed Dehestani and Natalia Savytska. Mohammed Dehestani helped me to integrate the GO terms for each gene and generate a table of GO term frequency. Natalia Savytska helped me to compose tables and set up a working pipeline of bubble plots for each GO term.

Thesis writing: I wrote the thesis independently and was supervised by Prof. Peter Heutink in the revision of the thesis.

In conclusion, the general framework of the project was designed by Prof. Peter Heutink, and I took the lead in the advancement of the project, including the pre-experiment, the operation of the experiment, the data processing and analysis, as well as the interpretation of the data.

Bibliography

Abeliovich, A, Y Schmitz, I Fariñas, D Choi-Lundberg, W H Ho, P E Castillo, N Shinsky, et al. 2000. “Mice Lacking Alpha-Synuclein Display Functional Deficits in the Nigrostriatal Dopamine System.” *Neuron* 25 (1): 239–52. https://doi.org/10.1016/s0896-6273(00)80886-7.

Al Amir Dache, Zahra, Amaëlle Otandault, Rita Tanos, Brice Pastor, Romain Meddeb, Cynthia Sanchez, Giuseppe Arena, et al. 2020. “Blood Contains Circulating Cell-Free Respiratory Competent Mitochondria.” The FASEB Journal 34 (3): 3616–30. https://doi.org/10.1096/fj.201901917RR.

Alexander, G E, M R DeLong, and P L Strick. 1986. “Parallel Organization of Functionally Segregated Circuits Linking Basal Ganglia and Cortex.” Annual Review of Neuroscience 9: 357–81. https://doi.org/10.1146/annurev.ne.09.030186.002041.

Antony, Paul M A, Nico J Diederich, Rejko Krüger, and Rudi Balling. 2013. “The Hallmarks of Parkinson’s Disease.” The FEBS Journal 280 (23): 5981–93. https://doi.org/10.1111/febs.12335.

Apicco, Daniel J, Evgeny Shlevkov, Catherine L Nezich, David T Tran, Edward Guilmette, Justin W Nicholatos, Collin M Bantle, et al. 2021. “The Parkinson’s Disease-Associated Gene ITPKB Protects against α-Synuclein Aggregation by Regulating ER-to-Mitochondria Calcium Release.” Proceedings of the National Academy of Sciences of the United States of America 118 (1). https://doi.org/10.1073/pnas.2006476118.

Arias-Fuenzalida, Jonathan, Javier Jarazo, Xiaobing Qing, Jonas Walter, Gemma Gomez-Giro, Sarah Louise Nickels, Holm Zaehres, Hans Robert Schöler, and Jens Christian Schwamborn. 2017. “FACS-Assisted CRISPR-Cas9 Genome Editing Facilitates Parkinson’s Disease Modeling.” Stem Cell Reports 9 (5): 1423–31. https://doi.org/10.1016/j.stemcr.2017.08.026.

Balestrino, R, and A H V Schapira. 2020. “Parkinson Disease.” European Journal of Neurology 27 (1): 27–42. https://doi.org/10.1111/ene.14108.

Baptista, Melisa J, Casey O'Farrell, Sneha Daya, Rili Ahmad, David W Miller, John Hardy, Matthew J Farrer, and Mark R Cookson. 2003. "Co-Ordinate Transcriptional Regulation of Dopamine Synthesis Genes by Alpha-Synuclein in Human Neuroblastoma Cell Lines." Journal of Neurochemistry 85 (4): 957–68. https://doi.org/10.1046/j.1471-4159.2003.01742.x.

Beevers, Christopher S, Fengjun Li, Lei Liu, and Shile Huang. 2006. "Curcumin Inhibits the Mammalian Target of Rapamycin-Mediated Signaling Pathways in Cancer Cells." International Journal of Cancer 119 (4): 757–64. https://doi.org/10.1002/ijc.21932.

Beitz, Janice M. 2014. "Parkinson's Disease: A Review." Frontiers in Bioscience (Scholar Edition) 6 (January): 65–74. https://doi.org/10.2741/s415.

Blanca Ramírez, Marian, Jesus Madero-Perez, Pilar Rivero-Rios, Mar Martinez-Salvador, Antonio J Lara Ordonez, Belen Fernandez, Elena Fdez, and Sabine Hilfiker. 2017. "LRRK2 and Parkinson's Disease: From Lack of Structure to Gain of Function." Current Protein & Peptide Science 18 (7): 677–86. https://doi.org/10.2174/1389203717666160311121748.

Blauwendraat, Cornelis, Mike A Nalls, and Andrew B Singleton. 2020. "The Genetic Architecture of Parkinson's Disease." Lancet Neurology 19 (2): 170–78. https://doi.org/10.1016/S1474-4422(19)30287-X.

Blue, E E, C E Yu, T A Thornton, N H Chapman, E Kernfeld, N Jiang, K M Shively, et al. 2018. "Variants Regulating ZBTB4 Are Associated with Age-at-Onset of Alzheimer's Disease." Genes, Brain, and Behavior 17 (6): e12429. https://doi.org/10.1111/gbb.12429.

Blumenreich, Shani, Or B Barav, Bethan J Jenkins, and Anthony H Futerman. 2020. "Lysosomal Storage Disorders Shed Light on Lysosomal Dysfunction in Parkinson's Disease." International Journal of Molecular Sciences 21 (14). https://doi.org/10.3390/ijms21144966.

Borsche, Max, Sandro L Pereira, Christine Klein, and Anne Grünewald. 2021. "Mitochondria and Parkinson's Disease: Clinical, Molecular, and Translational Aspects." Journal of Parkinson's Disease 11 (1): 45–60. https://doi.org/10.3233/JPD-201981.

Brunner, Janine D, Roman P Jakob, Tobias Schulze, Yvonne Neldner, Anna Moroni, Gerhard Thiel, Timm Maier, and Stephan Schenck. 2020. “Structural Basis for Ion Selectivity in TMEM175 K+ Channels.” ELife 9 (April). https://doi.org/10.7554/eLife.53683.

Burré, Jacqueline, Manu Sharma, Theodoros Tsetsenis, Vladimir Buchman, Mark R Etherton, and Thomas C Südhof. 2010. “Alpha-Synuclein Promotes SNARE-Complex Assembly in Vivo and in Vitro.” Science 329 (5999): 1663–67. https://doi.org/10.1126/science.1195227.

Cabin, Deborah E, Kazuhiro Shimazu, Diane Murphy, Nelson B Cole, Wolfram Gottschalk, Kellie L McIlwain, Bonnie Orrison, et al. 2002. “Synaptic Vesicle Depletion Correlates with Attenuated Synaptic Responses to Prolonged Repetitive Stimulation in Mice Lacking Alpha-Synuclein.” The Journal of Neuroscience 22 (20): 8797–8807. https://doi.org/10.1523/JNEUROSCI.22-20-08797.2002.

Cang, Chunlei, Kimberly Aranda, Young-jun Seo, Bruno Gasnier, and Dejian Ren. 2015. “TMEM175 Is an Organelle K(+) Channel Regulating Lysosomal Function.” Cell 162 (5): 1101–12. https://doi.org/10.1016/j.cell.2015.08.002.

Cao, Mian, Daehun Park, Yumei Wu, and Pietro De Camilli. 2020. “Absence of Sac2/INPP5F Enhances the Phenotype of a Parkinson’s Disease Mutation of Synaptojanin 1.” Proceedings of the National Academy of Sciences of the United States of America 117 (22): 12428–34. https://doi.org/10.1073/pnas.2004335117.

Cao, Yu-Lan, Ya-Ping Yang, Cheng-Jie Mao, Xiao-Qi Zhang, Chen-Tao Wang, Jing Yang, Dong-Jun Lv, Fen Wang, Li-Fang Hu, and Chun-Feng Liu. 2017. “A Role of BAG3 in Regulating SNCA/α-Synuclein Clearance via Selective Macroautophagy.” Neurobiology of Aging 60 (December): 104–15. https://doi.org/10.1016/j.neurobiolaging.2017.08.023.

Carvajal-Oliveros, Angel, Maritere Uriostegui-Arcos, Mario Zurita, Erika I Melchy-Perez, Verónica Narváez-Padilla, and Enrique Reynaud. 2022. “The BE (2)-M17 Cell Line Has a Better Dopaminergic Phenotype than the Traditionally Used for Parkinson´s Research SH-SY5Y, Which Is Mostly Serotonergic.” IBRO Neuroscience Reports 13 (December): 543–51. https://doi.org/10.1016/j.ibneur.2022.11.007.

Chattaragada, M S, C Riganti, M Sassoe, M Principe, M M Santamorena, C Roux, C Curcio, et al. 2018. “FAM49B, a Novel Regulator of Mitochondrial Function and Integrity That Suppresses Tumor Metastasis.” Oncogene 37 (6): 697–709. https://doi.org/10.1038/onc.2017.358.

Chen, Zhichun, Guanglu Li, and Jun Liu. 2020. “Autonomic Dysfunction in Parkinson’s Disease: Implications for Pathophysiology, Diagnosis, and Treatment.” Neurobiology of Disease 134 (February): 104700. https://doi.org/10.1016/j.nbd.2019.104700.

Choong, Chi-Jing, and Hideki Mochizuki. 2022. “Neuropathology of α-Synuclein in Parkinson’s Disease.” Neuropathology 42 (2): 93–103. https://doi.org/10.1111/neup.12812.

Chuang, Show-Mei, Li Chen, David Lambertson, Monika Anand, Terri Goss Kinzy, and Kiran Madura. 2005. “Proteasome-Mediated Degradation of Cotranslationally Damaged Proteins Involves Translation Elongation Factor 1A.” Molecular and Cellular Biology 25 (1): 403–13. https://doi.org/10.1128/MCB.25.1.403-413.2005.

Church, Frank C. 2021. “Treatment Options for Motor and Non-Motor Symptoms of Parkinson’s Disease.” Biomolecules 11 (4). https://doi.org/10.3390/biom11040612.

Cong, Wei, Bo Liu, Shuqing Liu, Mingzhong Sun, Han Liu, Yue Yang, Ru Wang, and Jing Xiao. 2014. “Implications of the Wnt5a/CaMKII Pathway in Retinoic Acid-Induced Myogenic Tongue Abnormalities of Developing Mice.” Scientific Reports 4 (August): 6082. https://doi.org/10.1038/srep06082.

Cookson, Mark R. 2012. “Parkinsonism Due to Mutations in PINK1, Parkin, and DJ-1 and Oxidative Stress and Mitochondrial Pathways.” Cold Spring Harbor Perspectives in Medicine 2 (9): a009415. https://doi.org/10.1101/cshperspect.a009415.

Cooper, Antony A, Aaron D Gitler, Anil Cashikar, Cole M Haynes, Kathryn J Hill, Bhupinder Bhullar, Kangning Liu, et al. 2006. “Alpha-Synuclein Blocks ER-Golgi Traffic and Rab1 Rescues Neuron Loss in Parkinson’s Models.” Science 313 (5785): 324–28. https://doi.org/10.1126/science.1129462.

Cunningham, Fiona, James E Allen, Jamie Allen, Jorge Alvarez-Jarreta, M Ridwan Amode, Irina M Armean, Olanrewaju Austine-Orimoloye, et al. 2022. “Ensembl 2022.” Nucleic Acids Research 50 (D1): D988–95. https://doi.org/10.1093/nar/gkab1049.

Day, Jacob Oliver, and Stephen Mullin. 2021. “The Genetics of Parkinson’s Disease and Implications for Clinical Practice.” Genes 12 (7). https://doi.org/10.3390/genes12071006.

Devi, Latha, Vijayendran Raghavendran, Badanavalu M Prabhu, Narayan G Avadhani, and Hindupur K Anandatheerthavarada. 2008. “Mitochondrial Import and Accumulation of Alpha-Synuclein Impair Complex I in Human Dopaminergic Neuronal Cultures and Parkinson Disease Brain.” The Journal of Biological Chemistry 283 (14): 9089–9100. https://doi.org/10.1074/jbc.M710012200.

Dickson, Dennis W. 2018. “Neuropathology of Parkinson Disease.” Parkinsonism & Related Disorders 46 Suppl 1 (Suppl 1): S30–33. https://doi.org/10.1016/j.parkreldis.2017.07.033.

Doi, Daisuke, Hiroaki Magotani, Tetsuhiro Kikuchi, Megumi Ikeda, Satoe Hiramatsu, Kenji Yoshida, Naoki Amano, et al. 2020. “Pre-Clinical Study of Induced Pluripotent Stem Cell-Derived Dopaminergic Progenitor Cells for Parkinson’s Disease.” Nature Communications 11 (1): 3369. https://doi.org/10.1038/s41467-020-17165-w.

Dumitriu, Alexandra, Chris D Pacheco, Jemma B Wilk, Katherine E Strathearn, Jeanne C Latourelle, Stefano Goldwurm, Gianni Pezzoli, Jean-Christophe Rochet, Susan Lindquist, and Richard H Myers. 2011. “Cyclin-G-Associated Kinase Modifies α-Synuclein Expression Levels and Toxicity in Parkinson’s Disease: Results from the GenePD Study.” Human Molecular Genetics 20 (8): 1478–87. https://doi.org/10.1093/hmg/ddr026.

Eldeeb, Mohamed A, Rhalena A Thomas, Mohamed A Ragheb, Armaan Fallahi, and Edward A Fon. 2022. “Mitochondrial Quality Control in Health and in Parkinson’s Disease.” Physiological Reviews 102 (4): 1721–55. https://doi.org/10.1152/physrev.00041.2021.

Engelender, S, Z Kaminsky, X Guo, A H Sharp, R K Amaravi, J J Kleiderlein, R L Margolis, et al. 1999. “Synphilin-1 Associates with Alpha-Synuclein and Promotes the Formation of Cytosolic Inclusions.” Nature Genetics 22 (1): 110–14. https://doi.org/10.1038/8820.

Fahn, Stanley. 2018. “The 200-Year Journey of Parkinson Disease: Reflecting on the Past and Looking towards the Future.” Parkinsonism & Related Disorders 46 Suppl 1 (January): S1–5. https://doi.org/10.1016/j.parkreldis.2017.07.020.

Fernandes, Hugo J R, Elizabeth M Hartfield, Helen C Christian, Evangelia Emmanoulidou, Ying Zheng, Heather Booth, Helle Bogetofte, et al. 2016. “ER Stress and Autophagic Perturbations Lead to Elevated Extracellular α-Synuclein in GBA-N370S Parkinson’s IPSC-Derived Dopamine Neurons.” Stem Cell Reports 6 (3): 342–56. https://doi.org/10.1016/j.stemcr.2016.01.013.

Foo, Jia Nee, Elaine Guo Yan Chew, Sun Ju Chung, Rong Peng, Cornelis Blauwendraat, Mike A Nalls, Kin Y Mok, et al. 2020. “Identification of Risk Loci for Parkinson Disease in Asians and Comparison of Risk Between Asians and Europeans: A Genome-Wide Association Study.” JAMA Neurology 77 (6): 746–54. https://doi.org/10.1001/jamaneurol.2020.0428.

Fort, Loic, José Miguel Batista, Peter A Thomason, Heather J Spence, Jamie A Whitelaw, Luke Tweedy, Jennifer Greaves, et al. 2018. “Fam49/CYRI Interacts with Rac1 and Locally Suppresses Protrusions.” Nature Cell Biology 20 (10): 1159–71. https://doi.org/10.1038/s41556-018-0198-9.

Franco-Iborra, Sandra, Miquel Vila, and Celine Perier. 2016. “The Parkinson Disease Mitochondrial Hypothesis: Where Are We At?” The Neuroscientist 22 (3): 266–77. https://doi.org/10.1177/1073858415574600.

Frezza, Christian, Sara Cipolat, Olga Martins de Brito, Massimo Micaroni, Galina V Beznoussenko, Tomasz Rudka, Davide Bartoli, et al. 2006. “OPA1 Controls Apoptotic Cristae Remodeling Independently from Mitochondrial Fusion.” Cell 126 (1): 177–89. https://doi.org/10.1016/j.cell.2006.06.025.

Gadhe, Laxmikant, Arunima Sakunthala, Semanti Mukherjee, Nitisha Gahlot, Riya Bera, Ajay Singh Sawner, Pradeep Kadu, and Samir K Maji. 2022. “Intermediates of α-Synuclein Aggregation:

Implications in Parkinson's Disease Pathogenesis." Biophysical Chemistry 281 (February): 106736. https://doi.org/10.1016/j.bpc.2021.106736.

Gallagher, Michael D, and Alice S Chen-Plotkin. 2018. "The Post-GWAS Era: From Association to Function." American Journal of Human Genetics 102 (5): 717–30. https://doi.org/10.1016/j.ajhg.2018.04.002.

Galloway, Chad A, Hakjoo Lee, and Yisang Yoon. 2012. "Mitochondrial Morphology-Emerging Role in Bioenergetics." Free Radical Biology & Medicine 53 (12): 2218–28. https://doi.org/10.1016/j.freeradbiomed.2012.09.035.

Gąssowska, Magdalena, Grzegorz A Czapski, Beata Pająk, Magdalena Cieślik, Anna M Lenkiewicz, and Agata Adamczyk. 2014. "Extracellular α-Synuclein Leads to Microtubule Destabilization via GSK-3β-Dependent Tau Phosphorylation in PC12 Cells." Plos One 9 (4): e94259. https://doi.org/10.1371/journal.pone.0094259.

Geisler, Sven, Kira M Holmström, Diana Skujat, Fabienne C Fiesel, Oliver C Rothfuss, Philipp J Kahle, and Wolfdieter Springer. 2010. "PINK1/Parkin-Mediated Mitophagy Is Dependent on VDAC1 and P62/SQSTM1." Nature Cell Biology 12 (2): 119–31. https://doi.org/10.1038/ncb2012.

Gladkova, Christina, Sarah L Maslen, J Mark Skehel, and David Komander. 2018. "Mechanism of Parkin Activation by PINK1." Nature 559 (7714): 410–14. https://doi.org/10.1038/s41586-018-0224-x.

Grazioli, Serge, and Jérôme Pugin. 2018. "Mitochondrial Damage-Associated Molecular Patterns: From Inflammatory Signaling to Human Diseases." Frontiers in Immunology 9 (May): 832. https://doi.org/10.3389/fimmu.2018.00832.

Gross, Stephane R, and Terri Goss Kinzy. 2005. "Translation Elongation Factor 1A Is Essential for Regulation of the Actin Cytoskeleton and Cell Morphology." Nature Structural & Molecular Biology 12 (9): 772–78. https://doi.org/10.1038/nsmb979.

Guelman, Sebastián, Kenji Kozuka, Yifan Mao, Victoria Pham, Mark J Solloway, John Wang, Jiansheng Wu, Jennie R Lill, and Jiping Zha. 2009. “The Double-Histone-Acetyltransferase Complex ATAC Is Essential for Mammalian Development.” Molecular and Cellular Biology 29 (5): 1176–88. https://doi.org/10.1128/MCB.01599-08.

Hargittai, István. 2023. “Arvid Carlsson Centenary—Discoverer of Chemical Transmissions in the Brain.” Structural Chemistry, March. https://doi.org/10.1007/s11224-023-02159-3.

Hatano, Taku, Shin-ichiro Kubo, Shigeto Sato, and Nobutaka Hattori. 2009. “Pathogenesis of Familial Parkinson’s Disease: New Insights Based on Monogenic Forms of Parkinson’s Disease.” Journal of Neurochemistry 111 (5): 1075–93. https://doi.org/10.1111/j.1471-4159.2009.06403.x.

Henderson, Emily J, Stephen R Lord, Matthew A Brodie, Daisy M Gaunt, Andrew D Lawrence, Jacqueline C T Close, A L Whone, and Y Ben-Shlomo. 2016. “Rivastigmine for Gait Stability in Patients with Parkinson’s Disease (ReSPonD): A Randomised, Double-Blind, Placebo-Controlled, Phase 2 Trial.” Lancet Neurology 15 (3): 249–58. https://doi.org/10.1016/S1474-4422(15)00389-0.

Hershko, A, and A Ciechanover. 1998. “The Ubiquitin System.” Annual Review of Biochemistry 67: 425–79. https://doi.org/10.1146/annurev.biochem.67.1.425.

Holdorff, Bernd. 2002. “Friedrich Heinrich Lewy (1885-1950) and His Work.” Journal of the History of the Neurosciences 11 (1): 19–28. https://doi.org/10.1076/jhin.11.1.19.9106.

———. 2006. “Fritz Heinrich Lewy (1885-1950).” Journal of Neurology 253 (5): 677–78. https://doi.org/10.1007/s00415-006-0130-2.

Hu, Xiaobo, Ruifang Wang, Zhigang Ren, Xiaorui Liu, Junsheng Gu, Guangying Cui, and Qinggang Li. 2019. “MiR-26b Suppresses Hepatocellular Carcinoma Development by Negatively Regulating ZNRD1 and Wnt/β-Catenin Signaling.” Cancer Medicine 8 (17): 7359–71. https://doi.org/10.1002/cam4.2613.

Jagadeesan, A J, R Murugesan, S Vimala Devi, M Meera, G Madhumala, M Vishwanathan Padmaja, A Ramesh, et al. 2017. “Current Trends in Etiology, Prognosis and Therapeutic Aspects

of Parkinson's Disease: A Review." Acta Bio-Medica : Atenei Parmensis 88 (3): 249–62. https://doi.org/10.23750/abm.v88i3.6063.

James, Dominic I, and Jean-Claude Martinou. 2008. "Mitochondrial Dynamics and Apoptosis: A Painful Separation." Developmental Cell 15 (3): 341–43. https://doi.org/10.1016/j.devcel.2008.08.011.

Jankovic, Joseph, and Eng King Tan. 2020. "Parkinson's Disease: Etiopathogenesis and Treatment." Journal of Neurology, Neurosurgery, and Psychiatry 91 (8): 795–808. https://doi.org/10.1136/jnnp-2019-322338.

Jansen, Iris E, Hui Ye, Sasja Heetveld, Marie C Lechler, Helen Michels, Renée I Seinstra, Steven J Lubbe, et al. 2017. "Discovery and Functional Prioritization of Parkinson's Disease Candidate Genes from Large-Scale Whole Exome Sequencing." Genome Biology 18 (1): 22. https://doi.org/10.1186/s13059-017-1147-9.

Jenco, J M, A Rawlingson, B Daniels, and A J Morris. 1998. "Regulation of Phospholipase D2: Selective Inhibition of Mammalian Phospholipase D Isoenzymes by Alpha- and Beta-Synucleins." Biochemistry 37 (14): 4901–9. https://doi.org/10.1021/bi972776r.

Jinn, Sarah, Cornelis Blauwendraat, Dawn Toolan, Cheryl A Gretzula, Robert E Drolet, Sean Smith, Mike A Nalls, Jacob Marcus, Andrew B Singleton, and David J Stone. 2019. "Functionalization of the TMEM175 p.M393T Variant as a Risk Factor for Parkinson Disease." Human Molecular Genetics 28 (19): 3244–54. https://doi.org/10.1093/hmg/ddz136.

Jinn, Sarah, Robert E Drolet, Paige E Cramer, Andus Hon-Kit Wong, Dawn M Toolan, Cheryl A Gretzula, Bhavya Voleti, et al. 2017. "TMEM175 Deficiency Impairs Lysosomal and Mitochondrial Function and Increases α-Synuclein Aggregation." Proceedings of the National Academy of Sciences of the United States of America 114 (9): 2389–94. https://doi.org/10.1073/pnas.1616332114.

Kampinga, Harm H, and Elizabeth A Craig. 2010. “The HSP70 Chaperone Machinery: J Proteins as Drivers of Functional Specificity.” Nature Reviews. Molecular Cell Biology 11 (8): 579–92. https://doi.org/10.1038/nrm2941.

Kaufman, Randal J, and Jyoti D Malhotra. 2014. “Calcium Trafficking Integrates Endoplasmic Reticulum Function with Mitochondrial Bioenergetics.” Biochimica et Biophysica Acta 1843 (10): 2233–39. https://doi.org/10.1016/j.bbamcr.2014.03.022.

Kennedy, Brian K, and Dudley W Lamming. 2016. “The Mechanistic Target of Rapamycin: The Grand Conductor of Metabolism and Aging.” Cell Metabolism 23 (6): 990–1003. https://doi.org/10.1016/j.cmet.2016.05.009.

Kikuchi, Tetsuhiro, Asuka Morizane, Daisuke Doi, Hiroaki Magotani, Hirotaka Onoe, Takuya Hayashi, Hiroshi Mizuma, et al. 2017. “Human IPS Cell-Derived Dopaminergic Neurons Function in a Primate Parkinson’s Disease Model.” Nature 548 (7669): 592–96. https://doi.org/10.1038/nature23664.

Klein, Christine, and Ana Westenberger. 2012. “Genetics of Parkinson’s Disease.” Cold Spring Harbor Perspectives in Medicine 2 (1): a008888. https://doi.org/10.1101/cshperspect.a008888.

Klug, Jason R, Brian N Mathur, Thomas L Kash, Hui-Dong Wang, Robert T Matthews, A J Robison, Mark E Anderson, et al. 2012. “Genetic Inhibition of CaMKII in Dorsal Striatal Medium Spiny Neurons Reduces Functional Excitatory Synapses and Enhances Intrinsic Excitability.” Plos One 7 (9): e45323. https://doi.org/10.1371/journal.pone.0045323.

Koopman, Werner J H, Henk-Jan Visch, Jan A M Smeitink, and Peter H G M Willems. 2006. “Simultaneous Quantitative Measurement and Automated Analysis of Mitochondrial Morphology, Mass, Potential, and Motility in Living Human Skin Fibroblasts.” Cytometry. Part A: The Journal of the International Society for Analytical Cytology 69 (1): 1–12. https://doi.org/10.1002/cyto.a.20198.

Koros, Christos, Athina Simitsi, and Leonidas Stefanis. 2017. “Genetics of Parkinson’s Disease: Genotype-Phenotype Correlations.” International Review of Neurobiology 132 (March): 197–231. https://doi.org/10.1016/bs.irn.2017.01.009.

Krohn, Lynne, Tuğba Nur Öztürk, Benoît Vanderperre, Bouchra Ouled Amar Bencheikh, Jennifer A Ruskey, Sandra B Laurent, Dan Spiegelman, et al. 2020. “Genetic, Structural, and Functional Evidence Link TMEM175 to Synucleinopathies.” Annals of Neurology 87 (1): 139–53. https://doi.org/10.1002/ana.25629.

LaVoie, M J, and T G Hastings. 1999. “Dopamine Quinone Formation and Protein Modification Associated with the Striatal Neurotoxicity of Methamphetamine: Evidence against a Role for Extracellular Dopamine.” The Journal of Neuroscience 19 (4): 1484–91. https://doi.org/10.1523/JNEUROSCI.19-04-01484.1999.

Lebkowski, Jane. 2011. “GRNOPC1: The World’s First Embryonic Stem Cell-Derived Therapy. Interview with Jane Lebkowski.” Regenerative Medicine 6 (6 Suppl): 11–13. https://doi.org/10.2217/rme.11.77.

Lees, Andrew J, Eduardo Tolosa, and C Warren Olanow. 2015. “Four Pioneers of L-Dopa Treatment: Arvid Carlsson, Oleh Hornykiewicz, George Cotzias, and Melvin Yahr.” Movement Disorders 30 (1): 19–36. https://doi.org/10.1002/mds.26120.

Lee, Richard G, Shanti Balasubramaniam, Maike Stentenbach, Tom Kralj, Tim McCubbin, Benjamin Padman, Janine Smith, et al. 2022. “Deleterious Variants in CRLS1 Lead to Cardiolipin Deficiency and Cause an Autosomal Recessive Multi-System Mitochondrial Disease.” Human Molecular Genetics 31 (21): 3597–3612. https://doi.org/10.1093/hmg/ddac040.

Lewis, Mechelle M, Shawna Galley, Samantha Johnson, James Stevenson, Xuemei Huang, and Martin J McKeown. 2013. “The Role of the Cerebellum in the Pathophysiology of Parkinson’s Disease.” The Canadian Journal of Neurological Sciences. Le Journal Canadien Des Sciences Neurologiques 40 (3): 299–306. https://doi.org/10.1017/s0317167100014232.

Lew, Mark. 2007. “Overview of Parkinson’s Disease.” Pharmacotherapy 27 (12 Pt 2): 155S-160S. https://doi.org/10.1592/phco.27.12part2.155S.

Le, Weidong. 2014. “Role of Iron in UPS Impairment Model of Parkinson’s Disease.” Parkinsonism & Related Disorders 20 Suppl 1 (January): S158-61. https://doi.org/10.1016/S1353-8020(13)70038-5.

Lin, Amy W, Kalbinder K Gill, Marisol Sampedro Castañeda, Irene Matucci, Noreen Eder, Suzanne Claxton, Helen Flynn, Ambrosius P Snijders, Roger George, and Sila K Ultanir. 2018. “Chemical Genetic Identification of GAK Substrates Reveals Its Role in Regulating Na+/K+-ATPase.” Life Science Alliance 1 (6): e201800118. https://doi.org/10.26508/lsa.201800118.

Ling, M, F Merante, H S Chen, C Duff, A M Duncan, and B H Robinson. 1997. “The Human Mitochondrial Elongation Factor Tu (EF-Tu) Gene: CDNA Sequence, Genomic Localization, Genomic Structure, and Identification of a Pseudogene.” Gene 197 (1–2): 325–36. https://doi.org/10.1016/s0378-1119(97)00279-5.

Linstow, Christian U von, Ziv Gan-Or, and Patrik Brundin. 2020. “Precision Medicine in Parkinson’s Disease Patients with LRRK2 and GBA Risk Variants - Let’s Get Even More Personal.” Translational Neurodegeneration 9 (1): 39. https://doi.org/10.1186/s40035-020-00218-x.

Liu, Chia-Hsin, and Y Peter Di. 2020. “Analysis of RNA Sequencing Data Using CLC Genomics Workbench.” Methods in Molecular Biology 2102: 61–113. https://doi.org/10.1007/978-1-0716-0223-2_4.

Lobo, D S S, L Aleksandrova, J Knight, D M Casey, N el-Guebaly, J N Nobrega, and J L Kennedy. 2015. “Addiction-Related Genes in Gambling Disorders: New Insights from Parallel Human and Pre-Clinical Models.” Molecular Psychiatry 20 (8): 1002–10. https://doi.org/10.1038/mp.2014.113.

Long, Lingyun, Jun Wei, Seon Ah Lim, Jana L Raynor, Hao Shi, Jon P Connelly, Hong Wang, et al. 2021. “CRISPR Screens Unveil Signal Hubs for Nutrient Licensing of T Cell Immunity.” Nature 600 (7888): 308–13. https://doi.org/10.1038/s41586-021-04109-7.

Losón, Oliver C, Zhiyin Song, Hsiuchen Chen, and David C Chan. 2013. “Fis1, Mff, MiD49, and MiD51 Mediate Drp1 Recruitment in Mitochondrial Fission.” Molecular Biology of the Cell 24 (5): 659–67. https://doi.org/10.1091/mbc.E12-10-0721.

Lou, Haiyan, Susana E Montoya, Tshianda N M Alerte, Jian Wang, Jianjun Wu, Xiangmin Peng, Chang-Sook Hong, et al. 2010. “Serine 129 Phosphorylation Reduces the Ability of Alpha-Synuclein to Regulate Tyrosine Hydroxylase and Protein Phosphatase 2A in Vitro and in Vivo.” The Journal of Biological Chemistry 285 (23): 17648–61. https://doi.org/10.1074/jbc.M110.100867.

MacVicar, Thomas D B, and Jon D Lane. 2014. “Impaired OMA1-Dependent Cleavage of OPA1 and Reduced DRP1 Fission Activity Combine to Prevent Mitophagy in Cells That Are Dependent on Oxidative Phosphorylation.” Journal of Cell Science 127 (Pt 10): 2313–25. https://doi.org/10.1242/jcs.144337.

Marino, Silvia, Rosella Ciurleo, Giuseppe Di Lorenzo, Marina Barresi, Simona De Salvo, Sabrina Giacoppo, Alessia Bramanti, Pietro Lanzafame, and Placido Bramanti. 2012. “Magnetic Resonance Imaging Markers for Early Diagnosis of Parkinson’s Disease.” Neural Regeneration Research 7 (8): 611–19. https://doi.org/10.3969/j.issn.1673-5374.2012.08.009.

Maroteaux, L, J T Campanelli, and R H Scheller. 1988. “Synuclein: A Neuron-Specific Protein Localized to the Nucleus and Presynaptic Nerve Terminal.” The Journal of Neuroscience 8 (8): 2804–15. https://doi.org/10.1523/JNEUROSCI.08-08-02804.1988.

Masliah, E, E Rockenstein, I Veinbergs, M Mallory, M Hashimoto, A Takeda, Y Sagara, A Sisk, and L Mucke. 2000. “Dopaminergic Loss and Inclusion Body Formation in Alpha-Synuclein Mice: Implications for Neurodegenerative Disorders.” Science 287 (5456): 1265–69. https://doi.org/10.1126/science.287.5456.1265.

Matsumine, H, M Saito, S Shimoda-Matsubayashi, H Tanaka, A Ishikawa, Y Nakagawa-Hattori, M Yokochi, et al. 1997. “Localization of a Gene for an Autosomal Recessive Form of Juvenile Parkinsonism to Chromosome 6q25.2-27.” American Journal of Human Genetics 60 (3): 588–96.

McCarron, John G, Calum Wilson, Mairi E Sandison, Marnie L Olson, John M Girkin, Christopher Saunter, and Susan Chalmers. 2013. “From Structure to Function: Mitochondrial Morphology, Motion and Shaping in Vascular Smooth Muscle.” Journal of Vascular Research 50 (5): 357–71. https://doi.org/10.1159/000353883.

Mehra, Surabhi, Shruti Sahay, and Samir K Maji. 2019. “α-Synuclein Misfolding and Aggregation: Implications in Parkinson’s Disease Pathogenesis.” Biochimica et Biophysica Acta. Proteins and Proteomics 1867 (10): 890–908. https://doi.org/10.1016/j.bbapap.2019.03.001.

Miller, Justine D, Yosif M Ganat, Sarah Kishinevsky, Robert L Bowman, Becky Liu, Edmund Y Tu, Pankaj K Mandal, et al. 2013. “Human IPSC-Based Modeling of Late-Onset Disease via Progerin-Induced Aging.” Cell Stem Cell 13 (6): 691–705. https://doi.org/10.1016/j.stem.2013.11.006.

Morais, Vanessa A, Dominik Haddad, Katleen Craessaerts, Pieter-Jan De Bock, Jef Swerts, Sven Vilain, Liesbeth Aerts, et al. 2014. “PINK1 Loss-of-Function Mutations Affect Mitochondrial Complex I Activity via NdufA10 Ubiquinone Uncoupling.” Science 344 (6180): 203–7. https://doi.org/10.1126/science.1249161.

Mullin, Stephen, and Anthony Schapira. 2013. “α-Synuclein and Mitochondrial Dysfunction in Parkinson’s Disease.” Molecular Neurobiology 47 (2): 587–97. https://doi.org/10.1007/s12035-013-8394-x.

———. 2015. “The Genetics of Parkinson’s Disease.” British Medical Bulletin 114 (1): 39–52. https://doi.org/10.1093/bmb/ldv022.

Muñoz, Yorka, Carlos M Carrasco, Joaquín D Campos, Pabla Aguirre, and Marco T Núñez. 2016. “Parkinson’s Disease: The Mitochondria-Iron Link.” Parkinson’s Disease 2016 (May): 7049108. https://doi.org/10.1155/2016/7049108.

Murphy, D D, S M Rueter, J Q Trojanowski, and V M Lee. 2000. “Synucleins Are Developmentally Expressed, and Alpha-Synuclein Regulates the Size of the Presynaptic Vesicular Pool in Primary Hippocampal Neurons.” The Journal of Neuroscience 20 (9): 3214–20. https://doi.org/10.1523/JNEUROSCI.20-09-03214.2000.

Nakamura, Ken, Venu M Nemani, Farnaz Azarbal, Gaia Skibinski, Jon M Levy, Kiyoshi Egami, Larissa Munishkina, et al. 2011. “Direct Membrane Association Drives Mitochondrial Fission by the Parkinson Disease-Associated Protein Alpha-Synuclein.” The Journal of Biological Chemistry 286 (23): 20710–26. https://doi.org/10.1074/jbc.M110.213538.

Nalls, Mike A, Cornelis Blauwendraat, Costanza L Vallerga, Karl Heilbron, Sara Bandres-Ciga, Diana Chang, Manuela Tan, et al. 2019. “Identification of Novel Risk Loci, Causal Insights, and Heritable Risk for Parkinson’s Disease: A Meta-Analysis of Genome-Wide Association Studies.” Lancet Neurology 18 (12): 1091–1102. https://doi.org/10.1016/S1474-4422(19)30320-5.

Nguyen, Thanh N, Benjamin S Padman, and Michael Lazarou. 2016. “Deciphering the Molecular Signals of Pink1/Parkin Mitophagy.” Trends in Cell Biology 26 (10): 733–44. https://doi.org/10.1016/j.tcb.2016.05.008.

Oh, SeCheol, Navid Paknejad, and Richard K Hite. 2020. “Gating and Selectivity Mechanisms for the Lysosomal K+ Channel TMEM175.” ELife 9 (March). https://doi.org/10.7554/eLife.53430.

Omura, Tomohiro, Masayuki Kaneko, Yasunobu Okuma, Yasuko Orba, Kazuo Nagashima, Ryosuke Takahashi, Noboru Fujitani, et al. 2006. “A Ubiquitin Ligase HRD1 Promotes the Degradation of Pael Receptor, a Substrate of Parkin.” Journal of Neurochemistry 99 (6): 1456–69. https://doi.org/10.1111/j.1471-4159.2006.04155.x.

Osellame, Laura D, Abeer P Singh, David A Stroud, Catherine S Palmer, Diana Stojanovski, Rajesh Ramachandran, and Michael T Ryan. 2016. “Cooperative and Independent Roles of the Drp1 Adaptors Mff, MiD49 and MiD51 in Mitochondrial Fission.” Journal of Cell Science 129 (11): 2170–81. https://doi.org/10.1242/jcs.185165.

Palacino, James J, Dijana Sagi, Matthew S Goldberg, Stefan Krauss, Claudia Motz, Maik Wacker, Joachim Klose, and Jie Shen. 2004. “Mitochondrial Dysfunction and Oxidative Damage in Parkin-Deficient Mice.” The Journal of Biological Chemistry 279 (18): 18614–22. https://doi.org/10.1074/jbc.M401135200.

Parkinson, J. 1969. “An Essay on the Shaking Palsy.” Archives of Neurology 20 (4): 441–45. https://doi.org/10.1001/archneur.1969.00480100117017.

Park, Jin-Sung, Ryan L Davis, and Carolyn M Sue. 2018. “Mitochondrial Dysfunction in Parkinson’s Disease: New Mechanistic Insights and Therapeutic Perspectives.” Current Neurology and Neuroscience Reports 18 (5): 21. https://doi.org/10.1007/s11910-018-0829-3.

Patten, B M. 1983. “A Personal Tribute to Dr. George C. Cotzias, Clinician and Scientist.” Perspectives in Biology and Medicine 27 (1): 156–61. https://doi.org/10.1353/pbm.1983.0011.

Pérez-Treviño, Perla, Mónica Velásquez, and Noemí García. 2020. “Mechanisms of Mitochondrial DNA Escape and Its Relationship with Different Metabolic Diseases.” Biochimica et Biophysica Acta. Molecular Basis of Disease 1866 (6): 165761. https://doi.org/10.1016/j.bbadis.2020.165761.

Perfeito, Rita, Teresa Cunha-Oliveira, and Ana Cristina Rego. 2012. “Revisiting Oxidative Stress and Mitochondrial Dysfunction in the Pathogenesis of Parkinson Disease--Resemblance to the Effect of Amphetamine Drugs of Abuse.” Free Radical Biology & Medicine 53 (9): 1791–1806. https://doi.org/10.1016/j.freeradbiomed.2012.08.569.

Perfettini, Jean-Luc, Thomas Roumier, and Guido Kroemer. 2005. “Mitochondrial Fusion and Fission in the Control of Apoptosis.” Trends in Cell Biology 15 (4): 179–83. https://doi.org/10.1016/j.tcb.2005.02.005.

Picard, Martin, Orian S Shirihai, Benoit J Gentil, and Yan Burelle. 2013. “Mitochondrial Morphology Transitions and Functions: Implications for Retrograde Signaling?” American Journal of Physiology. Regulatory, Integrative and Comparative Physiology 304 (6): R393-406. https://doi.org/10.1152/ajpregu.00584.2012.

Picca, Anna, Flora Guerra, Riccardo Calvani, Hélio José Coelho-Junior, Maurizio Bossola, Francesco Landi, Roberto Bernabei, Cecilia Bucci, and Emanuele Marzetti. 2020. "Generation and Release of Mitochondrial-Derived Vesicles in Health, Aging and Disease." Journal of Clinical Medicine 9 (5). https://doi.org/10.3390/jcm9051440.

Poewe, Werner, and Angelo Antonini. 2015. "Novel Formulations and Modes of Delivery of Levodopa." Movement Disorders 30 (1): 114–20. https://doi.org/10.1002/mds.26078.

Polymeropoulos, M H, C Lavedan, E Leroy, S E Ide, A Dehejia, A Dutra, B Pike, et al. 1997. "Mutation in the Alpha-Synuclein Gene Identified in Families with Parkinson's Disease." Science 276 (5321): 2045–47. https://doi.org/10.1126/science.276.5321.2045.

Quartarone, Angelo, Alberto Cacciola, Demetrio Milardi, Maria Felice Ghilardi, Alessandro Calamuneri, Gaetana Chillemi, Giuseppe Anastasi, and John Rothwell. 2020. "New Insights into Cortico-Basal-Cerebellar Connectome: Clinical and Physiological Considerations." Brain: A Journal of Neurology 143 (2): 396–406. https://doi.org/10.1093/brain/awz310.

Radhakrishnan, Divya M, and Vinay Goyal. 2018. "Parkinson's Disease: A Review." Neurology India 66 (Supplement): S26–35. https://doi.org/10.4103/0028-3886.226451.

Ren, Mindong, Yang Xu, Colin K L Phoon, Hediye Erdjument-Bromage, Thomas A Neubert, and Michael Schlame. 2023. "Knockout of Cardiolipin Synthase Disrupts Postnatal Cardiac Development by Inhibiting the Maturation of Mitochondrial Cristae." BioRxiv, March. https://doi.org/10.1101/2023.03.09.531996.

Riley, Joel S, and Stephen Wg Tait. 2020. "Mitochondrial DNA in Inflammation and Immunity." EMBO Reports 21 (4): e49799. https://doi.org/10.15252/embr.201949799.

Rodriguez-Sabate, Clara, Ingrid Morales, Jesus N Lorenzo, and Manuel Rodriguez. 2019. "The Organization of the Basal Ganglia Functional Connectivity Network Is Non-Linear in Parkinson's Disease." NeuroImage. Clinical 22 (February): 101708. https://doi.org/10.1016/j.nicl.2019.101708.

Ryan, Scott D, Nima Dolatabadi, Shing Fai Chan, Xiaofei Zhang, Mohd Waseem Akhtar, James Parker, Frank Soldner, et al. 2013. “Isogenic Human IPSC Parkinson’s Model Shows Nitrosative Stress-Induced Dysfunction in MEF2-PGC1α Transcription.” Cell 155 (6): 1351–64. https://doi.org/10.1016/j.cell.2013.11.009.

Scarffe, Leslie A, Daniel A Stevens, Valina L Dawson, and Ted M Dawson. 2014. “Parkin and PINK1: Much More than Mitophagy.” Trends in Neurosciences 37 (6): 315–24. https://doi.org/10.1016/j.tins.2014.03.004.

Schram, Andrea W, Roy Baas, Pascal W T C Jansen, Anne Riss, Laszlo Tora, Michiel Vermeulen, and H Th Marc Timmers. 2013. “A Dual Role for SAGA-Associated Factor 29 (SGF29) in ER Stress Survival by Coordination of Both Histone H3 Acetylation and Histone H3 Lysine-4 Trimethylation.” Plos One 8 (7): e70035. https://doi.org/10.1371/journal.pone.0070035.

Sena Brandine, Guilherme de, and Andrew D Smith. 2019. “Falco: High-Speed FastQC Emulation for Quality Control of Sequencing Data.” F1000Research 8 (November): 1874. https://doi.org/10.12688/f1000research.21142.2.

Sevlever, Daniel, Peizhou Jiang, and Shu-Hui C Yen. 2008. “Cathepsin D Is the Main Lysosomal Enzyme Involved in the Degradation of Alpha-Synuclein and Generation of Its Carboxy-Terminally Truncated Species.” Biochemistry 47 (36): 9678–87. https://doi.org/10.1021/bi800699v.

Shang, Wanjing, Yong Jiang, Michael Boettcher, Kang Ding, Marianne Mollenauer, Zhongyi Liu, Xiaofeng Wen, et al. 2018. “Genome-Wide CRISPR Screen Identifies FAM49B as a Key Regulator of Actin Dynamics and T Cell Activation.” Proceedings of the National Academy of Sciences of the United States of America 115 (17): E4051–60. https://doi.org/10.1073/pnas.1801340115.

Shiba-Fukushima, Kahori, Yuzuru Imai, Shigeharu Yoshida, Yasushi Ishihama, Tomoko Kanao, Shigeto Sato, and Nobutaka Hattori. 2012. “PINK1-Mediated Phosphorylation of the Parkin Ubiquitin-like Domain Primes Mitochondrial Translocation of Parkin and Regulates Mitophagy.” Scientific Reports 2 (December): 1002. https://doi.org/10.1038/srep01002.

Shiina, N, Y Gotoh, N Kubomura, A Iwamatsu, and E Nishida. 1994. “Microtubule Severing by Elongation Factor 1 Alpha.” Science 266 (5183): 282–85. https://doi.org/10.1126/science.7939665.

Sidransky, E, M A Nalls, J O Aasly, J Aharon-Peretz, G Annesi, E R Barbosa, A Bar-Shira, et al. 2009. “Multicenter Analysis of Glucocerebrosidase Mutations in Parkinson’s Disease.” The New England Journal of Medicine 361 (17): 1651–61. https://doi.org/10.1056/NEJMoa0901281.

Smith, Laura, and Anthony H V Schapira. 2022. “GBA Variants and Parkinson Disease: Mechanisms and Treatments.” Cells 11 (8). https://doi.org/10.3390/cells11081261.

Somayaji, Mahalakshmi, Zina Lanseur, Se Joon Choi, David Sulzer, and Eugene V Mosharov. 2021. “Roles for α-Synuclein in Gene Expression.” Genes 12 (8). https://doi.org/10.3390/genes12081166.

Spillantini, M G, M L Schmidt, V M Lee, J Q Trojanowski, R Jakes, and M Goedert. 1997. “Alpha-Synuclein in Lewy Bodies.” Nature 388 (6645): 839–40. https://doi.org/10.1038/42166.

Stafa, Klodjan, Elpida Tsika, Roger Moser, Alessandra Musso, Liliane Glauser, Amy Jones, Saskia Biskup, et al. 2014. “Functional Interaction of Parkinson’s Disease-Associated LRRK2 with Members of the Dynamin GTPase Superfamily.” Human Molecular Genetics 23 (8): 2055–77. https://doi.org/10.1093/hmg/ddt600.

Stefanis, Leonidas. 2012. “α-Synuclein in Parkinson’s Disease.” Cold Spring Harbor Perspectives in Medicine 2 (2): a009399. https://doi.org/10.1101/cshperspect.a009399.

Stoddard-Bennett, Theo, and Renee Reijo Pera. 2019. “Treatment of Parkinson’s Disease through Personalized Medicine and Induced Pluripotent Stem Cells.” Cells 8 (1). https://doi.org/10.3390/cells8010026.

Tahrir, Farzaneh G, Tijana Knezevic, Manish K Gupta, Jennifer Gordon, Joseph Y Cheung, Arthur M Feldman, and Kamel Khalili. 2017. “Evidence for the Role of BAG3 in Mitochondrial Quality Control in Cardiomyocytes.” Journal of Cellular Physiology 232 (4): 797–805. https://doi.org/10.1002/jcp.25476.

Tambasco, Nicola, Michele Romoli, and Paolo Calabresi. 2018. “Levodopa in Parkinson’s Disease: Current Status and Future Developments.” Current Neuropharmacology 16 (8): 1239–52. https://doi.org/10.2174/1570159X15666170510143821.

Tolosa, Eduardo, Alicia Garrido, Sonja W Scholz, and Werner Poewe. 2021. “Challenges in the Diagnosis of Parkinson’s Disease.” Lancet Neurology 20 (5): 385–97. https://doi.org/10.1016/S1474-4422(21)00030-2.

Tong, Tong, Junfang Ji, Shunqian Jin, Xianxing Li, Wenhong Fan, Yongmei Song, Minrong Wang, Zhihua Liu, Min Wu, and Qimin Zhan. 2005. “Gadd45a Expression Induces Bim Dissociation from the Cytoskeleton and Translocation to Mitochondria.” Molecular and Cellular Biology 25 (11): 4488–4500. https://doi.org/10.1128/MCB.25.11.4488-4500.2005.

Trist, Benjamin G, Dominic J Hare, and Kay L Double. 2019. “Oxidative Stress in the Aging Substantia Nigra and the Etiology of Parkinson’s Disease.” Aging Cell 18 (6): e13031. https://doi.org/10.1111/acel.13031.

Tseng, Wei-En Johnny, Chiung-Mei Chen, Yi-Chun Chen, Zhao Yi, Eng-King Tan, and Yih-Ru Wu. 2013. “Genetic Variations of GAK in Two Chinese Parkinson’s Disease Populations: A Case-Control Study.” Plos One 8 (6): e67506. https://doi.org/10.1371/journal.pone.0067506.

Tysnes, Ole-Bjørn, and Anette Storstein. 2017. “Epidemiology of Parkinson’s Disease.” Journal of Neural Transmission 124 (8): 901–5. https://doi.org/10.1007/s00702-017-1686-y.

“Updated Version of Image Data Storage and Analysis System. - Free Online Library.” n.d. Accessed June 5, 2023. https://www.thefreelibrary.com/Updated+version+of+image+data+storage+and+analysis+system-a0278510271.

Valente, Lucia, Valeria Tiranti, Rene Massimiliano Marsano, Edoardo Malfatti, Erika Fernandez-Vizarra, Claudia Donnini, Paolo Mereghetti, et al. 2007. “Infantile Encephalopathy and Defective Mitochondrial DNA Translation in Patients with Mutations of Mitochondrial Elongation Factors

EFG1 and EFTu." American Journal of Human Genetics 80 (1): 44–58. https://doi.org/10.1086/510559.

Viana, Matheus P, Aidan I Brown, Irina A Mueller, Claire Goul, Elena F Koslover, and Susanne M Rafelski. 2020. "Mitochondrial Fission and Fusion Dynamics Generate Efficient, Robust, and Evenly Distributed Network Topologies in Budding Yeast Cells." Cell Systems 10 (3): 287-297.e5. https://doi.org/10.1016/j.cels.2020.02.002.

Villar-Piqué, Anna, Tomás Lopes da Fonseca, and Tiago Fleming Outeiro. 2016. "Structure, Function and Toxicity of Alpha-Synuclein: The Bermuda Triangle in Synucleinopathies." Journal of Neurochemistry 139 Suppl 1 (October): 240–55. https://doi.org/10.1111/jnc.13249.

Wang, Wenzhang, Xinglong Wang, Hisashi Fujioka, Charles Hoppel, Alan L Whone, Maeve A Caldwell, Peter J Cullen, Jun Liu, and Xiongwei Zhu. 2016. "Parkinson's Disease-Associated Mutant VPS35 Causes Mitochondrial Dysfunction by Recycling DLP1 Complexes." Nature Medicine 22 (1): 54–63. https://doi.org/10.1038/nm.3983.

Wauer, Tobias, Kirby N Swatek, Jane L Wagstaff, Christina Gladkova, Jonathan N Pruneda, Martin A Michel, Malte Gersch, Christopher M Johnson, Stefan M V Freund, and David Komander. 2015. "Ubiquitin Ser65 Phosphorylation Affects Ubiquitin Structure, Chain Assembly and Hydrolysis." The EMBO Journal 34 (3): 307–25. https://doi.org/10.15252/embj.201489847.

Weber, Axel, Judith Marquardt, David Elzi, Nicole Forster, Sven Starke, Andre Glaum, Daisuke Yamada, et al. 2008. "Zbtb4 Represses Transcription of P21CIP1 and Controls the Cellular Response to P53 Activation." The EMBO Journal 27 (11): 1563–74. https://doi.org/10.1038/emboj.2008.85.

West, A Phillip, William Khoury-Hanold, Matthew Staron, Michal C Tal, Cristiana M Pineda, Sabine M Lang, Megan Bestwick, et al. 2015. "Mitochondrial DNA Stress Primes the Antiviral Innate Immune Response." Nature 520 (7548): 553–57. https://doi.org/10.1038/nature14156.

Wie, Jinhong, Zhenjiang Liu, Haikun Song, Thomas F Tropea, Lu Yang, Huanhuan Wang, Yuling Liang, et al. 2021. “A Growth-Factor-Activated Lysosomal K+ Channel Regulates Parkinson’s Pathology.” Nature 591 (7850): 431–37. https://doi.org/10.1038/s41586-021-03185-z.

Wright, Rebecca. 2022. “Mitochondrial Dysfunction and Parkinson’s Disease.” Nature Neuroscience 25 (1): 2. https://doi.org/10.1038/s41593-021-00989-0.

Wu, Bo, Qi Liu, Chunli Duan, Yaohua Li, Shun Yu, Piu Chan, Kenji Uéda, and Hui Yang. 2011. “Phosphorylation of α-Synuclein Upregulates Tyrosine Hydroxylase Activity in MN9D Cells.” Acta Histochemica 113 (1): 32–35. https://doi.org/10.1016/j.acthis.2009.07.007.

Yao, Jingyue, Jubo Wang, Ye Xu, Qinglong Guo, Yuening Sun, Jian Liu, Sichan Li, Yongjian Guo, and Libin Wei. 2022. “CDK9 Inhibition Blocks the Initiation of PINK1-PRKN-Mediated Mitophagy by Regulating the SIRT1-FOXO3-BNIP3 Axis and Enhances the Therapeutic Effects Involving Mitochondrial Dysfunction in Hepatocellular Carcinoma.” Autophagy 18 (8): 1879–97. https://doi.org/10.1080/15548627.2021.2007027.

Ying, Zhong-Ming, Qian-Kun Lv, Xiao-Yu Yao, An-Qi Dong, Ya-Ping Yang, Yu-Lan Cao, Fen Wang, Ai-Ping Gong, and Chun-Feng Liu. 2022. “BAG3 Promotes Autophagy and Suppresses NLRP3 Inflammasome Activation in Parkinson’s Disease.” Annals of Translational Medicine 10 (22): 1218. https://doi.org/10.21037/atm-22-5159.

Yin, Jiang-An, Lukas Frick, Manuel C. Scheidmann, Tingting Liu, Chiara Trevisan, Ashutosh Dhingra, Anna Spinelli, et al. 2022. “Robust and Versatile Arrayed Libraries for Human Genome-Wide CRISPR Activation, Deletion and Silencing.” BioRxiv, May. https://doi.org/10.1101/2022.05.25.493370.

Yuki, Kyoko E, Hadir Marei, Evgenij Fiskin, Megan M Eva, Angelica A Gopal, Jeremy A Schwartzentruber, Jacek Majewski, et al. 2019. “CYRI/FAM49B Negatively Regulates RAC1-Driven Cytoskeletal Remodelling and Protects against Bacterial Infection.” Nature Microbiology 4 (9): 1516–31. https://doi.org/10.1038/s41564-019-0484-8.

Yu, Tianzheng, Bong Sook Jhun, and Yisang Yoon. 2011. “High-Glucose Stimulation Increases Reactive Oxygen Species Production through the Calcium and Mitogen-Activated Protein Kinase-Mediated Activation of Mitochondrial Fission.” Antioxidants & Redox Signaling 14 (3): 425–37. https://doi.org/10.1089/ars.2010.3284.

Yu, Tianzheng, James L Robotham, and Yisang Yoon. 2006. “Increased Production of Reactive Oxygen Species in Hyperglycemic Conditions Requires Dynamic Change of Mitochondrial Morphology.” Proceedings of the National Academy of Sciences of the United States of America 103 (8): 2653–58. https://doi.org/10.1073/pnas.0511154103.

Zhang, Huili, Guangming Yang, Ning Zhong, Jun Shan, Xiaona Li, Yanhai Wu, Yazhou Xu, and Ye Yuan. 2020. “Possible Key MicroRNAs and Corresponding Molecular Mechanisms for Atrial Fibrillation.” Anatolian Journal of Cardiology 23 (6): 324–33. https://doi.org/10.14744/AnatolJCardiol.2020.39483.

Zhang, J H, T D Chung, and K R Oldenburg. 1999. “A Simple Statistical Parameter for Use in Evaluation and Validation of High Throughput Screening Assays.” Journal of Biomolecular Screening 4 (2): 67–73. https://doi.org/10.1177/108705719900400206.

Zhang, Xiaohua Douglas. 2011. “Illustration of SSMD, z Score, SSMD*, Z* Score, and t Statistic for Hit Selection in RNAi High-Throughput Screens.” Journal of Biomolecular Screening 16 (7): 775–85. https://doi.org/10.1177/1087057111405851.

Zhang, Xiaoling, Wenmin Huang, Yiyun Fan, Ying Sun, and Xiaoqun Ge. 2019. “Role of GTPases in the Regulation of Mitochondrial Dynamics in Parkinson’s Disease.” Experimental Cell Research 382 (1): 111460. https://doi.org/10.1016/j.yexcr.2019.06.005.

Zhong, Bi-Rou, Gui-Feng Zhou, Li Song, Qi-Xin Wen, Xiao-Juan Deng, Yuan-Lin Ma, Li-Tian Hu, and Guo-Jun Chen. 2021. “TUFM Is Involved in Alzheimer’s Disease-like Pathologies That Are Associated with ROS.” The FASEB Journal 35 (5): e21445. https://doi.org/10.1096/fj.202002461R.

Zhou, Leping, Wenzhang Wang, Charles Hoppel, Jun Liu, and Xiongwei Zhu. 2017. “Parkinson’s Disease-Associated Pathogenic VPS35 Mutation Causes Complex I Deficits.” Biochimica et Biophysica Acta. Molecular Basis of Disease 1863 (11): 2791–95. https://doi.org/10.1016/j.bbadis.2017.07.032.

Zhu, Yao-Feng, Wei-Ping Wang, Xue-Feng Zheng, Zhi Chen, Tao Chen, Zi-Yun Huang, Lin-Ju Jia, and Wan-Long Lei. 2020. “Characteristic Response of Striatal Astrocytes to Dopamine Depletion.” Neural Regeneration Research 15 (4): 724–30. https://doi.org/10.4103/1673-5374.266917.

Zhu, Zhou, Chuanbin Yang, Ashok Iyaswamy, Senthilkumar Krishnamoorthi, Sravan Gopalkrishnashetty Sreenivasmurthy, Jia Liu, Ziying Wang, et al. 2019. “Balancing MTOR Signaling and Autophagy in the Treatment of Parkinson’s Disease.” International Journal of Molecular Sciences 20 (3). https://doi.org/10.3390/ijms20030728.